Article:

Peakall, J orcid.org/0000-0003-3382-4578, Best, J, Baas, JH et al. (5 more authors) (2020) An integrated process-based model of flutes and tool marks in deep-water environments: Implications for palaeohydraulics, the Bouma sequence and hybrid event beds. Sedimentology, 67 (4). pp. 1601-1666. ISSN 0037-0746

https://doi.org/10.1111/sed.12727

An integrated process-based model of flutes and tool marks in deep-water environments: implications for palaeohydraulics, the Bouma sequence, and hybrid event beds

Jeff Peakall[1], Jim Best[2], Jaco H. Baas[3], David M. Hodgson[1], Michael A. Clare[4], Peter J. Talling[5], Robert M. Dorrell[6], David R. Lee[1]*

1. School of Earth and Environment, University of Leeds, Leeds, LS2 9JT, UK. (E-mail: j.peakall@leeds.ac.uk)

2. Departments of Geology, Geography and GIS, Mechanical Science and Engineering, and Ven Te Chow Hydrosystems Laboratory, University of Illinois at Urbana-Champaign, Urbana, IL 61801, USA

3. School of Ocean Sciences, Bangor University, Bangor, Menai Bridge, LL59 5AB, Wales, UK

4. National Oceanography Centre, Southampton, European Way, Southampton, SO14 3ZH, UK

5. Departments of Earth Sciences and Geography, University of Durham, Durham, DH1 3LE, UK

6. Energy and Environment Institute, University of Hull, Hull, HU6 7RX, UK

*Corresponding author

ABSTRACT

Flutes and tool marks are commonly observed sedimentary structures on the bases of sandstones in deep-water successions. These sole structures are universally used as palaeocurrent indicators but, in sharp contrast to most sedimentary structures, they are not used in palaeohydraulic reconstructions or to aid prediction of the spatial distribution of sediments. Since Kuenen's famous 1953 paper, flutes and tool marks in deep-water systems have been linked to turbidity currents, as reflected in the standard Bouma sequence taught to generations of geologists. Yet, these structures present a series of unaddressed enigmas. Detailed field studies in the 1960s and early 1970s observed that flutes are typically associated with thicker, more proximal beds, whilst tools are

generally prevalent in thinner, more distal, beds. Additionally, flutes and tool marks are rarely observed on the same surfaces, and flutes are seen to change downstream from larger wider parabolic to smaller narrower spindle shaped forms. No model has been proposed that explains these field-based observations.

Here, we undertake a radical re-examination of the formative flow conditions of flutes and tool marks, and demonstrate that they are the products of a wide range of sediment gravity flows, from turbulent flows, through transitional clay-rich flows, to debris flows. Flutes are not solely the product of turbulent flows, but can continue to form in transitional flows. Grooves are shown to be formed by *debris flows, slumps and slides*, not turbidity currents, and in many cases the debris flows are linked to the debritic component of hybrid flows. Discontinuous tool marks, including skim (bounce) marks, prod marks and skip marks, are shown to be formed by transitional mud-rich flows. Consequently, the observed spatial distribution of flutes and tool marks can be explained by a progressive increase in flow cohesivity downstream. This model of flutes and tool marks dovetails with models of hybrid flows that predict such a longitudinal increase in flow cohesivity. However, some deposits show grooves preferentially associated with Bouma T_A beds, and these are likely formed by flows transforming from higher to lower cohesion, and are present in basins where hybrid beds are absent or rare. The recognition that sole structures may have *no genetic link* to the later overlying turbidity current deposits, and can be formed by a wide range of flow types, indicates that the existing pictorial description of the Bouma sequence *is incorrect*. We propose a modified Bouma sequence that addresses these points. In utilising the advances in fluid dynamics since Kuenen's pioneering research, we demonstrate that it is possible to use flutes and tool marks to interpret flow type at the point of formation, the nature of flow transformations, and the mechanics of the basal layer. These advances suggest that it is then possible to predict the nature of deposit type down-dip. This new understanding, in combination with further testing in outcrop of the proposed relationships between sole marks and palaeohydraulics, opens up a wealth of possibilities for improving the understanding of deep-water clastic environments, with implications for developing more complete facies models, assessing subaqueous geohazards and the resilience of seafloor infrastructure, and advancing our understanding of deep-water sediments as archives of palaeoenvironmental change.

Keywords

Flutes, tool marks, sole structures, tools, Bouma sequence, transitional flow, debris flow, turbidity current, turbidite, sediment density flow, hybrid bed, substrate

Running title

Flutes and tool marks in deep-water environments

INTRODUCTION

The bases of sandstone beds in deep-water sedimentary successions are commonly ornamented with sole structures of inorganic origin that record the infilling of erosional bedforms generated in the underlying fine-grained substrate. Two categories of sole structures can be identified: scour marks such as flutes formed by turbulent scour, and tool marks formed by objects (tools) within the flow (Dżułyński & Sanders, 1962a; Collinson *et al*., 2006), which are subdivided further into continuous marks (*e.g*., grooves and chevron marks) and discontinuous marks (*e.g*., prod, bounce, skip, and roll marks) (Dżułyński & Sanders, 1962a). The use of sole structures as indicators of palaeocurrent direction is long-established (*e.g*., Hall, 1843) and every geoscience student is trained in their recognition, and their value for palaeogeographic reconstruction. However, their wider utility for the interpretation of palaeohydraulic conditions and flow-substrate interactions is limited. This is in stark contrast to aggradational bedforms, such as ripples, dunes, upper-stage plane beds and antidunes, which have been used extensively to provide information concerning processes during deposition in addition to palaeocurrent information (*e.g*., Harms, 1969; Allen, 1984; Cartigny *et al*., 2014; Baas *et al*., 2016a). In large part, the focus on palaeocurrent information from tool marks and flutes reflects the lack of understanding of their formative conditions.

Nonetheless, many important observations have been made concerning the distribution and association of flutes and tool marks. Exceptions exist, but flutes are typically associated with proximal locations, and tool marks with distal locations (*e.g.*, Hsu, 1959; Craig & Walton, 1962; Walker, 1967; Lovell, 1969; Ricci Lucchi, 1969b; Slacza & Unrug, 1976; Remacha & Fernández, 2003; Remacha *et al*., 2005; Collinson *et al*., 2006; Collinson & Mountney, 2019). Bed bases with both types are rare (*e.g*., Crowell, 1955; Wood & Smith, 1958; Sanders, 1965; Collinson *et al*., 2006), but where present commonly show cross-cutting relationships (Kuenen, 1957; Dżułyński & Sanders, 1962a; Enos, 1969a; Ricci Lucchi, 1969a; Draganits *et al*., 2008; Pyles & Jennette, 2009). Furthermore, although the Bouma sequence depicts flutes and grooves on the base of the T_A division, both types are also found under T_B and T_C beds (*e.g*., Bouma, 1962; Pett & Walker, 1971; Crimes, 1973; Table 1). These field observations are supported across systems of different ages and tectonic settings, but have proven enigmatic. As such, no process explanations or synoptic models have been presented to explain why flutes and tool marks exhibit these general spatial and temporal variations, or why there are exceptions. A better understanding of the relationship between erosional bedforms and their overlying deposits has profound implications for our general understanding of deep-water systems. In particular, the use of deep-marine sedimentary successions as archives of palaeoenvironmental change, for reducing uncertainty in geohazard assessment, and for determining the resilience of seafloor infrastructure, requires improved understanding of the interactions between flows and substrate conditions, and the formation of erosional bedforms. The most accessible resource for these investigations is the sole structures preserved on the base of deep-water sandstones.

In this paper, we aim to examine the formative mechanisms of flutes and the different types of tool marks. To achieve this aim, we utilise recent advances in the understanding of transitional flow processes between fully turbulent and laminar flow, and new data on seafloor substrates, to address the following objectives: i) to discuss flow rheology at the time of sole structure formation, and the likely downdip deposit type; ii) to use data from modern seafloor substrates to infer likely depths of erosion, nature of the ancient substrate, and amount of substrate entrainment; iii) to reassess the modern depiction of the Bouma sequence, which presents a genetic link between the basal erosive surface and the overlying deposit; iv) to use the dimensions of grooves to infer flow properties and interpret objects that generated the tools; and, v) to discuss the location under a flow where flutes and tool marks form, which is widely accepted as being under the density current head. This wide range of objectives is integrated into a new synoptic process-orientated model that explains the distribution and association of scour marks and tool marks, which can be employed to transform the information that can be gained from detailed investigations of these sedimentary structures in all modern and ancient deep-water successions.

BACKGROUND

Classification of sole marks

Sole marks (Kuenen, 1957) are features identified on the base of beds (typically sandstones), formed by infilling of topography that was eroded into an underlying fine-grained substrate, generally cohesive mud. Sole marks can include organic forms such as burrows (Kuenen, 1957), but here we restrict the discussion to inorganic structures. They are typically subdivided into two categories: scour marks formed by turbulent scour, and tool marks formed by objects (tools) within the flow (Dżułyński & Sanders, 1962a; Collinson *et al*., 2006). Scour marks include obstacle scours, longitudinal scours, mud ripples, and gutter casts (*e.g*., Dżułyński & Walton, 1965; Allen, 1984; Collinson *et al*., 2006), but for brevity we restrict ourselves to the most common structure, flutes (Enos, 1969a). Tool marks are further subdivided into continuous marks (grooves and chevron marks) and discontinuous marks (e.g., prod, bounce, skip, and roll marks) (Dżułyński & Sanders, 1962a). The term ‘continuous mark’ is not strictly true since grooves and chevrons do have terminations (e.g., Enos, 1969a). However, these structures are typically continuous on the scale of an individual outcrop. In contrast, discontinuous marks occur as individual or groups of structures centimetres to decimetres long (Dżułyński & Walton, 1965; Collinson *et al*., 2006).

Distribution and association of scour marks and tool marks

A number of key observations have been made concerning the distribution of scour and tool marks: i) scour marks and tool marks are comparatively rarely observed on the same surfaces (*e.g*., Crowell, 1955; Wood & Smith, 1958; Sanders, 1965; Collinson *et al*., 2006; Dirnerová & Janočko, 2014), albeit with exceptions where juxtapositions of scour and tool marks dominate successions (Crimes, 1973; Table 1); ii) where they are observed on the same surface, tool marks such as grooves can either pre-date (Kuenen, 1957; Dżułyński & Sanders, 1962a; Enos, 1969a; Ricci Lucchi, 1969a; Draganits *et al*., 2008) or post-date scour marks such as flutes (Dżułyński & Sanders, 1962a; Ricci Lucchi, 1969a; Pyles & Jennette, 2009); iii) scour marks are typically associated with thicker sands, and tool marks with thinner sands (Ricci Lucchi, 1969b; Tinterri & Muzzi Magalhaes, 2011; Collinson & Mountney, 2019), although other studies show only limited variation (*e.g*., Bouma, 1962 where grooves are on average in slightly thicker beds) or none at all (Enos, 1969a); iv) scour marks are typically associated with proximal environments, and tool marks with more distal environments, thus implying a longitudinal variation in the nature of erosive structures (Hsu, 1959; Craig & Walton, 1962; Dżułyński & Walton, 1965; Walker, 1967; Lovell, 1969; Slacza & Unrug, 1976; Remacha & Fernández, 2003; Remacha *et al*., 2005), although again exceptions do occur (Bouma, 1962; Crimes, 1973); and v) flutes and tool marks, including grooves, whilst commonly depicted as occurring solely under the T_A division of the Bouma sequence (*e.g*., Middleton & Hampton, 1976; Allen, 1985; Collinson *et al*., 2006; Leeder, 2011), are also associated with T_B and T_C units when these form the basal divisions in the Bouma sequence (*e.g*., Bouma, 1962; Pett & Walker, 1971; Crimes, 1973; Table 1). Observations (iii) and (iv) are partly linked since turbidites are well known to thin with distance downstream, often with an approximately exponential or power-law distribution (*e.g.*, Walker, 1967; de Rooij & Dalziel, 2001; Talling *et al*., 2007a,b; Kane *et al*., 2010).

Whilst these relationships are firmly embedded in the literature, it is interesting to note that in the quantitative data shown in Table 1 the relationship between Bouma divisions (and by inference downstream distance) and flutes and grooves is less clear. Grooves are more frequently observed in T_A beds in Bouma (1962) and Crimes (1973) whilst flutes are more common in Pett & Walker (1971). Such variations suggest that measuring and aggregating Bouma divisions at a given location might be an imperfect surrogate for downstream position in a system, compared with observations from different longitudinal positions (e.g., Lovell, 1969; Slacza & Unrug, 1976; Remacha & Fernández, 2003). Alternatively, these data may indicate that in some cases there can be a longitudinal variation from tool marks in proximal locations to scour marks downstream. What is clear is that there is a need for more quantitative documentation of the distribution of sole mark types in different settings. In particular, it is desirable to couple such quantitative data on the distribution of different sole structures to modern interpretations of sediment gravity flow processes, deposits and sub-environments.

STRUCTURE AND RATIONALE

To address the formative mechanisms, and thus utility, of flutes and tool marks, we start with a brief review of the fluid dynamics of mud-poor to mud-rich flows, in particular concentrating on transitional flows, between truly turbulent, and fully cohesive, laminar, flows. As will be demonstrated, the different types of flutes and tool marks can be linked to these differing flow types, and thus an understanding of these processes is critical when linking sole structures to flow dynamics. Sole structures are also dependent on the nature of the substrate, and thus the properties of modern seafloor substrates are examined next, and their applicability to older sediments considered. Once this key background on flow types and substrate properties is discussed, each of the sole structures is considered in turn, starting with flutes, then grooves and chevrons, and finally discontinuous tool marks. Lastly, we propose a new process-based model of flutes and tool marks, and examine the implications of this model for the Bouma sequence, hybrid event bed models, and for a number of other long-held paradigms within the field.

THE FLUID DYNAMICS OF MUD-POOR TO MUD-RICH FLOWS

Recent years have witnessed a step-change in our understanding of flows that are transitional in their behaviour between turbulent and laminar states, due to the addition of mud in suspension (Wang & Plate, 1996; Baas & Best, 2002, 2008, 2009; Baas *et al*., 2009, 2011, 2016a,b). As an increasing quantity of clay is added to a flow, the particles begin to form flocs and longer chains because of electrostatic bonding, and eventually gel, which may significantly influence the rheology of the flow. The nature of such modification can be viewed as a competition between the factors that favour particle aggregation and gelling, notably clay concentration, clay type and water chemistry, and the forces of shear (as both mean shear and turbulence) that can break the bonds between clays. Thus, formation of such transitional flows is highly variable in both time and space as flows accelerate, decelerate, entrain and deposit sediment, and encounter changing water chemistries.

Despite this complexity, experimental studies (Baas & Best, 2002; Baas *et al*., 2009, 2016a,b) have shown that, as clays are added to a flow through direct substrate entrainment or abrasion of muddy clasts, a series of predictable and consistent changes occur that modify the mean velocity profile and turbulence structure of the flow (Fig. 1). In a clearwater flow moving over a flat and smooth surface, the flow develops a canonical turbulent boundary layer, with a logarithmic profile of horizontal velocity, and turbulence generation occurring in the zone of shear adjacent to the bed (Fig. 1A). A small zone of flow near the bed, the viscous sublayer, is dominated by viscosity and is often less than ~1 mm in thickness for clearwater flows (Raudkivi, 1997; Bridge, 2003), with its thickness lessening at higher shear velocities. As clay is added to a flow, the first stage of turbulence modulation is characterised by an enhancement of turbulence near the bed when compared to the clearwater case, which appears linked to a thickening of the viscous sublayer (Wang & Plate, 1996; Baas *et al*., 2009). Such sublayer thickening has also been shown in studies of drag reduction in the presence of fine-grained sediment (Gust, 1976; Gust & Walger, 1976; Best & Leeder, 1993; Li & Gust, 2000) as well as in studies of polymer flows where such sublayer growth has been well documented (Ptasinski *et al*., 2001, 2003). A significant feature of this expanding viscous sublayer is that a zone of shear is established on its upper surface along which large-scale vortices, in the form of Kelvin-Helmholtz instabilities, are shed (Baas & Best, 2002; Baas *et al*., 2009). This thus provides an additional source of turbulence compared to clearwater flows, and this regime has been termed a turbulence-enhanced transitional flow (TETF; Fig. 1B; Baas *et al*., 2009, 2016a). As more mud is added to the flow, near the bed the enhanced viscous sublayer and region of enhanced turbulence continue to grow, but in the outer flow, where fluid shear is less, the clays begin to form chains that eventually establish a region of undeforming flow, or plug flow, at the top of the flow. This lower transitional plug flow (LTPF; Fig. 1C) is characterized by turbulence enhancement near the bed but turbulence attenuation near the flow surface. At still greater mud concentrations, turbulence near the bed is unable to break the increasingly numerous and strong clay chains and hence turbulence near the bed begins to lessen, leading to a significant increase in the thickness of the viscous sublayer (Baas *et al*., 2009) (Fig. 1D). At the same time, the region of undeforming plug flow extends down from the flow surface towards the bed. This regime, where turbulence attenuation occurs both near the bed and within the outer flow, has been termed an upper transitional plug flow (UTPF; Fig. 1D). Lastly, as increasing clay concentration fosters longer chains, or perhaps gelling, the flow eventually adopts a profile where horizontal velocity is invariant throughout the flow depth, except for a thin zone of shear near the bed on which the flow rides. This quasi-laminar plug flow (QLPF; Fig. 1E) possesses minimal turbulence throughout the flow depth and a thin near-basal shear zone with minor residual turbulence, overlying a thickened viscous sublayer (Baas *et al*., 2009). If the shear strength of the

QLPF flow is great enough, it may be able to transport particles within the body of the plug flow with minimal displacement or rotation.

The transitional flow experiments described here obtained maximum volumetric clay concentrations of 16.6% and 19.2% kaolinite (Baas *et al*., 2009, 2011, respectively), and 8.6% bentonite (Baas *et al*., 2016b) and thus the details of how flow structure develops at higher concentration remain unknown. The presence and importance of transitional flows in subaqueous density currents, and the presence of plug flow regions, has also been demonstrated recently in the laboratory experiments of Hermidas *et al.* (2018), who additionally noted the presence and importance of the free shear layer at the top of the current. Their experiments were run at slopes of 6-9.5°, with measurement durations of ~1 minute (40-100 s after the start of the experiments), and had maximum volumetric clay concentrations of 7% kaolinite (the clay formed 33% of the total sediment concentration, the rest consisting of sand, with or without silt). Estimates of the basal boundary layer, using viscosity values for the original mixtures measured *ex situ* by rheometer, predict laminar basal conditions for some flows (a plug flow, PF, in the classification of Hermidas *et al.*, 2018). However, turbulence data demonstrate that there was considerable residual turbulence in the basal boundary layer (Hermidas *et al*., 2018, their figure 7), and that this turbulence is much higher than in the plug flow itself, thus consistent with the transitional plug flows of Baas *et al*. (2009), although insufficient turbulence data are provided to ascribe the flows of Hermidas *et al*. (2018) to a specific transitional flow category of Baas *et al*. (2009). Consequently, it is unclear from the work of Baas *et al*. (2009, 2011, 2016b) and Hermidas *et al*. (2018) whether flows with higher clay concentrations transform from a QLPF to a fully laminar plug flow (herein termed LPF) where there is no residual turbulence at the base of the flow, or whether flows retain a thickened viscous sublayer and an overlying plug, with an intervening shear layer.

This sequence of transitional flow regimes can be expected in a wide range of flows, but the precise conditions at which each flow stage is reached is a function of three principal factors: i) the applied mean fluid shear that will act to break up the clay chains, such that greater clay concentrations are required to produce a given transitional flow regime at higher shear velocities (Baas & Best, 2002; Baas *et al*., 2009, 2016a); ii) the type of clay, or clays, present, such that clays that attain a higher viscosity and yield strength at lower volumetric concentrations (such as bentonite) will require a lower clay concentration to produce a given transitional flow regime at the same shear velocity (Baas *et al*., 2016b); and iii) the degree of turbulence generated from other sources, such as grain and form roughness. For instance, flow over a gravel surface will generate additional turbulence that will tend to break up any growing clay chains. As such, flows over a rough bed surface will require a higher clay concentration to generate a given transitional flow regime at the same shear velocity (Baas & Best, 2009). Form roughness, such as bedforms, or the topography on the top of debrites (*e.g*., Fonnesu *et al*., 2015), can also be expected to have the same effect. However, although the precise boundaries and phase space between these transitional flow regimes vary with applied fluid shear, additional sources of turbulence, and clay type (and also water chemistry), these various transitional flows will eventually be generated. This has been demonstrated by experiments examining transitional flows moving over a fixed ripple bedform (Fig. 1F-J; Baas & Best, 2008) that show that TETFs produce enhanced turbulence, when compared to a turbulent flow, associated with the shear layer formed around the leeside separation zone. However, as more clay is added to the flow, turbulence becomes dampened both near the bed and in the outer flow, producing LTPF, and then UTPF (Fig. 1G-I). Baas & Best (2008) distinguished two phases of flow within the UTPF regime for flow over fixed ripples, which they termed turbulence-attenuated transitional flow (TATF) (Fig. 1H-I). In the first of these phases, turbulence is attenuated within the separation zone, but the length of the separation zone is similar to that under TF and TETF regimes. As clay content increases, a subsequent phase is reached where the length of the separation zone shortens, alongside a further attenuation of turbulence (Fig. 1I). Eventually, with the addition of more clay, a QLPF forms where flow in the leeside is stagnant with little or no turbulence in the bedform lee (Fig. 1J). The corollary of these changing transitional flow regimes for decelerating flows of mud and sand was investigated by Baas *et al.* (2011), who demonstrated that ripples increased in height and wavelength under both TETF and LTPF (Fig. 2). These flows possessed enhanced turbulence near the bed that was reasoned to augment turbulence generated from the leeside flow separation zone. The enhanced near-bed turbulence increased erosion at flow reattachment and provided a greater sediment flux downstream, thereby increasing ripple height and wavelength (Baas *et al*., 2011; Fig. 2). However, in these experiments, at clay concentrations in either the upper part of the LTPF regime or the lower part of the UTPF regime, turbulence at the bed decreased — in part as a result of the rapidly thickening viscous sublayer — and led to a decrease in ripple height and wavelength (Fig. 2). As clay concentrations increased further in the LTPF and UTPF regimes, turbulence and bed sediment flux declined, leading to smaller bedforms and eventually a flat sediment bed.

Although the experiments of Baas *et al.* (2011) concerned aggradational bedforms, in the context of sole structure development they provide important insights into the patterns of turbulence and bed shear stress that may be expected over erosive bedforms generated in a mud bed. For instance, if a negative defect is formed in a mud bed, it can be speculated that bed erosion generated by flow separation over this defect is first enhanced within a TETF and lower LTPF, before decreasing and eventually ceasing under upper LTPF, and UTPF regimes. The significance of these speculations is revisited later.

Talling *et al*. (2012) and Talling (2013) examined the properties of subaqueous debris flows, concentrating solely on the plug flow component, and presented an analysis of the potential influence of yield strength (strictly ‘matrix strength’ *sensu* Middleton & Hampton, 1973, and Lowe, 1979) as a function of clay concentration (Fig. 3). On the basis of yield strength, flows were then subdivided into low (0.1-10 Pa, corresponding to 10-20% kaolin by volume), intermediate (10-100

Pa, 20-30% kaolin), and high-strength (100-1000 Pa, 30-40% kaolin) debris flows (Talling *et al*., 2012; Talling, 2013). This analysis highlights the likely maximum clast size that can be transported by a flow (for the case of a kaolinite-dominated debris flow), illustrating how this size decreases with decreasing suspended clay concentration (and hence yield strength), and increasing clast density (Fig. 3). These relationships are critical in both determining the shear stress exerted on a cohesive bed by an overriding flow, and in determining how clasts can be transported within the body of the flow to act as tools that generate erosive structures in the underlying substrate. Because such models of subaqueous debris flows concentrate solely on the plug flow component, they are not directly comparable to previous transitional flow experiments (Baas *et al*., 2009, 2011, 2016b). However, given the typical clay concentrations, the intermediate- and high- strength debris flows, which are of interest in the subsequent discussion, likely compare to the quasi-laminar plug flows (QLPF) and potentially the fully laminar plug flows (LPF) described previously. This comparison is supported by the subaqueous sediment gravity flow experiments of Baker *et al*. (2017), who demonstrated a change in flow type at similar kaolinite concentrations to those of Talling *et al*. (2012). The experiments of Baker *et al*. (2017) produced transitional flows with a dense, cohesive, lower layer (probably a QLPF / intermediate-strength debris flow; the experiments lacked turbulence data to confirm the former), at kaolinite concentrations of 22-25% by volume. Fully cohesive flows (likely an LPF / high-strength debris flow) were produced at volumetric concentrations of 27%. The experiments of Baker *et al*. (2017) also classify the low strength ‘debris flows’ of Talling *et al.* (2012) and Talling (2013) as high-concentration turbidity currents; in shallow water settings flows with such yield strengths are often referred to as fluid muds (Winterwerp & van Kesteren, 2004).

SEAFLOOR SUBSTRATES

Substrate controls on erosion

In addition to understanding flow dynamics, it is important to consider the role of the seafloor substrate in the formation of flutes and tool marks. The nature of the seafloor substrate not only governs the threshold at which an overriding flow will erode the bed, but is also an important control on the location, extent, depth, and morphology of the erosional features that form once this threshold is exceeded. Grain size is the primary control on the erosion threshold for non-cohesive sediment (i.e. coarse silt, sand, and gravel), and hence the prediction of erosion in granular media is generally straightforward (Soulsby & Whitehouse, 1997). Some notable exceptions exist, such as where biological factors inhibit sediment transport (*e.g.*, Parsons *et al*., 2016) or where the substrate is composed of calcareous or biogenic grains. In the latter case, density corrections are required to the classic Shields approach (*e.g.*, Oehmig, 1993; Miller & Komar, 1977). However, most of the world's oceans are floored with cohesive muddy substrates (Dutkiewicz *et al*., 2015), with the cohesive component composed of clay and non-sortable silt (≤10 µm; McCave *et al*., 1995), and this is the substrate in which scour and tool marks are most commonly found (Allen, 1984). So what effect does a cohesive substrate have on erosion at the base of a flow?

Identifying a single or dominant control on erodibility in cohesive sediment has proven elusive, with many studies yielding apparently contradictory results (McCave, 1984; Grabowski *et al*., 2011; Winterwerp *et al*., 2012). Factors that have been demonstrated to control how, where, and when erosion occurs include: i) *physical properties*, such as grain size (Roberts *et al*., 1998; Thomsen & Gust, 2000; Dickhudt *et al*., 2011), plasticity index (Smerdon & Beasley, 1959), particle size distribution (Panagiotopoulos *et al*., 1997; Houwing, 1999), shear strength (Kamphius & Hall, 1983; Dade *et al*., 1992; Winterwerp *et al*., 2012), bulk density, and water content (Amos *et al*., 1998, 2004; Winterwerp & van Kesteren, 2004; Bale *et al*., 2007); ii) *geochemical properties*, including organic content (Righetti & Lucarelli, 2007), clay mineralogy, and relative cation concentration (Mehta *et al*., 1989; Grabowski *et al*., 2011); and, iii) *biological modification* caused by bioturbation (Sgro *et al*., 2005; Fernandes *et al*., 2006; Widdows *et al*., 2009), feeding and egestion by organisms (Andersen *et al*., 2005), and the secretion of stabilising mucus-like substances such as extra-cellular polymeric substances (EPS) (Sutherland *et al*., 1998; Friend *et al*., 2003; Lundkvist *et al*., 2007;

Malarkey *et al*., 2015; Parsons *et al*., 2016). Of these factors, bulk density appears to exert the dominant control on the spatial extent and depth of erosion in cohesive sediments (Amos *et al*., 2004; Winterwerp *et al*., 2012), but erodibility is clearly a function of interactions between multiple competing and contributing processes (Grabowski *et al*., 2011). We therefore now specifically consider the syn- and post-depositional processes involved in the accumulation of primarily deep-water cohesive sediment that is most commonly found beneath flutes and tool marks.

The specific case of deep-water cohesive sediments

As cohesive sediment accumulates at the seafloor, it starts to consolidate under self-weight burial, which leads to a linear increase in bulk density and undrained shear strength with depth, known as normal consolidation (Skempton, 1954). The effect of this consolidation may serve to depth-limit erosion (Parchure & Mehta, 1985; Winterwerp & van Kesteren, 2004), although studies of modern deep-water sediments have revealed several deviations from a simple normally-consolidated profile that are detailed below.

Fluid-like benthic boundary layer

The first exception to the trend of strength linearly increasing with depth is found at the seawater-seafloor interface, which is typically composed of unconsolidated aggregates (Boudreau & Jorgensen, 2001) and in some cases may be treated more as a fluid than a sediment (Winterwerp & van Kesteren, 2004), because of high water content (>>50% of the mass is water, thus water content is >>100% relative to the dry mass), very low undrained shear strengths (<<1 kPa), and intense bioturbation (Baudet & Ho, 2004; Colliat *et al*., 2011; Hill *et al*., 2011; Kuo & Bolton, 2013). Whereas this interfacial 'benthic boundary' layer is often lost or disturbed by piston coring or *in-situ* geotechnical testing, shallow box coring of modern deep-water seafloor sediments commonly reveals a thin, centimetres-thick, layer of highly mixed fluid-like mud overlying a more competent mud that has begun to consolidate (Figs 4C, 5). This seafloor layer of low shear strength can be easily eroded under even relatively low bed shear stresses (e.g., Fig. 6A points a and b, which transition very rapidly into mass erosion).

Shallow strengthening

The second exception is based on *in-situ* shear strength measurements, which indicate that deep-water sediment is often much stronger within a zone a few tens of centimetres to approximately a metre below the seafloor than would be expected from normal consolidation alone, and sometimes by an order of magnitude (Fig. 4). None of the sites shown in Figure 4 have undergone any loading other than that experienced by progressive accumulation of sediment, nor is there any variation in lithology. Hence these cohesive sediments are *apparently* over-consolidated, or more correctly phrased, they have a high yield stress ratio (vertical yield stress / effective overburden pressure) (Burland, 1990). This enhanced strength is then lost at depth (>10s cm to ~1-2 m below seafloor; Fig. 4), where a normally consolidated trend is restored.

The exact reason for the zone of greater yield stress ratio is unclear, but it has been linked to biological influences related to food and chemical dependencies that may explain the depth-limitation. Possible explanations include: i) sediment strength mediation by sulphate-reducing bacteria that are abundant in the top 1-2 m of most of the world’s ocean substrates (Parkes *et al*., 2000); ii) stabilising effects of bioturbation by organisms such as polychaete worms (Colliat *et al*., 2011; Kuo & Bolton, 2013), and iii) particle-bonding effects by EPS secreted by organisms such as diatoms (Ehlers *et al*., 2005). Regardless of the cause, this enhanced strength will provide a much higher resistance to erosion than normally consolidated sediment and may strongly depth-limit and otherwise control the nature of erosion (Fig. 6). This shallow strengthening of muds may explain why some powerful sediment density flows only erode localised scours or grooves, but do not cause widespread erosion (*e.g.*, Amy & Talling, 2006; Talling *et al*., 2013a). Where some sediment density flows do succeed in ‘breaking through’ this strengthened layer, they may erode large volumes of cohesive sediment, potentially manifested as abundant intraclasts of substrate, transform to transitional flows or debris flows, and deposit hybrid event beds (*e.g.*, Haughton *et al*., 2003, 2009; Talling *et al*., 2004), whereas other slightly less powerful flows entrain little sediment and remain as lower-density turbidity currents.

Exposure of previously-buried sediment at the seafloor

Truly over-consolidated sediment can also be found at, or close to, the seafloor where erosion or uplift have exposed previously buried sediment (Burland, 1990). Experiments using clearwater flows have found that over-consolidated (remoulded shear strength, c_u, >200 kPa), cohesive (and also lithified or weakly cemented) sediment effectively inhibits the types of erosion observed in lower-strength clays (Annandale, 1995; Fig. 6). Erodibility in such materials may instead be controlled by localised weaknesses and imperfections within the sediment mass, such as discontinuities, joints, and bedding surfaces (Annandale, 1995), or where the sediment bed is homogeneous, erosion may be controlled largely by sediment abrasion (Yin *et al*., 2016).

Biological modification of the substrate

The final exception relates to the influence of benthic and microbial organisms, which are abundant in cohesive sediment within approximately the top metre below the seafloor worldwide (Parkes *et al*., 2000; Murray *et al*., 2002). The interactions of these organisms with the seafloor substrate and shallow subsurface sediment can significantly modify their geomechanical properties (Table 2). The magnitude, type, and depth-extent of such modifications are strongly controlled by physico-chemical factors that often strengthen the substrate (Murray *et al*., 2002), and thus aid the formation of flute and tool marks. For instance, internal burrow pressures of up to 40 kPa have been reported for some benthic organisms that exceed the typical shear strength of deep-water seafloor sediment (Murray *et al*., 2002; Fig. 4). The effects of such bioturbation-induced pressure lead to compaction and strengthening in cohesive sediment. Other exceptions undoubtedly exist, but the intention here is to highlight that the mechanical behaviour of modern deep-water cohesive sediments can be spatially and temporally complicated, and can exert a strong control on when, where, and how erosion occurs.

Seafloor substrates over geological time

A key question is whether the modern seafloor is a good analogue for sediment over geological time, and thus whether these variations with depth are typical. The level and type of bioturbation in deep-sea substrates experienced a major change during the Great Ordovician Biodiversification event (Orr, 2001; Màngano *et al*., 2016; Buatois & Mángano, 2018). Since the Ordovician, the diversity of deep-sea trace fossils has fluctuated — often related to large-scale changes in ocean circulation and oxygenation, such as basin-scale anoxic events — and some ichnotaxa, such as *Zoophycos* and *Ophiomorpha*, have changed their environmental range (*e.g*., Cummings & Hodgson, 2011a; Uchman & Wetzel, 2011). However, such changes appear unlikely to have dramatically altered the influence of these fauna on sediment properties. The successful application of ichnofacies and ichnofabric models that integrate modern and ancient traces to diagnose deep-sea environments (Heard & Pickering, 2008; Cummings & Hodgson, 2011b; Callow *et al.*, 2014; Heard *et al*., 2014; Knaust *et al*., 2014; Buatois & Mángano, 2018; Rodríguez-Tovar & Hernández-Molina, 2018) further suggests that bioturbation has not changed fundamentally, else this approach would not work.

Interestingly, work in shallow marine successions has argued that the mixed layer due to bioturbation, presently approximately the upper 10 cm, may have increased in thickness slowly through the Cambrian, only reaching modern conditions in the late Silurian (Tarhan *et al.,* 2015; Tarhan, 2018a). In marked contrast, a progressive decrease in near-bed substrate strength over the whole Phanerozoic has recently been inferred based on a decline in the number of studies reporting flutes and tool marks as a function of geological time period (Tarhan, 2018b). Tarhan (2018b), however, does not consider potential observational bias, and the process arguments supporting a link to substrates do not consider many of the processes discussed above.

Considering the evolution of trace fossils, and allowing for the postulated changes in mixed layer depth in shallow marine conditions, we conclude that modern deep-sea seafloors are likely a good analogue for deep-sea substrates since at least the late Silurian, albeit there is a need for further research.

FLUTES

Flute casts or flutes (after Crowell, 1955) are erosive features that widen downstream from a point, the 'nose', abruptly deepening downstream before gradually decreasing in depth towards their downstream end (Figs 7 and 8). They are formed by the erosion of a cohesive substrate that is subsequently infilled by sand, or in some cases gravel (Winn & Dott, 1977; Jobe *et al*., 2010), and thus are observed as sole marks on the base of beds. Flutes generally range in length from several centimetres to *c*. 0.50 m (Allen, 1971a), with widths of 0.01 – 0.20 m and depths of a few centimetres to 0.1 m (Collinson *et al*., 2006). However, flutes that are metres long, up to 1 m wide, and 1.5 m deep are known (Winn & Dott, 1977, 1979; Jobe *et al*., 2010). Even larger 'flutes', metres to 100s metres long, have been observed on the upper surface of beds where they are typically referred to as megaflutes (*e.g*., Elliott, 2000; Macdonald *et al*., 2011a,b; Hofstra *et al*., 2015), but here we restrict our analysis to sole marks. Allen (1971a) introduced a summary figure for flute morphology (Fig. 7A), later referred to as the 'ideal flute' (Allen, 1984), which in addition to the basic features described above, also exhibits lateral furrows and a median ridge (Fig. 8B). However, flutes can also consist of simple smooth forms that lack a median ridge and lateral furrows (Fig. 8B). Flutes exhibit a great variation in planform shape, from parabolic-transitional examples (Figs 7B and 8A) to long, thin spindles (Figs 7B and 8C), and asymmetric, and comet-shaped, forms (see Fig. 7B). Parabolic-transitional flutes are relatively rare, with parabolic flutes far more common (Figs 7B and

8B), the latter form representing the 'ideal flutes'. Parabolic forms range in size from a few centimetres to >0.50 m long, and have length to width ratios between 1 and 4 (Allen, 1971a). In contrast, spindle-shaped flutes are fairly common, 0.05-0.15 m long, typically lack median ridges and lateral structures, and are much longer than they are wide (Allen, 1971a, 1984). Comet-shaped flute marks are rare and tend to be smaller still, typically a few centimetres in length and rarely more than 0.1 m long, and they have sinuous edges in the downstream direction (Allen, 1971a, 1984). Polygonal flutes in mud beds were described by Allen (1971a; reproduced in Collinson *et al*., 2006 and Collinson & Mountney, 2019); however, our re-analysis of those examples listed therein fails to identify clear examples, perhaps reflected in the absence of this form in later summaries (Allen, 1984). We thus conclude that polygonal forms do not occur in muds, although such forms are well known from cave scallops where dissolution processes dominate (Allen, 1971a; Richardson & Carling, 2005). Flutes can be found covering entire bedding planes (conjugate), in clusters, or as individual marks (isolate), and typically many different types of flute can exist on the same bed (Allen, 1971a, 1984; Pett & Walker, 1971).

Longitudinal distribution of flutes

A number of observations have been made concerning the variation in flute occurrence and morphology with downstream distance, and as a function of variables such as bed thickness and Bouma division, that in turn vary downstream. Flutes at the base of T_A beds were observed to be wide and 'bulbous' (defined as very broad at the upstream end, *sensu* Dżułyński & Walton (1965), and used in this sense throughout the present paper; note that Allen (1984) defined 'bulbous' flutes differently, as having narrow deep heads), whilst those below T_B and T_C beds were narrow with pointed noses (Pett & Walker, 1971). Larger flutes have been observed on the base of thicker beds (Sestini & Curcio, 1965; Middleton, 1970; Tanaka, 1970, Allen, 1984), with Pett & Walker (1971) showing a clear relationship between flute width and bed thickness, but not between flute depth and bed thickness, suggesting that there may be a substrate control on flute depth. Such measurements assume that no later loading of flutes has occurred (e.g., Kelling & Walton, 1957). These field observations suggest that flutes become narrower, smaller, and have more pointed noses, with downstream distance. Furthermore, these relationships have been used to imply that larger flutes associated with thicker, more proximal sands, were formed by faster, thicker and longer-lived currents, and correspondingly, that smaller more distal flutes on thinner beds were formed by slower, thinner, shorter-lived currents (Allen, 1984). In addition to these field observations, Allen (1971a) modelled the distribution of flute marks with downstream distance, based on defect theory, and predicted that flutes would become smaller downstream and that they would change from whole bed surfaces covered in flutes (conjugate) to isolated flutes.

Experiments

The earliest experiments that were conceived to understand the development of flutes are those of Fuchs (1895; see Wetzel (2006) for an English translation of some key parts) who used sand and plaster-of-Paris to succeed in reproducing a range of 'bulges' on the bases of beds. Mutti *et al*. (2009) argued that Fuchs (1895) successfully reproduced small flutes experimentally, although none of his 'bulges' show much similarity with the planform and cross-sectional form of flutes (Dżułyński & Walton, 1963). Later work by Rücklin (1938) is more widely credited as forming the first flutes (Dżułyński & Walton, 1963; Allen, 1984), albeit the similarities are limited (Allen, 1971a) and these experiments were not in mud beds; the bed composition was 5.8% clay <10 μm and 94.2% coarse grains consisting of quartz (20-80 μm) and mica (50-200 μm). Subsequent work examined flute formation in weak mud beds with flows composed of plaster-of-Paris (Dżułyński & Walton, 1963; Dżułyński, 1965), but it is not clear if these features resulted directly from erosion, or from deformation and loading (Allen, 1971a). In contrast, the work of Allen (1968, 1969, 1971a) on flows over weak and higher-strength mud beds did demonstrate the formation of flutes, with conjugate forms in weak beds, and individual flutes in higher-strength modelling clay. The key breakthroughs in understanding flute formation have been derived principally from the seminal work of Allen (1971a, 1973, 1975) who employed clearwater flows to dissolve beds composed of plaster-of-Paris. Whilst the processes are different, *i.e.*, dissolution versus abrasion-driven erosion in muds, the experiments produced analogous forms, and enabled the formative processes to be studied in detail. However, the focus on studies using plaster-of-Paris has meant that the understanding of substrate controls on flute initiation and development remains limited.

The nature of formative flows for flutes

Allen (1968, 1971a) demonstrated that flutes are associated with turbulent flows that produce flow separation. The nature of flow separation changes as a function of flute morphology, from prominent horizontal rollers (with rotation in the downstream direction) within parabolic flutes (Figs 7 and 9), to a pair of rotating vortices (with rotation transverse to the main flow) within narrow flutes (Fig. 9) (Allen, 1971a). The initiation of flutes has been associated with the presence of defects in the bed, which can be produced by hollows formed by bioturbation, steps in bed height, or inhomogeneities within the substrate (Allen, 1984). Alternatively, flows over some very weak mud substrates can form their own defects that can then develop into flutes (Allen, 1969). Knowledge of flute development on stronger planar beds is largely lacking, since Allen's (1971a) experiments with modelling clay all used initial defects. Yin *et al*. (2016) also used modelling clay but with planar beds, but found that, whereas defects developed and grew with time, the resulting erosional structures were more analogous to bedrock erosion features in rivers (Richardson & Carling, 2005), rather than flutes in muds. However, the results of Yin *et al*. (2016) suggest that defects in planar mud beds can form purely from abrasion by a sediment-laden flow. These previous experiments on clay beds, although limited in number and in terms of substrate measurements (with the exception of Yin *et al*., 2016), also suggest that there is likely a strong substrate control on flute formation. Weak beds (*e.g.*, Fig. 5) may be unable to maintain the relatively steep slopes associated with flutes, notably at the nose, whilst beds that are too strong enable undercutting of the margins and the production of structures more analogous of bedrock rivers (Yin *et al*., 2016).

For a given substrate, the evolution of bed defects is dependent on initial defect size and the properties of the flow, with Allen (1971a) referring to these as 'unstable' forms leading to the development of parabolic flutes (Type I), and 'stable' forms producing spindle-shaped flutes (Type II) (Fig. 9). Allen (1971a) related this developmental divergence to the nature of separated flow within flutes, and in particular to the transition of the viscous sublayer upstream of the flute, to a turbulent flow, via the sublayer rolling up into a series of vortices. Based on theory derived from experiments on unstable laminar shear layers (Sato, 1956, 1959), and experimental data on flutes (Allen, 1971a), a criterion for the critical defect length, X_{crit}, was introduced, based on the downstream distance for transition to a turbulent flow (Allen, 1971a, 1984):

$$X_{crit} = 5.90d\,(1.25dU/v)^{-7/8} \quad (1)$$

where d is flow depth, U is mean downstream velocity, and v is kinematic viscosity. Consequently, when the downstream length of the initial bed defect, X, is greater than the critical defect length, X_{crit}, turbulent flow can directly act on the bed defect, and flutes will exhibit 'unstable' behaviour (Type I, Fig. 9), whereas if $X < X_{crit}$ then flutes are 'stable' (Type II, Fig. 9).

Allen (1971a) argued that, as flows travel downstream, flow velocity declines because of progressive sedimentation. He also assumed that the flow depth would either decrease downstream (Allen, 1984), or that flow depth was unlikely to increase downstream (Allen, 1971a). However, whereas this may not necessarily be true, the product of velocity and depth will decline, unless the flow is undergoing autosuspension (Pantin, 1979; Parker *et al*., 1986). Analysis of Equation 1, using the criterion that the product of velocity and depth decreases downstream, therefore predicts that the critical defect length, X_{crit}, increases with distance downstream. Assuming that there is no downstream variation in initial defect size, or substrate properties, this in turn predicts that parabolic forms are more prevalent upstream, and that spindle-shaped flutes are more likely downstream, as seen in field observations where larger bulbous flutes are observed below T_A beds, and smaller, narrower, and more pointed flutes are observed below Bouma T_B and T_C beds (Pett & Walker, 1971).

Downstream distribution of flutes: a paradox

The prediction that, as flows decelerate, flutes decrease in size whilst changing morphologically until flows are no longer able to erode the substrate, suggests that there should be a lack of erosive bedforms downstream of flutes. Paradoxically however, erosive bedforms in the form of tool marks are generally plentiful in more distal locations (*e.g.*, Walker, 1967; Lovell, 1969; Slacza & Unrug, 1976), whereas flutes are typically preferentially associated with more proximal locations (see 'Distribution and association of scour marks and tool marks'). Given that flows have decelerated to a point where they cannot erode the bed, then it is paradoxical that they are able to support grains large enough (order mm-cm diameter) to form the range of tool marks typically observed in these distal environments (see Tool marks section). The pioneering work of Allen (1971a, 1973, 1975, 1984) involved consideration of clearwater flows, and analogies with cohesionless turbidity currents. Here, we assess what the effects of cohesive transitional flows would be on flute dynamics and morphology, and whether these flows offer an answer to the apparently paradoxical distribution of flutes and tool marks.

Transitional flows and flute dynamics

As clay is added to an initial cohesionless turbulent flow, the flow is modified forming a turbulence-enhanced transitional flow (TETF; see 'The fluid dynamics of mud-poor to mud-rich flows' above), which occurred at kaolin clay concentrations as low as 0.046% in the experiments of Baas & Best (2008). As demonstrated in work on ripples, TETF is associated with enhancement of turbulence within the separation zone as a result of growth of the internal shear layer (Fig. 1; Baas & Best, 2008). The influence of this enhanced turbulence is most notable at the flow re-attachment point. If such TETFs erode into a cohesive bed, this may lead to enhanced erosion and increased maximum depth of flutes, as compared to turbulent flows, potentially producing wider and more bulbous flutes. With increasing clay content, turbulence-attenuated transitional flows (TATF) develop (Fig. 1; Baas & Best, 2008), marked by an initial decline in turbulence in the shear layer of the separation zone generated behind the leading edge of the flute, relative to turbulent flows. However, Baas & Best (2008) noted no corresponding decline in the length of the separation zone. Such turbulence attenuation likely leads to shallower flutes. Further increases in clay content within the TATF region (Fig. 1) will lead to additional declines in turbulence in the shear layer, and a progressive decrease in the length of the flow separation zone, likely leading to smaller, thinner flutes. At some point, the cohesive strength of the flow will destroy the flow separation zone entirely (Baas & Best, 2008), with the likely demise of further flute development at this point. Transitional flows over mobile beds showed a rapid decline in bedform height and wavelength, at some point between the upper part of the lower transitional plug flow regime and the lower part of the upper transitional plug flow regime. These morphological changes occur in response to decreasing turbulence in the flow separation zone, and potentially also because of the rapid increase in the thickness of the viscous sublayer (Fig. 2). By analogy, flutes may also cease to actively form around the transition between LTPF and UTPF conditions. This re-analysis of flutes demonstrates that flutes will continue to form, and indeed may be enhanced, under transitional flows. Thus the key conclusion of Allen (1968, 1971a) that flutes are the product of turbulent flows does not strictly hold, as they can also be formed under transitional flows, provided bed shear stress exceeds the critical erosion threshold.

If the criterion of Allen (1971a) for separating the development of initial bed defects (Eq. 1) is re-examined for transitional flows, we observe that transitional flows should have an effect through increases in the dynamic viscosity, which can increase by an order of magnitude, or more, in transitional flows (Baas *et al*., 2009). Changes in clay content may therefore produce the same downstream effects as changes in velocity. As flows become more transitional, and dynamic viscosity increases, the critical defect size, X_{crit}, should increase and thus flutes are more likely to become 'stable' and change from parabolic flutes to spindle-shaped flutes.

Examination of flow separation dynamics, and of the stability criterion for flute types, demonstrates that transitional flows likely influence flute evolution and morphology. Increases in turbulence in TETFs and LTPFs are postulated to lead to the development of wide, bulbous flutes. Further increases in suspended sediment concentration in the upper part of LTPFs or the lower part of UTPFs likely lead to progressive turbulence dampening and thus decreased flute sizes, more stable spindle-shaped flutes, and ultimately a loss of flute production or growth entirely.

In terms of understanding the downstream distribution of sole marks, the key question is how flows transform with downstream distance. Many turbidity currents have been postulated to gradually transform downstream from non-cohesive to cohesive through the erosion and ingestion of mud from the seafloor, and through the increasing importance of clay cohesion relative to turbulence generation (Haughton *et al*., 2003, 2009; Talling *et al*., 2004). In such cases, the increasing cohesion of the flow would work in tandem with the decreasing product of flow velocity and depth to encourage a transition to smaller spindle-shaped flutes, and ultimately to a lack of flute development. This offers a potential solution to the paradox of how erosive tool marks can be found downstream of flutes, but only if these tool marks are associated with more cohesive currents such as transitional flows or debris flows. The origin and development of tool marks are thus examined next.

TOOL MARKS

As noted earlier, tool marks can be subdivided into continuous and discontinuous forms; the former consist of grooves and chevron marks, and the latter of prod, bounce, skip, and roll marks. These structures are considered in turn, starting with the continuous forms. However, first the source of the tools is reviewed.

The nature of tools

The nature of the tools forming tool marks has been unclear in most past studies, because the tool is found rarely at the end of marks such as grooves. Examples include mudstone clasts, pieces of wood, pebbles, bones and shells (Dżułyński & Radomski, 1955; Dżułyński & Ślączka, 1958; McBride, 1962; Dżułyński & Walton, 1965; Glaessner, 1958; Enos, 1969a; Dżułyński, 1996). A number of authors have concluded that mudstone clasts are the most likely tools (Dżułyński & Radomski, 1955; Wood & Smith, 1958; Dżułyński & Walton, 1965; Middleton & Hampton, 1973, 1976), although Kuenen (1957) argued that mudstone clasts were improbable as tools since they would undergo rapid rounding through abrasion and therefore would not produce grooves with internal striations. Kuenen (1957) instead suggested that stones or shells pulled by "a sail of seaweed" would enable clasts to be dragged along rather than rolling along (see also Dżułyński & Ślączka, 1958). The potential for abrasion of mudstone clasts is examined later, after the nature of individual tool marks has been described, and potential formative mechanisms considered.

An alternative approach to identifying the nature of the formative tools is to consider the availability of tools in deep-water clastic environments. Extrabasinal pebbles are typically restricted to high-gradient, tectonically active systems (Hsu, 1959; Winn & Dott, 1977; Leszczyński, 1989; Jobe *et al*., 2010). Plant fragments, many of which are too small or fragile to act as tools, are thought to be preferentially associated with hyperpycnal currents (Zavala *et al*., 2012; Deville *et al*., 2015; Zavala & Arcuri, 2016) or the collapse of shelf-edge deltas (Hodgson, 2009), and may be concentrated towards the lower energy parts of the flow, *i.e.* the top and back of the flow (Haughton *et al*., 2003; Kneller & McCaffrey, 2003; Hodgson, 2009). Consequently, plant fragments are less likely to be in direct contact with the bed. Furthermore, tool marks are widely reported from Palaeozoic deep-water strata prior to the advent of plants that were greater than a few centimetres in size, and before the development of significant internal structure, in the Devonian (Kenrick *et al*., 2012), and therefore before plant fragments as likely tool makers (*e.g*., Craig & Walton, 1962; Enos, 1969a; Parkash & Middleton, 1970; Clayton, 1994; Haines *et al*., 2001).

Additional sources of tools, such as bones and shells, appear to be unusual and relatively rare. In contrast, mudstone clasts are ubiquitous in deep-water clastic systems across a wide range of environments, including broad sediment bypass zones such as channel-lobe transitions, channel lag deposits, and in the deposits of debris flows and hybrid events (Mutti & Nilsen, 1981; Johansson & Stow, 1995; Haughton *et al*., 2003, 2009; Posamentier & Kolla, 2003; Stevenson *et al.*, 2015; Brooks *et al*., 2018a). These mudstone clast-rich deposits extend from proximal areas on the slope, through submarine channels, all the way to the fringes of basin-floor lobes (Posamentier & Kolla, 2003; Talling *et al*., 2004; Luthi *et al*., 2006; Hodgson, 2009; Talling, 2013; Stevenson *et al.*, 2015). Many of these mudstone clasts are intra-basinal as a result of the erosion of seafloor muds, but mudstone clasts incorporated into debris flows can be very far-travelled (Talling, 2013; Stevenson *et al*., 2015). As highlighted earlier, the generation of such intraclasts may be favoured by the presence and erosive break-up of a near-surface over-consolidated layer.

Groove casts

Groove casts, also referred to as groove marks or grooves, were first named by Shrock (1948), and subdivided into drag marks and slide marks by Kuenen & Sanders (1956) and Kuenen (1957), referring to those features observed below greywackes (*i.e*., muddy sands) and those formed from slumping, respectively. However, later research found that it is difficult to differentiate these two types (Dżułyński & Ślączka, 1958; Bouma, 1962). The term ‘drag mark’ has since been used more generally to refer to grooves in deep-water systems and other environments, as well as glacial striae, features formed by drifting grounded ice, and boulders on playa floors (Allen, 1984).

Groove casts are recognised as one of the most common sole marks in deep-water sediments (Dżułyński & Walton, 1965), and are the most common tool mark (Middleton & Hampton, 1973, 1976), with Enos (1969a) estimating that 69% of sole marks in coarse-grained, mud-rich, sandstones of the Ordovician Cloridorme Formation are grooves. Grooves appear as elongate ridges on the base of sandstone beds (Fig. 10), infilling erosion surfaces in cohesive sediment, typically mud, although Dakin *et al*. (2013) reported grooves in partially lithified sandstones. Most grooves extend for the full length of a given outcrop (Enos, 1969a) and can be up to 35 m in length (Draganits *et al*., 2008), are remarkably straight, typically exhibit constant depth and width, and may have smooth rounded internal surfaces, or internal parallel longitudinal striae (Figs. 10, 11; Dżułyński & Walton, 1965; Allen, 1984). Exceptionally, groove casts can exhibit spiralling of the internal striae (Dżułyński & Ślączka, 1958; Dżułyński & Sanders, 1962a). Margins of grooves are typically sharp, although raised lateral ridges are associated with some grooves (Dżułyński & Walton, 1965; Fig. 12). Grooves vary from <1 mm to up to 4 m wide and can be up to 0.2 m deep (Dżułyński & Walton, 1965; Draganits *et al*., 2008). Whilst groove widths cover a wide range, the width of typical grooves is poorly constrained. Dirnerová & Janočko (2014) reported widths of 5-50 mm for a series of units, and 5-100 mm appears typical of many examples (Dżułyński & Walton, 1965; Enos, 1969a; Ricci Lucchi, 1995; Collinson *et al*., 2006). The number and spacing of internal striae are not reported, although examples show 1-10s of internal striae, with sub-millimetric to centimetric spacing (Fig. 10E; Dżułyński & Sanders, 1962a; Potter & Pettijohn, 1963; Pettijohn & Potter, 1964; Dżułyński & Walton, 1965; Lanteaume *et al*., 1967; Ricci Lucchi, 1995), up to decimetres for very large grooves (Draganits *et al*., 2008). Large numbers of grooves can cover entire surfaces (Figs. 10, 11), where they may show a range of sizes, or grooves can be present as isolated examples (Fig. 21A). Where present in groups, they are typically parallel or sub-parallel to each other (Kuenen, 1957; Allen, 1984; Collinson *et al*., 2006). However, grooves may also show cross-cutting relationships with angles of up to 90°, although typically <40° (Fig. 10B; Dżułyński & Walton, 1965; Enos, 1969a; Ricci Lucchi, 1969a). Groove casts have been seen to commence at an “irregular bulge” (Dżułyński & Ślączka, 1958) representing the counterpart of the original irregular depression, or from chevron marks (Fig. 16A,B), whilst terminations can consist of either: i) a tapering of the groove to meet the original substrate surface; ii) a rounded end, sometimes with an associated small mud ridge in the downstream direction; or, iii) an abrupt, twisted end (Dżułyński & Sanders, 1962a; Dżułyński & Walton, 1965). Terminations are, however, very rarely seen, with Enos (1969a) reporting just 10 terminations across >1500 beds. Even when terminations are present, most lack their formative tools. Key unaddressed questions concern how the tools are transported away from the ends of their grooves, and ultimately where these tools are deposited. Grooves have primarily been associated with turbidites (*e.g.*, Kuenen, 1957; Bouma, 1962; Crimes, 1963; Dżułyński & Walton, 1965; Enos, 1969a; Ricci Lucchi, 1969a; Pett & Walker, 1971; Allen, 1984) and have, along with other tool marks, been incorporated into the Bouma sequence (Middleton & Hampton, 1973, 1976; Collinson *et al*., 2006; Talling *et al*., 2012a). However, grooves have also been observed in association with hybrid event beds (Talling *et al*., 2004, 2012a,b; Patacci *et al*., 2014; Southern *et al*., 2015; Fonnesu *et al*., 2016, 2018), with high-strength cohesive debris flows (Johns *et al*., 1981; Kastens, 1984; Labaume *et al*., 1987; Payros *et al*., 1999; Talling *et al*., 2012a; Dakin *et al*., 2013), and with slumps (Kuenen, 1957; Crimes, 1973). Outcrop examples of high-strength debris flows rarely show grooves, perhaps in part because of associated large-scale deformation of the substrate (Johns *et al*., 1981; Labaume *et al*., 1987). In contrast, Kastens (1984) imaged a spectacular example from the modern seafloor, where a debris flow had left a series of parallel grooves immediately upslope of the debris flow deposit, with the grooves approximately matching the diameter of the largest clasts (Fig. 12).

Mapping of grooves beneath individual event beds suggests that grooves may cover lengths and areas far in excess of those identified from individual outcrops, as shown in Figure 14. In these examples from the basin plain deposits of the Miocene Marnoso-arenacea Formation in the Italian Apennines (see Table 3 for context) grooves are present for distances in excess of 40 km and over areas up to ~300 km^2. It is unknown whether individual grooves are continuous for these distances or whether these consist of a succession of individual isolated grooves.

The highly parallel nature of groove casts, their large longitudinal and areal extent, and the frequent occurrence of internal parallel striae (Fig. 10E), all suggest that the tools were dragged in a single position (without rotating), at a constant height (no bouncing), through a substrate that was sufficiently strong that it could not be deformed by fluid stresses or flow back into the eroded space once the groove had been cut. The occasional spiralling of internal laminae and twisted termination suggest that in these rare cases the clasts are able to rotate, albeit relatively slowly with respect to their downstream movement in the case of the internal striae.

Experiments

Crowell (1955) claimed that Rücklin (1938) had produced groove marks, but the feature produced has little in common with groove marks (Dżułyński & Walton, 1965), and furthermore these experiments were not in mud beds (5.8% clay <10 µm; 94.2% silt and sand). The very first work to produce grooves was thus Kuenen (1957; see his Plate 1D) who produced grooves ('slide marks' of Kuenen, 1957) from experimental slumps, using a 2 cm thick sandy cover sliding over a clay layer at inclinations from a few degrees to 10-20°. Subsequently, Ten Haaf (1959; reported in Dżułyński & Sanders, 1962a) studied erosive marks caused by snowballs catapulted over a surface of fresh snow, and concluded that groove marks were linked to flows with great current velocity, interpreted as the product of turbidity currents. Later experiments using plaster-of-Paris for the currents and kaolin clay or gelatine for the substrate were undertaken to examine sole structures formed under 'artificial turbidity currents' (Dżułyński & Walton, 1963, 1965; Dżułyński, 1965; Dżułyński & Simpson, 1966; Dżułyński, 1996). A variety of tools (fish bones, hardened mud, or plaster-of-Paris fragments; numbers and sizes unknown) were placed at the base of a short ramp and on the clay floor of the tank, and plaster-of-Paris currents were then released down the ramp. The experiments succeeded in making short individual grooves, including one that showed internal laminae that spiralled longitudinally (Dżułyński, 1965). However, sub-parallel groups of grooves that characterise outcrop examples were not reproduced. The grooves were also associated with a range of other tool marks including prod, bounce and skip marks (Dżułyński & Walton, 1963, 1965; Dżułyński, 1965, 1996; Dżułyński & Simpson, 1966). This is in contrast to outcrop examples where these features are commonly separated in space or time, implying that the optimal conditions for groove formation were not achieved in these experimental studies.

A key question concerning the experiments of Dżułyński and co-workers is how representative the flows that formed these grooves and associated tool marks are of turbidity currents, even allowing for the scale of the experiments (Peakall *et al*., 1996). Relatively few details of the experiments were given, but basic flow parameters can be estimated. Densities and viscosities were not measured, but the proportions of water to plaster-of-Paris were 3:2 or 2:1 (Dżułyński & Walton, 1965), 3:1 in the case of the experiments on tool marks (Dżułyński & Walton, 1963), or 2:1 / 3:1 (Dżułyński & Simpson, 1966). No details of the mixtures used in Dżułyński (1965) were provided. Whereas plaster-of-Paris is quite a variable material, assuming a typical bulk density of 785 kg m^{-3} and an absence of changes in volume as a result of the dissolution of the plaster-of-Paris and initial hydration of the calcium sulphate hemihydrate minerals (note these volume changes are small; Jørgensen & Posner, 1959), gives flow densities of ~1520 kg m^{-3}, ~1390 kg m^{-3}, and ~1260 kg m^{-3} for the 3:2, 2:1, and 3:1 mixtures, respectively. Viscosities at the time of mixing can be estimated at ~1-2.5 Pa s^{-1} (Murakami & Hanada, 1956), about the same as runny honey (Yanniotis *et al*., 2006), albeit plaster-of-Paris increases in viscosity rapidly after just a few minutes, if there were any delays in the experiments (Murakami & Hanada, 1956). The yield strength of the plaster-of-Paris flows used in these experiments is harder to estimate, although plaster-of-Paris does exhibit yield strength at high concentrations (Rees, 1983). In summary, the experiments of Dżułyński & Walton (1963, 1965) likely had viscosities equivalent to kaolin suspensions with approximately 20% by volume concentration (*cf*., Talling, 2013, his figure 9A), had densities representative of kaolin suspensions with volumes of 15->30% (*cf*., Fig. 3), and likely had some yield strength. These flows consequently had densities largely in the intermediate-strength debris flow field (Fig. 3), had viscosities equivalent to the lower boundary of the intermediate-strength debris flow field (Talling, 2013), and had a yield strength likely in the broad range for the low strength debris flows (0.1-10 Pa) of Talling (2013), or the lower and upper transitional plug flows of Baas *et al*. (2009, 2011). In turn, flow rheology is also dependent on applied stress and thus velocity (Baas *et al*., 2009, 2011; Talling, 2013). Whereas velocities are unknown, and thus the exact rheology cannot be specified, it is clear that the experiments are more representative of transitional plug flows, or intermediate-strength debris flows, than the turbidity currents that these workers compared them to.

A beautiful example of apparently well-defined parallel grooves has been observed in an experimental subaqueous debris flow composed of kaolinite-water slurries with approximately 40% by weight kaolinite, where the coherent head had broken off from the body of the flow because of hydroplaning (Fig. 15; Hampton, 1970; Middleton & Hampton, 1973). Presumably, the grooves were formed by: clasts that were larger than the thickness of the basal water layer beneath the hydroplaning block; at the back of the broken-off debris flow component; or as fluid dissipated underneath the flow as it came to rest. Small clasts of kaolinite are observed behind the flow, and likely formed the tools. Kastens (1984) noted the similarities between the grooves shown in these experiments and those observed on the modern seafloor (Fig. 12). However, it should be noted that there was no initial substrate in these experiments (Hampton, 1970), unlike Kuenen’s (1957) experiments with slumps, and therefore the grooves were cutting into a deposit formed by the passing current.

Chevron marks

Chevron marks (Dunbar & Rodgers, 1957) consist of a series of open and continuous V-shaped, or U-shaped, ridges that are aligned in a given direction (Fig. 16). The chevrons have been shown to close in the downstream direction (Craig & Walton, 1962; Dżułyński & Sanders, 1962a). Chevrons comprise a continuum of forms from uninterrupted chevrons (V- or U-shaped ridges), when the whole form is present, through cut chevrons consisting of V-shaped forms that are cut down the middle, to interrupted chevrons, with ridges and furrows either side of a clear groove mark (Fig. 17; Craig & Walton, 1962; Dżułyński & Sanders, 1962a). Chevron marks have been observed to occasionally transition downstream between these different forms: from uninterrupted, to cut, or interrupted chevrons (Craig & Walton, 1962; Dżułyński & Sanders, 1962b), and from interrupted to uninterrupted chevrons (Dżułyński & Sanders, 1962a). Allen (1984) suggested that these transitions represent the concave-up trajectory of the clast as it gets closer to (and/or cuts) the bed, and then moves away again. However, as with grooves, transitions are unusual and they are typically constant in form where observed, coming under the 'continuous' class of tool marks. The different forms are consequently associated with different positions of the tool relative to the bed, with the tool cutting into the bed (interrupted chevrons, cut chevrons) or presumably at a constant height above the bed (uninterrupted chevrons). Chevrons are typically a few millimetres wide, with greater widths typically associated with interrupted chevrons (Craig & Walton, 1962). In longitudinal cross-section, the downstream end of the chevron ridge is steepest and is folded over on itself (Fig. 17; Dżułyński & Sanders, 1962a; Allen, 1984). The chevrons appear to form by fluid stressing of weak ductile muds, and thus are partly a function of the bed substrate properties (Dżułyński & Walton, 1965). The fluid stressing itself is believed to be caused by wakes that form around the moving tool, and have been likened to the wakes that form behind ships (Craig & Walton, 1962; Dżułyński & Sanders, 1962a; Allen, 1984). In some cases, transitions occur from uninterrupted chevrons to regular groove marks (Kuenen, 1957; Fig. 16A,B), indicating that the formative tool was moving downward through the flow, and then into contact with the bed. The loss of chevrons when the tool makes contact with the bed potentially implies an abrupt increase in substrate strength. However, abrupt changes in the cohesive strength of the seafloor may be relatively unusual, albeit that biological controls and/or oxygenation may create these. Alternatively, such transitions may suggest that the fluid dynamics around the tool itself alter the strength of wakes impacting the substrate. Here, the potential for variations in the strength of wakes is explored by further considering ship wakes.

Ships form interrupted chevrons because the vessel itself cuts the bow wave, in the same way as the interrupted chevrons are assumed to form. In contrast, the bow wave of a tool above the surface of a bed may be able to propagate downwards forming uninterrupted chevrons. For ships, the magnitude of the transverse waves forming the wake is a strong function of the length-based Froude number, $F_L = U/\sqrt{(gL)}$, where U is streamwise velocity, g is acceleration due to gravity and L is the length of the ship's waterline (*e.g.*, Parnell & Kofoed-Hansen, 2001; Soomere, 2007). A so-called "hump speed" occurs when F_L is ~0.56, producing increased wave energy. This can be further exacerbated if the vessel is in shallow water, as characterised by the depth-averaged Froude number $F_h = U/\sqrt{(gh)}$, where h is the water depth. As F_h increases, wave heights increase, and if the critical value of F_h coincides with the "hump speed" very large waves can be generated, which is a problem for some fast ferries (Parnell & Kofoed-Hansen, 2001). It is not clear how far such analogies can be taken with respect to a fully submerged tool with wakes rather than waves, but it does suggest that different regimes may exist that could lead to major changes in the size and strength of the wakes generated around a moving tool. Consequently, the absence of chevrons in most grooves may suggest that the uppermost part of the substrate was too consolidated, and the particle velocity and orientation were suboptimal, for the generation of sufficiently strong wakes capable of deforming the substrate.

Experiments

Experiments with i) plaster-of-Paris flows crossing weak clay beds, ii) or sandy suspensions crossing beds of soft plaster-of-Paris produced from settled suspensions, enabled tools to form incredibly realistic chevron marks (Dżułyński & Walton, 1963; Dżułyński & Simpson, 1966; Dżułyński, 1996). Matchsticks manually moved across, but above, the surface of an experimental mud-bed that had been left long enough to develop a thin cohesive 'skin' were also observed to form chevrons (Dżułyński & Walton, 1963, 1965; Kelling *et al*., 2007). Similarly, dragging a stick through the mud, produced cut chevron marks (Dżułyński & Walton, 1963, 1965).

The nature of formative flows for grooves and chevrons

Here, we review the possible mechanisms for the formation of grooves and chevrons, in terms of the evidence from groove orientations and cross-cutting relationships, and flow type (low- and high-density turbidity currents, granular flows, liquefied/fluidised flows, and debris flows, the latter equivalent to quasi-laminar plug flows and laminar plug flows, described earlier) (Fig. 18), in the light of progress in understanding the dynamics of sediment gravity flows.

Groove orientations

As noted earlier, grooves are typically parallel to one another, but they can also show cross-cutting relationships. There has been much debate concerning the interpretation of cross-cutting groove marks, with interpretations as the product of a single flow (*e.g*., Kuenen & Ten Haaf, 1958; Enos, 1969a; Allen, 1971b) or multiple flows (*e.g*., Crowell, 1958; Mulder *et al*., 2002). Multiple flows should exhibit two or more maxima in terms of the distribution of crossing groove directions, and a consistent relationship between the age of the mark and orientation. However, these relationships are not typically observed (Enos, 1969a; Allen, 1984). A key consideration here is that in contrast to flutes, which form over a period of time, grooves are thought to be cut by a tool near-instantaneously, so individual marks can reflect small-scale changes in current direction, rather than time-averaged properties (Allen, 1971b; see later discussion). Explanations for cross-cutting relationships from single flows include: i) variations in turbulent flow related to the growth and decay of lobes (and clefts) at the head of a turbidity current, which are associated with secondary flows (Kuenen & Ten Haaf, 1958; Allen, 1971b); ii) flow divergence in an expanding current (Potter & Pettijohn, 1963); iii) a 'meandering' migration of the flow over time (Walker, 1970); iv) variations in flow direction between split debrite blocks in a transforming flow (*sensu* Felix & Peakall, 2006; Draganits *et al*., 2008); and, v) rotation of blocks in the flow that are much larger than the grooves (Draganits *et al*., 2008). Rotation of blocks in the flow can explain even the largest angular differences (90°) between grooves (Draganits *et al*., 2008). Other ideas discussed by Ricci Lucchi (1969a), including Coriolis force, flows in the ambient fluid, irregularities on the bed, and transverse slopes, were all considered untenable by Allen (1971b).

Low-density turbidity currents (Fig. 18A)

The formation of grooves was first linked to turbidity currents by Kuenen (1953; see also Kuenen & Sanders, 1956) although the density of these turbidity currents was not inferred. Turbulent, low-density turbidity currents as agents for the formation of grooves were postulated by the catapulting snowball experiments of Ten Haaf (1959), in the experiments of Dżułyński and co-workers (Dżułyński & Walton, 1963; Dżułyński, 1996, 2001), and through consideration of suspended sediment within the head (Allen, 1971b). However, the experiments of Dżułyński and co-workers have been shown here to be more comparable to transitional plug flows and intermediate-strength debris flows, and in any case only succeeded in generating isolated grooves over short distances. Similarly, snowballs only generate straight grooves in very soft substrates, by momentum alone, and leave the tool at the end of the groove (Ten Haaf, 1959). Key questions are whether low-density turbulent turbidity currents can: i) transport groups of particles in near-parallel straight lines; ii) transport particles that are partially 'submerged' and erode into a substrate, at a constant depth, particularly where this substrate has sufficient strength to avoid fluid stressing; iii) keep a particle in a fixed position with respect to the bed surface (*i.e*., without rotation), thus maintaining grooves of constant width and form; iv) hold particles at constant heights above the bed, as required for the formation of chevrons; and v) preserve the grooves and chevrons in a pristine form. Video analysis of cobbles in bedload-rivers shows that sliding of particles is typically limited to events of less than one grain diameter in length, rolling events consist of short sub-parallel straight segments a few grain diameters in length, and that particles are dispersed laterally within the flow relatively quickly (Drake *et al*., 1988; see also Seizilles *et al*., 2014). Overpassing of gravels across much finer sands is likely more applicable to transport of tools over muds, and might lead to clasts travelling in near-parallel straight lines. However, analysis of gravel overpassing shows that clasts typically roll, and sometimes bounce, rather than move across the bed in a fixed orientation (Allen, 1983), such as via sliding. Particles above the bed in a turbulent flow typically move either as saltation load with characteristic ballistic profiles, or in suspension, where particles move within the flow (Bagnold, 1973; Francis, 1973; Lee & Hsu, 1994). In both cases, particles would not be expected to maintain a constant height above the bed, as is postulated to occur in the formation of chevron marks. It is also unclear why forms associated with turbulent flow, such as flutes (see earlier) do not form. Perhaps the substrate is too firm for the applied turbulent bed shear stresses to cause erosion (*cf*., Fig. 6A), and thus flutes do not form. A similar argument might explain why grooves and chevrons are typically preserved pristinely, apparently unmodified by turbulent flow.

Consequently, the different observations combined (Fig. 18A) indicate that low-concentration turbulent currents are highly unlikely to produce and preserve groups of parallel to sub-parallel grooves, or chevron marks. Nonetheless, it may be possible for isolated short grooves to form from the movement of individual particles overpassing a deformable bed, in a manner similar to the snowball effect, albeit the grooves may not be as regular if particles roll, and the tool would be expected to be present at the end (see for instance figure 2 of Shchepetkina *et al*. (2018) from estuarine systems).

High-density turbidity currents (HDTCs) with traction carpet (Fig. 18B)

Many of the postulated mechanisms in the literature for groove formation involve high-concentration layers at the base of turbidity currents. Dżułyński & Sanders (1962a) suggested turbulent traction carpets that restrict the impact of large-scale turbulent eddies from the main body of the flow. Dense concentrations of near-bed sand, approaching laminar conditions, were: i) inferred for some thin, closely spaced groove marks by Dżułyński & Walton (1965); ii) invoked in the form of a thin high-viscosity fluidized sheet at the base of turbidity currents by Hsu (1959; see also Sanders, 1965); and, iii) proposed as having formed in flows exhibiting turbulence suppression because of high near-bed concentrations of suspended particles (Ricci Lucchi, 1995). Draganits *et al*. (2008) also suggested that the basal layer of the flow was laminar, and might be formed by the head of concentrated density flows (*sensu* Mulder & Alexander, 2001). These high-concentration layers are associated with flows that are interpreted in current classifications as high-density turbidity currents (Kneller & Branney, 1995; Talling *et al*., 2012a; equivalent to the concentrated density flows of Mulder & Alexander, 2001). Such flows form massive or graded Bouma T_A deposits, possibly with inversely graded layers at their base (T_{B-3} of Talling *et al*., 2012a), as a result of incremental deposition under high-concentration turbulence-damped conditions (Sohn, 1997; Talling *et al*., 2012a) or velocity fluctuations on the scale of seconds (Cartigny *et al.*, 2013). The key controlling difference is the sediment fall-out rate, with lower rates associated with inversely graded layers, and higher rates with massive or normally graded T_A deposits (Sumner *et al*., 2008). The highest-concentration basal layers have been called 'traction carpets' (Dżułyński & Sanders, 1962a; Lowe, 1982) or laminar shear layers (Vrolijk & Southard, 1997; Sumner *et al*., 2008), and are thought to be at most a few centimetres thick (Hiscott, 1994; Sohn, 1997; Talling *et al*., 2012a), although the experiments of Sumner *et al*. (2008) only produced layers <5 mm thick. Inverse grading, where present, occurs as a result of larger particles moving away from the bed, through a geometrical mechanism of larger particles moving over smaller ones, and kinetic sieving as smaller particles migrate downwards (Sohn, 1997; Dasgupta & Manna, 2011). Dispersive pressure is not an important process in traction carpets as implied in earlier work (Sohn, 1997; Dasgupta & Manna, 2011). High-speed imaging of large particles close to the bed in the experiments of Postma *et al*. (1988) also reveals that particles do not remain at fixed heights within the flow, but rather move vertically and rotate within the flow. Experimental work has also shown that clasts higher in the flow preferentially glide along the top of these high-concentration basal layers (traction carpets) rather than settle through them (Postma *et al*., 1988), explaining discontinuous mudstone clast layers in discrete horizons within Bouma T_A beds, at bed amalgamations, or dispersed within the flow (Hiscott *et al*., 1997; Talling *et al*., 2012a).

Given these processes, it does not appear that larger clasts would be incorporated and maintained within traction carpets and therefore be dragged along the bed and form grooves (Fig. 18B). In many cases, the clasts, as shown by groove dimensions, are considerably larger (typically a few tens of mm, and rarely >1 m in diameter (Allen, 1984)) than the thickness of the traction carpets. In fact, typical grain sizes within these layers are less than a tenth of the thickness of the traction carpet (Sohn, 1997). Furthermore, larger particles preferentially move away from the bed if initially incorporated into a traction carpet that is forming, or glide along the upper surface of the traction carpet rather than sinking in once a high-concentration layer has formed. Both mechanisms also militate against the formation of repeated chevrons, where a tool needs to be held at a constant height above the bed, or partly within the bed. The dense medium of a traction carpet that extends to the bed would also appear incapable of enabling the formation and propagation of the ‘bow’ waves around clasts that are thought to form chevrons.

High-density turbidity currents (HDTCs) with high-concentration basal layer (Fig. 18C)

High-concentration basal layers can also be formed in HDTCs in the absence of traction carpets (*e.g.*, Lowe, 1982; Baker *et al*., 2017), either during initial tractional sedimentation prior to the development of traction carpets (Lowe, 1982), or during bypass of the HDTC (Baker *et al*., 2017). Failure of the sediment bed in canyon systems has also been postulated to lead to the downstream formation of a high-concentration basal layer beneath a turbidity current (Paull *et al*., 2018). Tractional sedimentation in sand-rich HDTCs is typically dominated by upper-stage plane beds and dune-like bedforms, associated with a turbulent flow regime, prior to increasing sediment concentrations near the base leading to the development of traction carpets (Lowe, 1982). In a supercritical regime, high-concentration basal layers have been postulated to develop over cyclic steps (Hughes Clarke, 2016; Paull *et al*., 2018). This initial turbulence-driven tractional regime is highly unlikely to be able to maintain larger clasts in fixed positions and at a constant height within the flow, and thus form grooves, for the reasons discussed above for 'low-density turbidity currents'. In the postulated high-concentration basal layers of Monterey Canyon, associated with upslope migrating bedforms, large (~0.45 m diameter) spherical and cuboid instrumented 'artificial-clasts' are observed to rotate within the flow, and are thought to be rafted in, or at the upper interface of, the dense layer (Paull *et al*., 2018). These 'artificial-clasts' further suggest that clasts are not dragged in a fixed position at the base of high concentration basal layers. In the same campaign, an 800 kg tripod was moved several kilometres down canyon. Whilst the movement of the tripod demonstrates the power of such flows, we do not consider the density or dimensions of the structure to be representative of a natural clast (6000 kg/m^3; 2.5 tall, 1.5 m long legs and a large basal cross-sectional area, see Fig. 4b of Paull *et al*., 2018) and once tipped over it is likely to be hydrodynamically stable. Furthermore, the tripod was observed to stop and start during a flow event (Fig. 4c of Paull *et al*., 2018) indicating that it was not fixed in place in the flow. Thus, the available evidence suggests that these postulated high-concentration basal portions of turbidity currents are not capable of holding clasts in a fixed position. For coarser gravel-rich HDTCs, few tractional structures are formed, and traction carpets are thought to dominate (Lowe, 1982).

Most of our knowledge of HDTCs is based on their depositional characteristics, in the form of bedforms and traction carpets, as discussed above. However, HDTCs may also exhibit a bypass phase, as can be observed in laboratory experiments (Baker *et al*., 2017). Little is known about the structure of HDTCs during bypass, with wide variation in estimated flow concentrations for what constitutes HDTCs: between 5 and 9% (Mulder & Alexander, 2001), >10% (Talling *et al*., 2012a), >20-30% (Lowe, 1982), or from ~7 to 45% (Kuenen, 1966; Middleton, 1967). Density stratification of gravity currents is also known to be important, and thus these estimates of flow concentration are likely not bulk concentrations but instead reflect basal conditions (e.g., Peakall *et al*., 2000; Peakall & Sumner, 2015). During sediment bypass, HDTCs may have lower basal sediment concentrations (less pronounced stratification), with these only increasing as flows decelerate and sediment falls out from suspension rapidly (Peakall & Sumner, 2015). However, here we consider the possibility that flows may bypass with basal concentrations at which hindered settling and dispersive pressure become important (*e.g*., Lowe, 1982). This would dampen turbulence and potentially lead to near-bed turbulence being extinguished through reduction of mixing (Cantero *et al*., 2012, 2014), and/or near-bed turbulence suppression through the transitional behaviour of clays present within the flow (Baas & Best, 2002; Baas *et al*., 2009, 2011, 2016b). This, in turn, may lead to laminar basal layers. However, larger particles would not be expected to remain at a constant height within a hindered settling zone, with large particles either falling through the layer, or moving away from the bed if dispersive pressure is important enough (Fig. 18C). If turbulence is extinguished entirely, flows may undergo rapid sedimentation with little if any tractional component (Cantero *et al*., 2012). Consequently, larger particles are unlikely to remain at fixed heights within the flow and be dragged through a substrate to form grooves (Fig. 18C).

Granular flows (Fig. 18D)

Grain or granular flows are sediment gravity flows composed of cohesionless grains maintained by dispersive pressure induced by grain-to-grain collisions (Bagnold, 1956; Lowe, 1976a). Groove marks formed by granular flows have been interpreted from pyroclastic flows, with Pittari & Cas (2004) interpreting the formative flow as a highly concentrated granular flow that was capable of keeping clasts in a fixed position, and noting that the flows had 35-40% fine-grained ash. Similarly, Sparks *et* *al*. (1997) argued for a dense concentrated granular avalanche, and assumed this had a fine-grained component. Grooves have also been recognised in other pyroclastic flow deposits (Cole *et al*., 2002; Sparks *et al*., 2002), albeit Sparks *et al*. (2002) attributed groove formation to a turbulent flow component at the head.

Grain flows, particularly polymodal sand and gravel flows, are able to form in deep-water environments (*e.g*., Middleton, 1970; Middleton & Hampton, 1973, 1976; Lowe, 1976a; Iverson *et al*., 1997; Henstra *et al*., 2016), but they may be restricted to comparatively steep slopes (more than a few degrees; Lowe, 1976a). Furthermore, in subaqueous deep-water environments, the fine-grained silt-clay component, if more than a few percent, is likely coupled to the water phase producing a debris flow (Lowe, 1976a; Iverson, 1997; Pittari & Cas, 2004), and so the prevalence of granular flows will be restricted. It is unclear whether subaqueous granular flows without a significant fine-grained component are able to maintain clasts in a fixed position without clast rotation (Fig. 18D). This might be possible only if the grains in the basal part of the flow lock together and the flow then glides downslope by inertia (*pers. comm.*, George Postma). However, grooves beneath granular flows have not been reported in deep-water systems, suggesting that this is unlikely.

Fluidised, liquefied and nearly-liquefied flows (Fig. 18E, F)

Fluidised flows with an overriding gravity current (Sanders, 1965), or thin fluidised traction carpets as discussed earlier (Hsu, 1959; Sanders, 1965), have been suggested as mechanisms for the formation of grooves. Truly liquefied flows are produced where pore pressure equals the weight of the grains, leading to the grains temporarily losing contact with each other and floating within the surrounding fluid (Lowe, 1976b). Re-sedimentation then occurs from the base upwards as grains settle through the fluid. Consequently, subaqueous liquefied flows, even of coarse silts and sands, are unlikely to move more than a kilometre, since resettling takes place relatively quickly (Lowe, 1976b). In contrast, truly fluidised flows have an external source of fluid that enables the upward velocity of water to match, or exceed, the settling velocity of the grains (Lowe, 1976b). Fluidised flows are therefore likely restricted to very thin flows generated from the tops of liquefied flows, and thus are considered to be unimportant in deep-water settings (Lowe, 1976b). In both cases, flows have no strength and cannot hold a tool in place and drag it through a substrate; consequently, such flows will not be associated with groove or chevron formation (Fig. 18E).

However, in some cases, usage of the terms 'liquefied' and 'fluidised' flows has altered from these definitions, leading to potential confusion. Liquefied flows (Talling *et al*., 2013a) and liquefied debris flows (Talling *et al*., 2012a) were defined where "it is unknown whether all, or a significant part of the sediment weight is borne by excess pore fluid pressure" (Talling *et al*., 2013a), and "where excess pore pressures primarily support the grains" (Talling *et al*., 2012a), respectively. Both definitions extend liquefied flows to those with pore fluid pressures below where liquefaction occurs, thus reflecting different flow processes. Analogies are made with subaerial debris flow experiments where pore pressures in excess of the total normal stress have been recorded, implying that these experimental flows were sometimes liquefied (Iverson, 1997; Major & Iverson, 1999; Iverson *et al*., 2010). However, the measurements in those experiments were local, recorded by sensors at the base of the flow (Major & Iverson, 1999). Typical pore pressures within such subaerial debris flows were well below the liquefaction limit, balancing about 80% or more of the total normal stress (Major & Iverson, 1999), and they were described as 'nearly liquefied' (Iverson, 1997; Major & Iverson, 1999; Iverson *et al*., 2010). Driving forces for these elevated pore pressures are contractive shearing, where sediment undergoes rapid contraction as a result of shear from an overlying flow, which can lead to a very rapid rise of pore pressure (Iverson *et al*., 2000; Iverson, 2005), and sediment consolidation (Iverson, 1997); note that contractive shearing may be a mechanism for Bouma T_A formation (see Supplementary Information). In the case of sediment consolidation, it will be progressively hindered (rather than monotonic; Iverson, 1997) as pore pressures rise, and thus the process of pore pressure increase from this mechanism is self-regulating, with compaction unable to drive the flow towards true liquefaction. The elevated pore pressures in the body of these flows enhance flow mobility and keep shear strength very low (Major & Iverson, 1999; Iverson *et al*., 2010). Consequently, tools are unlikely to be held in fixed positions at the base of these flows whilst dragged through a substrate, and grooves and chevrons should not form below the body of such flows (Fig. 18F). In contrast, the fronts of these nearly-liquefied flows in subaerial environments do not exhibit elevated pore pressures as they are relatively dry and thus have higher shear strengths (Iverson, 1997; Major & Iverson, 1999; Iverson *et al*., 2010). Whilst the pore pressure distribution in the fronts of subaqueous debris flows is unknown, these flows will be wet, and thus we postulate that shear strength will not be as high, and thus grooves and chevrons are much less likely to be formed at the flow front in subaqueous flows (Fig. 18F).

Fluidised subaqueous density flows have been claimed to be long-lived based on experiments and field studies. These studies are critiqued in the Supplementary data, which concludes that the experiments (Ilstad *et al*., 2004a; Breien *et al*., 2010) are neither fluidised nor liquefied, and the F5 facies of Mutti and co-workers (Mutti, 1992; Tinterri *et al*., 2003; Mutti *et al*., 2009) is not formed by fully fluidised flow. Consequently, fluidised subaqueous flows are not considered further as a mechanism for groove formation. We thus recommend a return to the definitions of liquefied and fluidised flows as envisaged by Lowe (1976b), reflecting the mechanisms of liquefaction and fluidisation themselves. The elevated pore pressures recognised in experimental subaerial debris flows (Iverson, 1997; Major & Iverson, 1999) may be typical of some subaqueous debris flows; the ‘liquefied flows’ and ‘liquefied debris flows’ of Talling *et al*. (2012a, 2013a), are herein renamed ‘nearly-liquefied flows’ (Iverson, 1997). However, the presence of clasts that have been transported over long distances in most debris flows in deep-water systems indicates significant yield strength (and thus lower pore pressures). These latter examples are discussed below in the ‘Debris flow’ section.

Debris flows and hybrid events (Fig. 18G, H, I)

Processes of groove formation: Based on outcrop studies, only Draganits *et al*. (2008) and Pyles & Jennette (2009) have suggested that grooves on the base of sand beds might be the product of debris flows (equivalent to quasi-laminar plug flows and laminar plug flows; see earlier), and in the former case this was one of two suggestions (see Section on HDTCs). Pyles & Jennette (2009) inferred that grooves in the Carboniferous-aged Ross Formation, Ireland, were formed by shale clasts being dragged by a laminar flow, interpreted as a debris flow, and noted that the clasts in the overlying debrite scaled with the width of the grooves. However, no other process arguments were provided to substantiate this interpretation. Additionally, the 'slide marks' of Kuenen & Sanders (1956) and Kuenen (1957), a sub-classification of grooves (see introduction to the Groove Casts section), were interpreted as formed from slumping, although debris flows were not specifically considered. Here we argue that debris flows, and the debritic flow components of hybrid events, can account for the observed attributes of grooves, in addition to those formed from slumps and slides. In contrast to the other mechanisms discussed above, debris flows have been shown to form multiple parallel to sub-parallel grooves in a natural seafloor example (Fig. 12; Kastens, 1984). Such flows have cohesive strength, are loaded with clasts, and can exhibit laminar conditions, thus enabling clasts to be held in position at the base of the flow. However, in order for clasts to erode the substrate there needs to be a slip condition at the base of the flow — that is the clasts need to be moving relative to the substrate. A slip condition can occur in one of two ways. If the plug flow extends all the way to the flow base (a laminar plug flow; Figure 18G), then there can be a slip condition at the base (e.g., Fig. 13). Alternatively, the flow may exhibit a shear-layer that separates the plug flow region from the basal viscous sub-layer (quasi-laminar plug flow), as shown experimentally in Baas *et al*. (2009) and in our re-analysis of data from Hermidas *et al*. (2018). In this QLPF case, then although at the base of the flow the velocity goes to zero, there is still slip between the base of the plug flow, where the clasts are attached, and the bed (Figs. 18H and 18I). In both cases, clasts (tools) at the base of the plug zone are moving faster than the substrate and therefore can be dragged through a substrate in straight lines at a fixed depth, thus forming grooves (Fig. 18H).

Subaerial debris flows are known to transport particles adjacent to the bed in their heads where there is a slip condition, followed by basal particles moving vertically and laterally away from the bed (Johnson *et al*., 2012; Fig. 13). The migration of these particles would explain both cross-cutting grooves (*i.e*., the distribution of groove orientations around a single maximum direction; see 'Evidence from groove directions'), and also the absence of particles at the ends of grooves (Fig. 18G, H). Particles are simply uplifted into the main debris flow and transported down system away from the site of groove formation (Fig. 13). Lobes and clefts, which have been postulated as a mechanism for cross-cutting grooves in turbidity currents, may occur, but they have not been observed in subaqueous debris flows in the laboratory (Sohn, 2000). A cohesive flow also explains the lack of particle rotation observed in most groove casts, since particles are held in place by the cohesive strength of the flow (Fig. 18G, H, I). Debris flows are known to concentrate larger particles towards the front of the flow (Iverson, 1997; Gray & Kokelaar, 2010; Johnson *et al*., 2012), and these outsized clasts may therefore be the primary tools for groove formation, explaining the limited cross-cutting of grooves (Fig. 18G, H). In subaerial debris flows, large clasts also accumulate at lateral margins, but these are rapidly deposited so are less likely to form grooves (Gray & Kokelaar, 2010). Similar parallel longitudinal grooves have been observed in experiments with subaqueous debris flows where hydroplaning at the front provides a slip-component (Fig. 15; Hampton, 1970; Middleton & Hampton, 1973). Grooves are also observed in other natural flows where the tools are supported by flows with cohesive strength, as shown by the giant grooves (kilometres to 10s of kilometres long) at the base of large-scale mass transport deposits (MTDs) observed in three-dimensional seismic reflection data (*e.g*., Posamentier & Kolla, 2003; Gee *et al*., 2005; Ortiz-Karpf *et al*., 2017; Soutter *et al*., 2018). The longitudinal continuity of these MTD grooves raises the question as to what the longitudinal extent of individual grooves is in deep-water clastic systems (see later discussion). Analogies can also be made with glacial striae on rock (Allen, 1984), where the tools are 'welded' onto the bottom of an ice sheet, to the formation of mega-scale glacial lineations by fractured ice at the base of ice-sheets (Clark, 1993; Piasecka *et al*., 2018), and to a lesser extent the grounding of ice in sediments in oceans (Reimnitz *et al*., 1977; Vogt *et al*., 1994; Piasecka *et al*., 2018), where the weight of ice maintains the tool on the substrate. A further groove-like feature, referred to as 'glide tracks', is formed by large outrunner blocks in front of debris flows (Prior *et al*., 1984; Nissen *et al*., 1999). However, unlike grooves formed beneath the parent flow, these typically exhibit depth changes along the track at distances on the order of the glide track width, reflecting the lack of stability of the blocks (Kuijpers *et al*., 2001; De Blasio *et al*., 2006). This is in marked contrast to the uniformity in depth observed in grooves in outcrop.

Chevron tool marks are also more readily explained by QLPF debris flows, as these allow a particle to be held at a fixed height above, or partly within, the substrate, thus enabling a series of repeated bow waves to form around the particle, and the formation of the chevrons (Fig. 18I). In contrast, as noted earlier, it is hard to envisage a mechanism for maintaining a particle at a fixed height above the bed for either turbulent low-density turbidity currents or high-density turbidity currents with a high-concentration basal layer. The generation of chevrons would, however, suggest that the basal layer is sufficiently fluidal that bow waves are able to propagate through it to the substrate surface (Fig. 18I). The type of chevron (uninterrupted, cut, interrupted, Fig. 17) may in turn reflect — and in deposits, predict — the thickness of this fluidal layer, and thus the depth from the bed to the base of the plug layer, relative to the size of the cutting clasts.

Nature of debris flows forming grooves: Taking groove widths in the range 10-100 mm (see earlier discussion), and assuming that the clasts that created them are of the same diameter (in agreement with the observations of Kastens, 1984; Fig. 12) rather than asperities of much larger particles, the minimum cohesive strength of the debris flow required to support the clasts can be calculated. Using the approach of Talling *et al*. (2012a), based in part on Hampton (1975), suggests that grains of 10-100 mm diameter and of typical densities (based on mud densities 0-10 m below the seafloor taken from Flemings *et al*. (2006)) can be transported by low- (1-10 Pa) to intermediate-strength (10-100 Pa) debris flows. The boundary between low and intermediate densities is at an approximate diameter of 20 mm, and thus most of these clast sizes would require intermediate-strength debris flows (Fig. 3). These strengths equate to volumetric kaolinite concentrations of between >13-30%, although more cohesive clays, such as bentonite, would produce the same strengths at considerably lower volumetric concentrations (Marr *et al*., 2001; Baas *et al*., 2016b; Baker *et al*., 2017). These intermediate-strength debris flows are mobile enough to traverse low-gradient slopes and reach fan fringes, and to produce relatively thin (<2 m thick) deposits (Schwab *et al*., 1996; Talling *et al*., 2004, 2010, 2012a; Ducassou *et al*., 2013). Hydroplaning of debris flows, where ambient fluid is injected beneath the head (Hampton, 1970; Mohrig *et al*., 1998), may occur in these intermediate-strength flows (*cf*., Baker *et al*., 2017) but preferentially occurs for high-strength debris flows (Ilstad *et al*., 2004b; Talling *et al*., 2012a), albeit that flow velocity is also a controlling factor in hydroplaning. Where flows undergo hydroplaning, tools will groove the bed if larger than the thickness of the basal water layer beneath the debris flow, or grooves may be formed by the debris flow immediately behind the hydroplaning head. The likely rarity of hydroplaning in these intermediate-strength debris flows suggests, however, that outsized clasts towards the front of the flow may be responsible for the formation of grooves, albeit flow in the body of the current may also be able to generate grooves.

Hybrid events and groove formation: The debritic component of clast-rich hybrid event beds is typically associated with intermediate-strength cohesive debris flow (Talling, 2013), and these can reach the very distal portions of submarine lobes and basin plains (Talling *et al*., 2004; Hodgson, 2009). Hybrid event beds, including clast-rich types, are common in these distal locations (Haughton *et al*., 2003, 2009; Talling, 2013), with hybrid event beds accounting for >31% (Fonnesu *et al*., 2018), and >83% (Spychala *et al*., 2017a), respectively, of total thickness in the basin plain and lobe frontal fringes. Some flows may erode and generate clasts a considerable distance up-dip, as shown by exotic mud clasts (Haughton *et al*., 2003, 2009; Talling *et al*., 2007a, 2012b). In combination with the absence of the debritic component of hybrid event beds in proximal areas, this observation of extensive clast transport suggests that hybrid event beds are capable of bypassing a debritic component over large longitudinal distances; for instance, tens of kilometres in the case of the Marnoso-arenacea (Fig. 14; Talling *et al*., 2012b; Talling, 2013). Other hybrid event beds likely source mudstone clasts more distally (Hodgson, 2009; Kane *et al*., 2017; Fonnesu *et al*., 2018). However, given that flows must transition from being primarily erosive, thus generating mudstone clasts, to primarily depositional, and that debris flows deposit *en masse*, bypass of the clast-rich component likely also occurs.

Some models of hybrid events assume that the debritic component travels across an underlying sand (e.g. Haughton *et al*., 2009) or above a sand-rich 'high density flow' (Fonnesu *et al*., 2016), in which case it is unlikely that the debritic component can groove the seafloor through this layer. However, such models are largely based on studies of depositional hybrid events. Models of hybrid events transforming from an initial debris flow do show a separate debritic component bypassing (Haughton *et al*., 2003, their Fig. 11C). Furthermore, the evidence for large-scale bypass of some hybrid events and the absence of deposits in proximal areas, suggests that the hybrid events were not depositional at all points and thus travelling over sand beds. Similarly, the evidence for active erosion of the seafloor, demonstrates that the hybrid event cannot be travelling over a pre-existing sand-layer. Furthermore, the process arguments presented herein suggest that a sand-rich high-density flow as envisaged by Fonnesu *et al*. (2016) has insufficient cohesive and frictional strength to hold tools in a rigid position and thus groove the bed. Instead, these process mechanisms strongly suggest that the debritic component must be a separate component in touch with the bed during the bypass phase. These observations and arguments are in keeping with those of Talling (2013) who tackled the question of why the debritic component almost always ends up above the deposits of a high density turbidity current deposit, and is capped by the deposit of a low density turbidity current. Talling (2013) concluded that this is due to the longitudinal structure of the flow, with the basal sand likely deposited by a forerunning HDTC that moves faster than the debris flow component, which in turn moves faster than the LDTC (Fig. 19).

Intermediate-strength debris flows, not associated with hybrid event beds, can also occur in distal areas, albeit more rarely (*e.g.*, Ducassou *et al*., 2013; Spychala *et al*., 2017b), and these bypassing flows should also act to form grooves up-dip. Therefore, the presence of grooves and chevrons indicates that they were cut by a clast-rich intermediate-strength debris flow (QLPF to LPF), and given their prevalence, in many cases by a debritic component of a hybrid event.

Grooves and hybrid event beds: implications for hybrid event bed processes

Some studies show that hybrid event beds often lack grooves at their base (*e.g.*, Haughton *et al*., 2009; Jackson *et al*., 2009; Talling *et al*., 2012a; Grundvåg *et al*., 2014), although in some cases grooves may be observed up-dip where outcrop allows such correlation (*e.g.*, Figs. 11A, 14A; Fonnesu *et al*., 2018). However, grooves have been observed on the bases of some hybrid event beds (HEBs) containing both clast-rich and clast-less debrite units (Figs. 11B, 14A; Talling *et al*., 2004, 2012a,b; Patacci *et al*., 2014; Southern *et al*., 2015; Fonnesu *et al*., 2016, 2018), albeit it should be noted that debrites in HEBs can show significant spatial variations (Fig. 14B; Fonnesu *et al*., 2015). A more detailed assessment of the presence or absence of grooves at the base of hybrid event beds is not possible at present, as grooves are often reported for entire outcrop sections, usually as palaeocurrent indicators, rather than specifically linked to hybrid beds (*e.g.*, Spychala *et al*., 2015, 2017b; Malkowski *et al*., 2017, 2018), or tool marks are treated as a single category, and thus grooves are not specified (*e.g.*, Hodgson, 2009). Here we concentrate on those examples where grooves are present. Examples of grooved hybrid event beds have been interpreted following the standard paradigm that views them as the product of erosion under the head of a turbulent turbidity current, potentially with a dense stratified basal layer (Fonnesu *et al*., 2016; Fig. 19A). However, as argued previously, low- and high-density turbidity currents are unable to explain groove formation, and the grooves themselves indicate erosion by a dominantly bypassing debris flow component. The grooved surfaces are, in turn, overlain by clean sand, followed by a debritic interval and finally more sand (Talling *et al*., 2004; Patacci *et al*., 2014; Fonnesu *et al*., 2016, 2018), to produce the typical tripartite hybrid event bed signature (Haughton *et al*., 2003, 2009; Talling *et al*., 2004; Fig. 19B).

The presence of grooves up-dip from the deposits of hybrid event beds (e.g., Figs. 11A, 14, Beds 3 and 5) may signify erosion by a clast-rich debritic component, with or without a forerunning turbidity current, followed by deposition from a later turbiditic component (Fig. 20A). Beds 1, 3 and 6 (Fig. 14) show examples of clast-less debrites running to the limits of the outcrop suggesting that if there is a clast-rich unit towards the front of the flow then it is beyond the outcrop limits. This model has analogies with the model of hybrid event beds where a debris flow erodes or bypasses material up-dip, before undergoing flow transformation and successive deposition of sand from a forerunning turbidity current, followed by debritic deposition, to form the hybrid bed down-dip (Talling *et al*., 2004). However, in these models (Talling *et al*., 2004), the trailing turbidity current that forms the capping component of the tripartite hybrid event bed, and that might be expected to be deposited on the grooved surfaces, is low-density, forming thin beds characterised by T_{CDE} divisions. Consequently, this model cannot explain the presence of high-density turbidity current deposits overlying grooved surfaces, up-dip of hybrid event beds (*e.g*., Figs. 11A, 14; Fonnesu *et al*., 2018). The dominant model of hybrid event bed formation, where flows gradually transform down-dip from non-cohesive to cohesive, would have the same issue (Fig. 19B; Haughton *et al*., 2003, 2009; Talling *et al*., 2004); assuming that a debritic component does interact with the substrate at some point, and therefore forms grooves, the deposits overlying such erosive surfaces would be expected to be composed of low density turbidites.

In cases where grooves are present at the base of hybrid event beds, the longitudinal flow transformation model from turbulent turbidity current at the front, through a following debris flow and then a dilute turbidity current (Fig. 19B; Talling *et al*., 2004; Haughton *et al*., 2009), is inapplicable because, as argued earlier, the basal surface is the product of a debris flow, as also is the division above the basal sand. Three models can be postulated to explain the observations. First, erosion by the head of a turbidity current may lead to increasing mud and mud-clast content and local transformation into a debris flow (*e.g*., Talling *et al*., 2004; Kane *et al*., 2017), which cuts the basal grooves (Fig. 20B). This debris flow may then be followed by a turbidity current component and then the debritic component, as in the model of Haughton *et al.* (2009; Fig. 20B). Secondly, the flow may be broken longitudinally into a series of debritic and turbiditic components, reflecting retrogressive failure up-dip (Piper *et al*., 1999; Brooks *et al*., 2018b), or the debris flow component may split into a series of discrete blocks during flow transformation (Felix & Peakall, 2006; Felix *et al*., 2009). In this case, the first debritic pulse cuts the grooves, followed by deposition from the subsequent turbidity current and debritic components (Fig. 20C). However, such processes would be expected to form multiple stacked debrites, in contrast with vertical sequences of hybrid event beds (Haughton *et al*., 2003, 2009; Talling *et al*., 2004; Fig. 19B). Thirdly, the deposits may reflect a bypassing debris flow that cuts the grooves and then starts to become vertically stratified, with sand deposition from the debris flow followed by deposition of the debrite component (Fig. 20D). The influence of vertical stratification in hybrid event beds has previously been suggested from both laboratory (Baas *et al*., 2009, 2011; Sumner *et al*., 2009) and field studies (Fig. 19C; Talling *et al*., 2004, 2010, 2012a). However, sand separating from a mud-sand debris flow is physically simpler (and has been modelled experimentally), than from a debritic phase with larger mud clasts. In the latter case, the mudstone clasts would need to be less dense than the flow, whereas the sand would have to be denser than the flow and thus able to settle. However, as flow density must be high for the larger mudstone clasts to remain supported then yield strength would be expected to be significant. Given this, the sand would have to settle through a dense, possibly high strength, material. Alternatively, if a clast-rich debrite is at the front of the flow, followed up-dip by a clast-less debrite, sand may separate from this component. It remains unclear how feasible such a mechanism is.

In summary, with the possible exception of the case where the front of the turbidity current develops into a debris flow through erosion (Fig. 20B), all of the models suffer from limitations. Flow transformation from an initial debris flow (Fig. 20A) does not predict high-concentration turbiditic deposits above grooves. Longitudinal flow segregation with multiple debritic components (Fig. 20C) predicts too many debrites in the hybrid event bed. Finally, in the case of the vertical segregation model (Fig. 20D), there are issues concerning how sand segregates from a mixture of mud and large mud clasts, or whether there are longitudinal variations from clast-rich to clast-less debrite. Flows forming hybrid event beds therefore potentially have more complex longitudinal and temporal changes than have hitherto been postulated, and these account for observations such as high-density turbidity current deposits overlying grooved surfaces up-dip of hybrid beds.

An alternative to the different models of hybrid event beds is that the flow forming the grooved surface is *entirely separate* from the flow forming the overlying deposits (Fig. 20E). In this case, an initial debris flow, slide or slump cuts a grooved surface on the seafloor after the flow bypasses down-dip. Given that debris flows typically either deposit *en masse* or not at all, the grooves may be left in pristine form on the seafloor as the flow bypasses, as seen in Figure 12 (Kastens, 1984), or may be covered by a thin layer of unconsolidated mud from minor flow transformation of the top of the debris flow, as well as any subsequent hemipelagic deposition. A subsequent turbidity current may 'ingest' any unconsolidated mud (of low strength, see Substrate section) and deposit onto the grooved surface.

Here, we also note that flutes can be present at the base of some hybrid event beds (*e.g.*, Patacci *et al.*, 2014), often in beds without clast-rich components (Talling *et al.*, 2004, 2012a; Fonnesu *et al.*, 2018), or on the same surfaces as grooves and other tool marks (Fonnesu *et al.*, 2016). This indicates that turbulent or transitional flows also eroded the basal erosion surface, and in the case of mixed groove-flute assemblages that flow evolution took place, or a later turbulent or transitional flow event eroded grooves from an earlier event. The presence of flutes in the absence of grooves may suggest the occurrence of a forerunning turbidity current, or a cohesive transitional flow.

Morphology and abrasion of mudstone clasts

Kuenen (1957) argued against mudstone clasts being the primary source of tools on the grounds that they would undergo rapid rounding through abrasion. Mudstone clasts do indeed abrade on time scales of tens of minutes to hours depending on applied shear stress and composition (Smith, 1972). Such abrasion is observed in turbidity currents, with transported clasts typically showing rounded to sub-rounded clasts (Johansson & Stow, 1995). Similarly, hybrid event bed debrites can show rounded to angular clasts, again likely reflecting transport distance (*e.g.*, Davis *et al.*, 2009; Hodgson, 2009). Grooves show both smooth curved internal surfaces and surfaces marked by parallel striae. Consequently, these surfaces likely reflect the nature of clasts that cut them, with longer-travelled sub-rounded clasts likely cutting the smooth surfaces. Striae are likely formed by clast asperities perhaps from recently eroded clasts, although potentially they may be the product of armoured mudstone clasts in some cases. The nature of the groove morphology may, in part, be a reflection of the time period of formation; although the true length of grooves is unknown because of outcrop extent, they are known to be up to tens of metres long. Current velocities for deep-water flows are poorly known (Talling *et al.*, 2013b; Peakall & Sumner, 2015). However, Talling *et al.* (2012a) calculated that a 1 m thick, intermediate-strength, kaolin-rich debris flow on a slope of 0.1° (typical of mid to lower fans; Pirmez & Imran, 2003) would require a velocity of ~0.5-1 ms^{-1}. Such flow velocities are in-line with velocities measured or estimated for distal turbidity currents (Klaucke *et* *al*., 1997; Pirmez & Imran, 2003; Vangriesheim *et al*., 2009; Stevenson *et al*., 2014; Peakall & Sumner, 2015). Assuming a velocity of 1 ms^{-1}, the clast travel time over the length of grooves observed in outcrop equates to seconds to tens of seconds, which is too short a period to result in significant abrasion (*e.g*., Smith, 1972). Moreover, the mudstone clasts are likely more indurated than the substrate into which they are cutting.

For cases where the extent of individual grooves is not limited by the timescale between initial impingement of a clast on a bed, and being uplifted vertically at the flow front (Johnson *et al*., 2012; Fig. 13; see earlier discussion), then consideration of mudstone abrasion rates enables estimates of maximum groove lengths to be made. Groove lengths of hundreds of metres (timescale of minutes) to kilometres (10s of minutes) would appear possible, dependent on the composition of the mudstone clasts (Smith, 1972). Nonetheless, individual grooves are likely to be shorter than the tens of kilometres observed under large MTDs, likely reflecting that in MTDs they are cut by much larger tools (*e.g*., Gee *et al*., 2005; Ortiz-Karpf *et al*., 2017; Soutter *et al*., 2018) where abrasion relative to clast size will be less important, and in at least some cases by stronger tools (*e.g*., Soutter *et al*., 2018).

Discontinuous tool marks

Prod, bounce, skip and roll marks form from the impact of tools with a soft substrate (Dżułyński & Sanders, 1962a; see Fig. 21). Prod marks (Figs 21 and 22; Dżułyński & Ślączka, 1958) are considered to be the most useful for palaeocurrent analyses since they are asymmetric, with a longer shallower upstream slope, and a shorter steeper downstream slope; the shallower slope may be ornamented with longitudinal striae (Dżułyński *et al*., 1959; Lanteaume *et al*., 1967; Allen, 1984). Bounce marks (Figs 21 and 22; Wood & Smith, 1958), also called skim marks (Allen, 1984), are symmetrical to slightly asymmetrical and typically 10s to 100s mm long (>3 m in exceptional cases), <50 mm wide, less than a few millimetres deep, and may contain parallel internal striae (Lanteaume *et al*., 1967;

Allen, 1984). Skip marks (Fig. 22; Dżułyński *et al*., 1959) are a series of discontinuous tool marks, typically at a similar spacing, that are produced by a single tool. The morphology of each mark may be almost identical, or variable but similar enough to be recognisable as being formed by the same tool (Dżułyński & Walton, 1965). Skip marks can include tumble marks (Fig. 22; Allen, 1984), formed from a tool somersaulting, such as fish vertebrae and angular mud clasts (Dżułyński & Walton, 1965; Allen, 1984). Skip marks can also consist of a series of bounce marks that can sometimes become almost continuous, approaching the appearance of grooves (Collinson *et al*., 2006). Lastly, roll marks (Fig. 22; Dżułyński & Ślączka, 1958) are made by cylindrical objects (*e.g*., fish vertebrae, ammonite and straight orthocone shells) that enable the tool to roll over the bed (Dżułyński & Sanders, 1962a; Dżułyński & Walton, 1965; Bates, 1974). Discontinuous tool marks can be superimposed on, and consequently can be younger than, both flutes and grooves (Fig. 21B; Dżułyński & Sanders, 1962a; Dżułyński & Walton, 1965; Ricci Lucchi, 1995). Given their small size and erosion depths (typically mm to 10s mm) (Dżułyński & Walton, 1965; Collinson *et al*., 2006) relative to flutes and grooves, any evidence of their formation prior to flutes and grooves may be lost, although where erosion by later forms is limited, evidence for discontinuous tool marks that formed earlier can be found (Fig. 21C).

The nature of formative flows for discontinuous tool marks

Roll marks require a flow where the particles are not periodically lifted from the bed by buoyant or turbulent forces, and thus flow concentration is likely comparatively low, and turbulence limited. Furthermore, roll marks will be hindered by high viscosity, and the development of thickened viscous boundary layers. Consequently roll mark formation will be favoured by relatively fluidal flows with comparatively low viscosity, low concentration, and limited turbulence; these likely include weak turbulent flows (TF), and lower-concentration transitional flows (TETF, LTPF). Similarly, skip marks are formed by tumbling particles that are in close contact to the bed, but the tools are either more angular than those involved in roll marks, or experience sufficient lift forces to periodically lose contact with the bed. These tumble marks may also be favoured by weak turbulent flows, or transitional flows (TETF, LTPF). However, a greater spacing between tumble marks implies that a significant buoyant force is present that supports the particle, and thus an association with higher-concentration transitional flows (*e.g.*, UTPF).

The asymmetric morphology of prod marks suggests that tools may exhibit ballistic trajectories like saltating grains, and thus approach the bed at comparatively low angles, before rebounding from the bed and being lifted up at a higher angle (Bagnold, 1973; Francis, 1973; Lee & Hsu, 1994). Experiments with large saltating particles, up to 6 mm diameter, showed a narrow range of incidence angles (10°-35°) and a take-off angle range of 21°-87°, with a mean of *c*. 65° (Ancey *et al*., 2002), in keeping with qualitative observations of prod marks. Saltation is normally linked to turbulent flows (Pilotti & Menduni, 1997), but Francis (1973) demonstrated experimentally that in higher-viscosity flows composed of glycerine-water mixtures saltation could also occur under laminar conditions, suggesting that for clay-rich flows, transport under transitional flow conditions (Baas & Best, 2002) would also be possible. Laminar or transitional clay-rich flows would also act to provide a buoyant force aiding transport of larger tools.

The presence of fine striae on the upstream slope of some prod marks suggests that the incident grain was not spinning when it impacted the bed. This is surprising since grains typically rotate during saltation, driven by bed collisions, grain-to-grain collisions, and velocity gradients across the particle (Best, 1998). Larger particles, like those observed to form tool marks, are known to rotate more slowly than smaller particles, for instance *c*. 4-5 rotations per second for *c*. 4.8 mm diameter particles in water (Francis, 1973; Best, 1998) in contrast to ~40 rotations per second for *c*. 1.4 mm diameter particles in water (Lee & Hsu, 1994; Best, 1998). Two mechanisms, in addition to increased particle size, may act to reduce or eliminate rotation of tools: increased viscosity (Best, 1998) and reduction in the velocity gradient. Transitional flows possess enhanced viscosities (potentially an order of magnitude or more increase relative to a clearwater flow), and also exhibit greatly reduced shear immediately adjacent to the bed, notably for lower and upper transitional flows, and quasi-laminar plug flow (Baas *et al.*, 2009, 2016b). This basal zone of low shear, representing a thickened viscous sublayer, was *c.* 6 mm thick in the experiments of Baas *et al*. (2009), representing *c.* 4-5% of flow thickness. Although how the thickness of this low shear zone scales with flow thickness for larger flows is unknown, for flows that are metres to tens of metres deep the thickness of this basal zone might be expected to be of the order of centimetres to ten centimetres. Given that particle saltation heights are typically about 2-4 times the grain diameter for rotating particles in liquids (Francis, 1973; Fernandez Luque & Van Beek, 1976; Krecic & Hanes, 1997), and potentially as low as a third of this in the absence of rotation (Krecic & Hanes, 1997), saltation trajectories may well be expected to be restricted to this basal zone of low shear if occurring in transitional flows. Consequently, the presence of this basal zone of low shear, in combination with enhanced viscosities, suggests that the formative flows in prod marks exhibiting striae are transitional flows, most likely upper transitional plug flows (see later). An additional control on particle rotation may be the interaction of tools — particularly for mudstone clasts — with a cohesive bed, leading to markedly inelastic collisions. The loss of kinetic energy associated with inelastic collisions might result in a corresponding reduction in imparted angular momentum (Wiberg & Smith, 1985) and thus rotation rates. A reduction or cessation of particle rotation in turn affects particle trajectories through reduction of lift associated with the Magnus effect (Rubinow & Keller, 1961), leading to much shorter saltation hop lengths and lower trajectories (Krecic & Hanes, 1997). Moreover, the reduction or absence of rotation further reduces turbulence generation towards the base of the flow, because rotating grains have been shown to generate additional turbulence (Best, 1998).

In sharp contrast to prod marks, bounce marks are formed by particles that graze the bed with a concave-up trajectory (Allen, 1984). This concave trajectory is atypical of grains in a bedload layer, which typically roll, slide or saltate (*e.g.*, Lee & Hsu, 1994), and suggests that the tool is largely supported by the flow, presumably by the buoyant force. However, the tool is not fully supported, in contrast to particles transported in a well-developed plug flow, such as an intermediate-strength debris flow. Skip marks consisting of repeated bounce marks further argue for a significant buoyant force, since the morphologies do not fit with saltating tools in terms of their longitudinal symmetry and length to width ratio. The observation that some skip marks consist of bounce marks that are almost continuous and start to look like grooves, suggests that in these cases the particles are further supported by the flow, and close to becoming intermediate-strength debris flows that fully support the tools (see Section on grooves). Given the processes identified herein, 'bounce marks' is a remarkably poor choice of term for these features, since unlike prod marks the particles do not really bounce, but rather skim the surface. Consequently the term 'skim marks' used by Allen (1984) is recommended here, as it reflects the key process.

As noted earlier, the change in the morphology of flute marks and the ultimate cessation of their formation is interpreted to be caused by a change from turbulent flow to transitional flow, with a corresponding reduction of the size, and eventual elimination, of the flow separation zones at the flow-bed interface integral to flute formation (*cf*., Baas & Best, 2008; see Section on Flutes). Discontinuous tool marks do not appear to form simultaneously with flutes, although they can overprint them. Furthermore, as observed here, some types of tool mark, such as skim (bounce) marks, provide evidence for a substantial buoyant force that enables particles to graze the bed in gentle arcs. Here, we interpret discontinuous marks to be typically the product of transitional flows. If the flow is either fully turbulent, or in the turbulence-enhanced transitional flow (TETF), or lower transitional plug flow (LTPF) regimes, flutes are likely to form (see section on Flutes), assuming substrate conditions enable mass erosion from the bed. In such flow regimes, substantial bed turbulence is present encouraging scour, and the mud clasts responsible for discontinuous tool marks may not be supported within the flow. Cessation of flute development likely occurs in the upper part of the lower transitional plug flow regime, or the lower part of the upper transitional plug flow regime (UTPF), because of a loss of turbulence (see section on Flutes), at a stage where increasing concentration and viscosity may enable support for tools within the flow. At the other end of the spectrum, if the flow is a plug flow of sufficient cohesive strength to form an intermediate-strength debris flow (upper part of the quasi-laminar plug flow regime, QLPF, or a fully laminar plug flow, LPF), tools will be held rigidly in place within the flow and form grooves. Between these two end members, transitional flows of progressively increasing strength can support clasts, with: i) prod marks envisaged as forming in the upper part of the UTPF regime (*e.g.*, Baas & Best, 2008); ii) prod marks with striae at their upstream end likely reflecting stronger flows (uppermost part of the UTPF regime); and iii) skim marks forming in stronger transitional flows (uppermost part of the UTPF and lower part of the QLPF regimes; Baas *et al*., 2009) that possess sufficient density to provide significant buoyant force (Fig. 23). Skip marks dominated by relatively short marks will be the product of an upper UTPF regime, whereas skip marks consisting of repeated longer skim marks are likely formed in the lower QLPF regime. Roll marks are most likely the product of low concentration, low viscosity flows with limited turbulence (TF, TETF, LTPF), whereas skip marks that involve tumbling may reflect either i) low concentration, low viscosity conditions, or ii) if the spacing between tumble marks is greater, a higher buoyancy associated with transitional flows such as UTPF. Both forms require relatively planar beds to pass over, are unlikely to be able to form over surfaces composed of flutes, and cannot form under higher concentration flows such as upper QLPFs (Fig. 23).

The influence of tool properties on the nature of discontinuous tool marks

The nature of the tools themselves, and the availability of tools, also helps determine the character of tool marks. However, the tools carried by a flow are at least partially controlled by the fluid dynamics, which will limit the maximum size and density of the particles. Particle shape is a more independent parameter, although as noted earlier (see Morphology and abrasion of mudstone clasts) it is in part a function of travel distance for tools such as mudstone clasts. The shape of particles will affect the nature of the tool marks, and in some cases, notably where fossils are the tools, they can produce very characteristic tool marks (e.g., Dżułyński & Ślączka, 1958, 1960; Dżułyński & Walton, 1965; Howe, 1999). Similarly, the presence of fine striae in some prod marks and skim marks, implies particles with sharp asperities. Particle shape is also known to affect saltation with trajectories becoming longer and lower, and thus flatter, with decreasing sphericity (Williams, 1964; Rice, 1991), thus potentially affecting contact angles with the substrate.

DISCUSSION

Distribution and association of scour marks and tool marks: a process explanation

The present analysis of formative mechanisms for the range of different sole structures enables an explanation for their observed spatial and temporal distributions. As discussed earlier, flutes are typically associated with thicker sandstones in proximal locations, whilst tool marks are frequently associated with thinner, more distal sandstones, and flutes and tool marks are typically found on different bedding planes at a given point spatially. Furthermore, large bulbous flutes are typically found up-dip from small spindle-shaped flutes (Pett & Walker, 1971). To summarise the key process mechanisms proposed herein, large bulbous flutes are likely formed by turbulent and turbulence-enhanced transitional flows, whereas spindle-shaped flutes are associated with stronger transitional flows (LTPF and lower UTPF). Discontinuous tool marks may be formed by a variety of flow types, from laminar to turbulent. However skim marks are associated with flows with significant buoyant force that enable the tools to gently graze the bed in low curving arcs. Similarly, prod marks with striae at their up-dip ends indicate flows that are comparatively viscous with thickened basal sublayers. Finally, grooves and chevrons can only be formed by debris flows exhibiting a slip condition that have the cohesive strength needed to maintain tools, primarily mudstone clasts, in fixed positions at a given height within the flow that are dragged through the substrate. In the case of chevrons, this requires a fluidal layer at the base of the debris flow plug, suggesting a quasi-laminar plug flow. Observed examples of longitudinal variation from large bulbous flutes, to spindle-shaped flutes, to discontinuous and continuous tool marks therefore suggest increasing flow cohesion downstream, and enables a process-orientated model to be proposed (Fig. 24A).

Increasing flow cohesion downstream

This progressive increase in cohesion is in agreement with the standard model for the formation of hybrid event beds (Haughton *et al*., 2003, 2009; Talling *et al*., 2004) that proposes flows gradually transform downstream from non-cohesive to cohesion-dominated. In this model, as flows ingest mud, and decelerate as slopes decline, cohesive forces begin to progressively dominate over turbulent forces. These rheological changes would lead to a successive decline in flute size and their eventual disappearance, through the development of more transitional flows and discontinuous tool marks, and lastly the formation of grooves and chevrons as flows form debritic components that are likely associated with hybrid event beds (Fig. 24A). This longitudinal relationship between discontinuous tool marks, and grooves and chevrons, has not been demonstrated in the field, as tool marks have not typically been subdivided. However, the presence of hybrid event beds at the distal fringes of submarine lobes and basin plains (Talling *et al*., 2004; Hodgson, 2009; Spychala *et al*., 2017a) suggests that in these cases grooves and chevrons are preferentially found in distal locations. However, it should be noted that transformations can start and finish anywhere along the transport profile shown in Figure 24.

Decreasing flow cohesion downstream

Whereas the postulated model of longitudinal change from low to high cohesion explains the typical field observations of flutes and tool marks as summarised in the literature, some field observations predict the opposite transition from grooves in T_A beds to flutes in T_C beds (Table 1, Bouma, 1962; Crimes, 1973). These observations are in keeping with flows that start as high-concentration debris flows (or slumps and slides) and progressively dilute downstream, reducing flow cohesion. In such cases where initial high-cohesion flows transform to lower-cohesion flows (*e.g.*, Piper *et al*., 1999;

Talling *et al*., 2004; Felix *et al*., 2009), the distribution of flutes and tool marks should be reversed relative to the hybrid event bed model of increasing flow cohesion, with grooves up-dip, then discontinuous tool marks, and finally flutes, assuming the flow remains erosive throughout (Fig. 24B). Such a scenario is supported by observations of the Annot Sandstone, Peïra Cava, France, where grooves are present but hybrid beds and mass transport deposits are very rare, and decrease as a proportion of beds downstream (Table 3; Cunha *et al*., 2017). Some slumps with coeval overlying sands ('welded slump-graded sand couplets') do occur in Peïra Cava, and are interpreted as the products of partial flow transformation from high- to low-concentration (Stanley, 1982). Similarly, extensive grooves are observed in the Zumaia section of the Basque Basin, Spain (Tables 1 and 3; Crimes, 1973) yet hybrid beds are not reported in that time interval (Table 3). Analysis of the distribution of recurrence intervals suggests that the basin-plain beds at Zumaia were sourced from large-scale disintegrating slope collapses (Clare *et al*., 2014, 2015). Furthermore, a large, transversely sourced slump, down dip from Zumaia, exhibits grooves at its base (Crimes, 1976). Both the recurrence intervals and the observed slump with basal grooves suggest that in this basin, the grooves were likely formed from flows transforming from high- to low-cohesion flows. Again, it should be appreciated that Figure 24 is schematic, and flows may initiate with different flow properties and may not transform entirely.

Other sole type distributions

Some debris flows may travel very large distances without undergoing significant flow transformation (Ducassou *et al*., 2013), and therefore may be able to form grooves at any point. Similarly, turbulent flows that do not undergo flow transformation to more cohesive flows may just form flutes, with velocity and flow depth controlling the change from larger to smaller flutes without a viscosity change, as envisaged by Allen (1971a). Potentially, other scenarios are also possible. We postulate that some sediment gravity flows may first transform from high- to low-cohesion through a range of dilution mechanisms (*e.g.*, Felix & Peakall, 2006; Felix *et al*., 2009), prior to the flow decelerating, and viscous forces becoming more important towards the end of the flow (*e.g.*, Talling *et al.*, 2004). The accompanying changes in flow cohesion would be expected to result in changes from grooves to sole structures associated with lower cohesion (Fig. 24A), and then a switch back to sole structures related to increasing cohesion (Fig. 24B), with the point of lowest flow cohesion determining the range of the more fluidal sole structures. It should also be noted that whereas the present discussion only considers longitudinal changes in flow properties and thus sole structures, there will also be changes laterally, depending on how flow structure changes from on-axis to off-axis.

Temporal changes in sole structures

The prevalence of flutes or tool marks on a given surface suggests that in many flows, at a given point spatially, the erosive phase of the flow only comprises a single flow type, and thus the major changes in flow type are longitudinal. However, flutes can pre- or post-date tool marks (Fig. 21B,C), indicating that in some examples there is also a temporal variation in the nature of flow types within a given event. This assertion assumes that the erosive surface formed from a single event. Flutes followed by tool marks suggests an increased cohesive flow strength over time, which may be associated with a forerunning more turbulent flow phase and a slower, more viscous, later flow component (*e.g.*, Figs 19B and 20A), or potentially with increased seafloor erosion (see Fig. 4 and discussion in the 'Seafloor substrates' section). Flutes post-dating tool marks indicates that flows have become more turbulent, suggesting that a more dilute turbulent flow phase followed a faster, higher-concentration, flow phase. Amy *et al*. (2005a) demonstrated experimentally that for stratified gravity currents, both of these scenarios are possible, and that the variation in the vertical distribution of viscosity controls whether the lower viscosity, more turbulent, layer either outruns or lags the higher viscosity layer. These temporal changes in flow properties have been postulated previously as explanations for flutes cutting tool marks or *vice versa* (Dżułyński & Sanders, 1962a; Draganits *et al*., 2008; Pyles & Jennette, 2009).

Implications for the Bouma Sequence

The formation of grooves by dominantly bypassing debritic flow components, and the successive development of grooves and then flutes (or *vice versa*), demonstrate that the erosive surface and overlying deposits can be produced by different types of current. Thus many sole structures *do not* have a genetic link to the overlying turbidity current deposit, as encapsulated in the present pictorial Bouma sequence. We note that Bouma (1962) and early workers (Dżułyński & Walton, 1965; Harms & Fahnestock, 1965; Walker, 1965, 1967) only considered the five internal divisions of the sequence, and did not incorporate a basal erosive surface. However, later workers added the erosive surface to the base of the Bouma T_A division in summary diagrams of the Bouma sequence (Blatt *et al*., 1972), and then explicitly linked this surface to sole marks including tool marks (Middleton & Hampton, 1973, 1976), to yield the standard pictorial Bouma sequence we know today and that has been almost universally adopted (*e.g*., Bridge & Demicco, 2008; Leeder, 2011; Talling *et al*., 2012a; Boggs, 2014; Pickering & Hiscott, 2016; Collinson & Mountney, 2019; Fig. 25).

The recognition of erosion by one phase of the flow, for instance grooved surfaces formed by debris flows, and deposition by a subsequent phase of the flow, producing turbidity current deposits, also implies that the temporal gap between erosion and deposition can be considerable. Whilst a time gap between the erosive surface and the underlying deposit is implicit in the Bouma sequence, this time gap has been assumed to be very short for heterolithic and unconfined settings, based on the pioneering work of Kuenen (1957, p. 242) who stated "the conclusion is inevitable that flute casts and drag marks [grooves] result from the same current that deposited the covering bed a moment later". For bypass surfaces, such as channel bases and scours, no genetic linkage between erosive surface and overlying surface is typically implied (e.g., Stevenson *et al*., 2015), albeit the dominant sand-on-sand surfaces in axial locations (e.g., Hubbard *et al*., 2014) in these environments may limit the frequency of sole structures. Herein, we challenge the belief for unconfined and heterolithic settings that there is a genetic linkage between erosive surface and overlying deposit, and argue that the time gap in the Bouma sequence can be orders of magnitude greater than that previously envisaged.

The erosively grooved surface, if present, can be overlain by the full range of sandy Bouma sub-divisions (T_A-T_C) (Table 1; Fig. 11; Bouma, 1962; Pett & Walker, 1971; Crimes, 1973), again illustrating that there can be a temporal disconnect between the erosive and depositional phases of the same event. A grooved erosive surface, therefore, is neither a part of the sedimentological record of a waning turbidity current, nor the classical Bouma sequence. Here, we suggest a new pictorial version of the Bouma sequence (Fig. 26), that returns to the original Bouma (1962) sequence as a record of waning turbidity currents, and recognises that the basal components of the Bouma sequence at a given longitudinal or lateral position can be deposited on an erosive surface that may record waxing turbidity currents, and processes other than turbidity currents. These additional processes recorded by the erosive surface may include debritic flow components, and transformation of flows between debritic and turbiditic components where flutes and groove marks are superimposed.

There remains debate as to whether the erosive surface and the overlying deposit are the product of the same flow, albeit one that may have multiple rheological components. As discussed earlier, most workers suggest that cross-cutting groove marks likely represent the product of single flows (*e.g.*, Kuenen & Ten Haaf, 1958; Allen, 1971b), yet others have argued for multiple flows (*e.g.*, Crowell, 1958; Mulder *et al.*, 2002). The present study suggests that debritic flow components are able to erode grooved surfaces whilst bypassing almost all sediment, as demonstrated by a modern example from the eastern Mediterranean (Fig. 12; Kastens, 1984). Furthermore, there is no record of a mudstone clast lag or coarse granules (particles >1 mm) immediately overlying these surfaces (*cf.*, Talling *et al.*, 2007c; Talling, 2013) and only occasional examples of clasts deposited at the ends of grooves. Consequently, this suggests that intermediate-strength debris flows can bypass the surface entirely, thus allowing successive debris flows to produce cross-cutting marks. Such intermediate-strength debris flows may exhibit limited shear mixing and consequently only generate small-scale turbidity currents (Talling *et al*., 2010; Talling, 2013). A key question is whether the tails of these dilute flows might be expected to lead to deposition of turbiditic sands or just to muds on top of the grooves. The pristine grooves observed on the modern seafloor immediately up-dip of a debris flow deposit (Fig. 12; Kastens, 1984) show that some grooves can be preserved without any overlying deposit from the flow. It thus raises the clear possibility that the erosive surface and overlying deposits within the Bouma sequence may *not* be formed by a *single* flow event.

Formation of flutes and tool marks under the head?

It has long been argued that flutes and tool marks form during erosion by the head of the turbidity current and that deposition takes place in the body (*e.g*., Kuenen & Ten Haaf, 1958; Middleton, 1967; Allen, 1971b; Cantero *et al*., 2008). Here, we have shown that some tool marks, such as grooves, form under debris flows. Additionally, the presence of superimposed grooves and flutes, formed by debritic and turbulent turbidity current components of the same flow, show that sole marks cannot always form under the head of a flow. Where grooves precede flutes (Kuenen, 1957; Dżułyński & Sanders, 1962a; Enos, 1969a; Ricci Lucchi, 1969a; Draganits *et al*., 2008), there must be erosion in some part of the turbiditic body of the flow, and for the opposite case of flutes preceding grooves, the debris flow component must form grooves under the body of the flow (Dżułyński & Sanders, 1962a; Ricci Lucchi, 1969a), unless grooves and flutes are formed by separate flows. In systems with long flow run-outs, there may also be a substantial temporal gap between the erosion of grooves and flutes or *vice versa*, given that the lengths of clast-rich and clastless debritic components can be up to several tens of kilometres (Fig. 14; Amy *et al*., 2005b; Amy & Talling, 2006; Talling *et al*., 2012b). The hypothesis that flutes and tool marks can only form in the head is also at odds with the evidence that many turbidity currents bypass for much of their duration, with variations between bypass and erosion (Stevenson *et al.*, 2015). Similar arguments can be made based on the superimposition of discontinuous tool marks on flutes (Fig. 21B) and *vice versa* (Fig. 21C), representing a change from turbulent flow to transitional flow in the former case, and the opposite in the latter case (Fig. 23). In both cases, this transition between turbulent and transitional flow is unlikely to happen within the spatial extent of the head. It would therefore appear that scour and tool marks are not limited to the head of the flow, and could instead form for a far greater proportion of some flows.

Implications for palaeocurrent measurements

The present synthesis illustrates that when taking palaeocurrent measurements it is important to note the type of sole structures measured, as this can provide a host of other information that can aid interpretation of flow properties and enhance prediction. However, there may also be a link between palaeocurrents and sole structure type, at least in areas where interaction with topography is important. Kneller and McCaffrey (1999) pointed out that flow density, and density stratification, influence the nature of topographic interaction. Herein, we have demonstrated that different sole structures are related to flows that have different density, stratification, and rheology. Consequently, it might be expected that at-a-given-point, different flow types, and therefore sole structure type, may give different palaeocurrent measurements when flows interact with topography. Beautiful examples of this are shown from the Marnoso-arenacea, Italy, where grooves show an enhanced variability relative to flutes, which is interpreted to be a result of topographic interaction (Muzzi Magalhaes & Tinterri, 2010, their figure 20; Tinterri & Muzzi Magalhaes, 2011; see also Bell *et al*., 2018). However, in other examples of interaction with topography flutes and grooves show similar palaeocurrents (Tinterri *et al*., 2016; Cunha *et al*., 2017). Such variations might reflect the nature of topography, and incident angles, as well as the aforementioned flow properties (cf. Kneller & McCaffrey, 1999).

CONCLUSIONS

This paper presents a radical re-examination of the formative flow conditions of flutes and tool marks formed in deep-water environments, and demonstrates that flutes are not solely the product of turbulent flows, but can also be formed by transitional flows. We also show that discontinuous tool marks — such as skim marks, and prod marks with up-dip striae — are the product of more cohesive transitional flows than flutes. Although, since the pioneering work of Kuenen (1953), grooves and chevron marks have been almost universally assumed to have been formed by turbidity currents, herein we propose that they are formed by debris flows, as well as slumps and slides as Kuenen (1957) recognised. Chevron marks further indicate that there must be a fluidal layer at the base of the debris flow, as seen in quasi-laminar plug flows (*sensu* Baas *et al*., 2009). The cross-cutting nature of some flutes and tool marks indicates that flows can also undergo transitions in flow type at a given spatial location. Flutes and tool marks are thus the product of a range of sediment gravity flow types, but in most cases they are not the product of low- or high- density non-cohesive turbidity currents, as envisaged in past literature. We use this fluid dynamic linkage to propose the first synoptic model that explains the observed longitudinal distribution of flute type, and different tool mark types, in terms of progressive changes in cohesion of flows down-dip, with flows transforming from turbulent non-cohesive flows, through transitional flows, to debris flows, or *vice-versa*. This model also provides a tool for more detailed analysis of the relationships between sole marks and palaeohydraulic conditions in outcrop.

The recognition that grooves and chevrons are dominantly the product of debris flows (and also slumps and slides) demonstrates that existing pictorial descriptions of the Bouma sequence incorrectly assume a genetic link between the basal erosive surface and the overlying deposit. We introduce a new pictorial version of the Bouma sequence that incorporates this insight and illustrates that the erosive surface can represent significant sediment bypass. In addition, we show that the formation of flutes and tool marks is not restricted to the head of gravity currents. It is also evident that substrate characteristics are crucial for sole structures, yet remain poorly understood.

Here we show that modern seafloor substrates exhibit a narrow (<1 m thick) zone of shallow strengthening — up to an order of magnitude stronger than predicted by consolidation — in the top few decimetres to approximately two metres. This variation in shear strength with depth may lead to rapid flow bulking if erosion breaks through this layer, and account for the bimodality in flow transformation.

Although knowledge of aggradational bedforms has increased through decades of flow measurement and experimentation, almost no work has been undertaken on flutes and tool marks since the pioneering work of the 1950s to the early 1970s, thus restricting their utility to palaeocurrent indicators. In the interim, our knowledge of the fluid dynamics of sediment gravity currents, and the nature of the shallow seafloor substrate, have advanced enormously. Here, we demonstrate that it is possible to use flutes and tool marks to interpret: i) flow type at deposition; ii) the nature of flow transformation; and, iii) the nature of the basal layer within debris flows where chevron marks are present. This new understanding suggests that it is then possible to predict the nature of deposit type down-dip. The present study demonstrates that there is much information to be gleaned from a greater understanding of these sole structures, and that there is much more to be learnt from refocusing on these under-utilised sedimentary structures.

ACKNOWLEDGEMENTS

JP, JLB and JHB are grateful to the UK Natural Environment Research Council for grant NE/C514823/1 that enabled our initial work on transitional flows. We also thank NERC (NER/S/A/2006/14147), the National Oceanography Centre, and a Leeds-CSC scholarship for funding work on erosive bedforms from which some of these ideas nucleated. MAC thanks NERC (NE/P009190/1; NE/P005780/1) for funding that has supported his contributions. Heather Macdonald Averill and Daowei Yin are thanked for discussions and their early work investigating erosive bedforms in the laboratory. JP and DH thank Juan Pablo Milana for showing us the sole marks of Quebrada de las Lajas, Argentina. JP, JLB and JHB thank Alfred Uchman, Piotr Łapcik, and Tomasz Pyrcz for access to the Natural Sciences Education Centre at the Jagiellonian University, and for showing us sole marks in and around the Carpathians. JP thanks Paul Wignall for first aid after looking at sole marks in the field proved rather more dangerous than anticipated. We are also grateful to Hannah Brooks for her help with several of the figures, and to Kathryn Amos for discussions and her photographic skills. We thank Peter Haughton, George Postma, Roberto Tinterri, and an anonymous reviewer, along with associate editor Fabrizio Felletti and editor Ian Kane, for their critique and insights that greatly improved this State of the Science paper.

NOMENCLATURE

C_u	Remoulded shear strength (Pa)
d	Flow depth (m)
F_h	Depth-averaged Froude number
F_L	Length based Froude number
g	Acceleration due to gravity (9.81 m s^{-1})
h	Water depth (m)
L	Length of ship’s waterline (m)
U	Mean downstream velocity (m s^{-1})
X	Length of initial bed defect (m)
X_{crit}	Critical bed defect length (m)
ν	Kinematic viscosity (m^2 s^{-1})
σ	Shear stress (Pa)

REFERENCES

Allen, J.R.L. (1968) Flute marks and flow separation. *Nature*, **219**, 602-604.

Allen, J.R.L. (1969) Erosional current marks of weakly cohesive beds. *Journal of Sedimentary Petrology*, **39**, 607-623.

Allen, J.R.L. (1971a) Transverse erosional marks of mud and rock: Their physical basis and geological significance. *Sedimentary Geology*, **5**, 167-385.

Allen, J.R.L. (1971b) Mixing at turbidity current heads, and its geological implications. *Journal of Sedimentary Petrology*, **50**, 227-234.

Allen, J.R.L. (1973) Development of flute-mark assemblages, 1. Evolution of pairs of defects. *Sedimentary Geology*, **10**, 157-177.

Allen, J.R.L. (1975) Development of flute-mark assemblages, 2. Evolution of trios of defects. *Sedimentary Geology*, **13**, 1-26.

Allen, J.R.L. (1983) Gravel overpassing on humpback bars supplied with mixed sediment: examples from the Lower Old Red Sandstone, southern Britain. *Sedimentology*, **30**, 285-294.

Allen, J.R.L. (1984) *Sedimentary Structures: Their Character and Physical Basis*. Elsevier, Amsterdam, 1256 pp.

Allen, J.R.L. (1985) *Principles of Physical Sedimentology*. Allen and Unwin, London, 272 pp.

Allen, J.R.L. (1991) The Bouma division A and the possible duration of turbidity currents. *Journal of Sedimentary Petrology*, **61**, 291-295.

Amos, C.L., Bergamasco, A., Umgiesser, G., Cappucci, S., Cloutier, D., DeNat, L., Flindt, M., Bonardi, M. and **Cristante, S.** (2004) The stability of tidal flats in Venice Lagoon—the results of in-situ measurements using two benthic, annular flumes. *Journal of Marine Systems*, **51**, 211-241.

Amos, C.L., Brylinsky, M., Sutherland, T.F., O'Brien, D., Lee, S. and **Cramp, A.** (1998) The stability of a mudflat in the Humber estuary, South Yorkshire, UK. In: *Sedimentary Processes in the Intertidal Zone* (Eds K.S. Black, D. Paterson and A. Cramp). *Geological Society London Special Publications*, **139**, 25-43.

Amy, L. and **Talling, P.J.** (2006) Anatomy of turbidites and linked debrites based on long distance (120 x 30 km) bed correlation, Marnoso Arenacea Formation, Northern Apennines, Italy. *Sedimentology*, **53**, 161–212.

Amy, L.A., Peakall, J. and **Talling, P.J.** (2005a) Density- and viscosity-stratified gravity currents: Insights from laboratory experiments and implications for flow deposits. *Sedimentary Geology*, **179**, 5-29.

Amy, L.A., Talling, P.J., Peakall, J., Wynn, R.B. and **Arzola Thynne, R.G.** (2005b) Bed geometry used to test recognition criteria of turbidites and (sandy) debrites. *Sedimentary Geology*, **179**, 163-174.

Amy, L.A., Kneller, B.C. and **McCaffrey, W.D.** (2007) Facies architecture of the Grès de Peïra Cava, SE France: landward stacking patterns in ponded turbiditic basins. *Journal of the Geological Society*, **164**, 143-162.

Ancey, C., Bigillon, F., Frey, P., Lanier, J. and **Ducret, R.** (2002) Saltating motion of a bead in a rapid water stream. *Physical Review E*, **66**, 036306.

Andersen, T.J., Lund-Hansen, L.C., Pejrup, M., Jensen, K.T. and **Mouritsen, K.N.** (2005) Biologically induced differences in erodibility and aggregation of subtidal and intertidal sediments: a possible cause for seasonal changes in sediment deposition. *Journal of Marine Systems*, **55**, 123-138.

Annandale, G.W. (1995) Erodibility. *Journal of Hydraulic Research*, **33**, 471-494.

Apps, G.M., Peel, F. and *Elliott, T.* (2004) The structural setting and palaeogeographic evolution of the Grès d'Annot Basin. In: *Deepwater Sedimentation in the Alpine Foreland Basin of SE France: New Perspectives on the Grès D'Annot and Related Systems* (Eds P. Joseph, and S.A. Lomas), *Geological Society of London Special Publication*, **221**, 65-96.

Awadallah, S.A.M. and **Hiscott, R.N.** (2004) High-resolution stratigraphy of the deep-water lower Cloridorme Formation (Ordovician), Gaspé Peninsula based on K-bentonite and megaturbidite correlations. *Canadian Journal of Earth Sciences*, **41**, 1299-1317.

Baas, J.H. and **Best, J.L.** (2002) Turbulence modulation in clay-rich sediment-laden flows and some implications for sediment deposition. *Journal of Sedimentary Research*, **72**, 336-340.

Baas, J.H. and **Best, J.L.** (2008) The dynamics of turbulent, transitional and laminar clay-laden flow over a fixed current ripple. *Sedimentology*, **55**, 635-666.

Baas, J.H. and **Best, J.L.** (2009) On the flow of natural clay suspensions over smooth and rough beds. *European Research Community on Flow, Turbulence and Combustion (ERCOFTAC) Bulletin*, **78**, 58-63.

Baas, J.H., Best, J.L., Peakall, J. and **Wang, M.** (2009) A phase diagram for turbulent, transitional, and laminar clay suspension flows. *Journal of Sedimentary Research*, **79**, 162-183.

Baas, J.H., Best, J.L. and **Peakall, J.** (2011) Depositional processes, bedform development and hybrid flows in rapidly decelerated cohesive (mud-sand) sediment flows. *Sedimentology*, **58**, 1953–1987.

Baas, J.H., Best, J.L. and **Peakall, J.** (2016a) Predicting bedforms and primary current stratification in cohesive mixtures of mud and sand. *Journal of the Geological Society*, **173**, 12-45.

Baas, J.H., Best, J.L. and **Peakall, J**. (2016b) Comparing the transitional behaviour of kaolinite and bentonite suspension flows*. Earth Surface Processes and Landforms*, **41**, 1911–1921.

Bagnold, R.A. (1956) The flow of cohesionless grains in fluids. *Philosophical Transactions of the Royal Society of London*, **A249**, 235-297.

Bagnold, R.A. (1973) The nature of saltation and of 'bed-load' transport in water. *Proceedings of the Royal Society of London A*, **332**, 473-504.

Baker, M.L., Baas, J.H., Malarkey, J., Silva Jacinto, R., Craig, M.J., Kane, I.A. and **Barker, S.** (2017) The effect of clay type on the properties of cohesive sediment gravity flows and their deposits. *Journal of Sedimentary Research*, **87**, 1176-1195.

Bale, A.J., Stephens, J.A. and **Harris, C.B.** (2007) Critical erosion profiles in macro-tidal estuary sediments: Implications for the stability of intertidal mud and the slope of mud banks. *Continental Shelf Research*, **27**, 2303-2312.

Baltzer, A., Cochonat, P. and **Piper, D.J.** (1994) In situ geotechnical characterization of sediments on the Nova Scotian Slope, eastern Canadian continental margin. *Marine Geology*, **120**, 291-308.

Bates, D.E.B. (1974) Probable orthocone skip and roll marks from the Aberystwyth Grits. *Geological Magazine*, **111**, 31-34.

Baudet, B.A. and **Ho, E.W.L.** (2004) On the behaviour of deep-ocean sediments. *Géotechnique*, **54**, 571-580.

Bell, D., Stevenson, C.J., Kane, I.A., Hodgson, D.M. and **Poyatos-Moré, M.** (2018) Topographic controls on the development of contemporaneous but contrasting basin-floor depositional architectures. *Journal of Sedimentary Research*, **88**, 1166-1189.

Best, J.L. (1998) The influence of particle rotation on wake stability at particle Reynolds numbers, $Re_p < 300$—implications for turbulence modulation in two-phase flows. *International Journal of Multiphase Flow*, **24**, 693-720.

Best, J.L. and **Leeder, M.R.** (1993) Drag reduction in turbulent muddy seawater flows and some sedimentary consequences. *Sedimentology,* **40**, 1129-1137.

Blatt, H., Middleton, G. and **Murray, R.** (1972) *Origin of Sedimentary Rocks*. Prentice-Hall, New Jersey, 634 pp.

Boggs, S., Jr. (2014) *Principles of Sedimentology and Stratigraphy*, 5th edition, Pearson, Harlow, 564 pp.

Boudreau, B.P. and **Jorgensen, B.B.** (Eds.) (2001) *The Benthic Boundary Layer: Transport Processes and Biogeochemistry*. Oxford University Press, New York, 404 pp.

Bouma, A. (1962) *Sedimentology of some Flysch Deposits: A Graphic Approach to Facies Interpretation*. Elsevier, Amsterdam/New York, 168 pp.

Breien, H., De Blasio, F.V., Elverhøi, A., Nystruen, J.P. and **Harbitz, C.B.** (2010) Transport mechanisms of sand in deep marine environments – insights based on laboratory experiments. *Journal of Sedimentary Research*, **80**, 975–990.

Bridge, J.S. (2003) *River and Floodplains: Forms, Processes and Sedimentary Record*. Blackwell Publishing, Oxford, 491 pp.

Bridge, J.S. and **Demicco, R.V.** (2008) *Earth Surface Processes, Landforms and Sediment Deposits*. Cambridge University Press, Cambridge, 815 pp.

Bromley, R.G. (1996) *Trace Fossils: Biology, Taxonomy and Applications*. Chapman and Hall, London, 361 pp.

Brooks, H.B., Hodgson, D.M., Brunt, R.L., Peakall, J., Hofstra, M. and **Flint, S.S.** (2018a) Deepwater channel-lobe transition zone dynamics: processes and depositional architecture, an example from the Karoo Basin, South Africa. *Geological Society of America Bulletin*, **130**, 1723-1746, doi:10.1130/B31714.1.

Brooks, H.L., Hodgson, D.M., Brunt, R.L., Peakall, J. and **Flint, S.S.** (2018b) Exhumed lateral margins and increasing infill confinement of a submarine landslide complex. *Sedimentology*, **65**, 1067-1096, doi: 10.1111/sed.12415

Buatois, L.A. and **Mángano, M.G.** (2018) The other biodiversity record: Innovation in animal-substrate interactions through geological time. *GSA Today*, **28** (10), 4-10, doi:10.1130/GSATG371A.1

Burland, J.B. (1990) On the compressibility and shear strength of natural clays. *Géotechnique*, **40**, 329-378.

Callow, R.H.T., Kneller, B., Dykstra, M. and **McIlroy, D.** (2014) Physical, biological, geochemical and sedimentological controls on the ichnology of submarine canyon and slope channel systems. *Marine and Petroleum Geology*, **54**, 144-166.

Cantero, M.I., Balachandar, S., García, M.H. and **Bock, D.** (2008) Turbulent structures in planar gravity currents and their influence on the flow dynamics. *Journal of Geophysical Research*, **113**, C08018.

Cantero, M.I., Cantelli, A., Pirmez, C., Balchander, S., Mohrig, D., Hickson, T.A., Yeh, T-h, Naruse, H. and **Parker, G.** (2012) Emplacement of massive turbidites linked to extinction of turbulence in turbidity currents. *Nature Geoscience*, **5**, doi: 10.1038/NGEO1320

Cantero, M.I., Balachander, S., Cantelli, A. and **Parker, G.** (2014) A simplified approach to address turbulence modulation in turbidity currents as a response to slope breaks and loss of lateral confinement. *Environmental Fluid Mechanics*, **14**, 371-385.

Cartigny, M.J.B., Eggenhuisen, J.T., Hansen, E.W.M. and **Postma, G.** (2013) Concentration-dependent flow stratification in experimental high-density turbidity currents and their relevance to turbidite facies models. *Journal of Sedimentary Research*, **83**, 1047-1065.

Cartigny, M.J.B., Ventra, D., Postma, G. and **Van Den Berg, J.H.** (2014) Morphodynamics and sedimentary structures of bedforms under supercritical-flow conditions: New insights from flume experiments. *Sedimentology*, **61**, 712-748.

Clare, M.A., Talling, P.J., Challenor, P., Malgesini, G. and **Hunt, J.** (2014) Distal turbidites reveal a common distribution for large (>0.1 km^3) submarine landslide recurrence. *Geology*, **42**, 263-266.

Clare, M.A., Talling, P.J. and **Hunt, J.E.** (2015) Implications of reduced turbidity current and landslide activity for the initial Eocene Thermal Maximum – evidence from two distal, deep-water sites. *Earth and Planetary Science Letters*, **420**, 102-115.

Clark, C.D. (1993) Mega-scale glacial lineations and cross-cutting ice-flow landforms. *Earth Surface Processes and Landforms*, **18**, 1-29.

Clayton, C.J. (1994) Contrasting sediment gravity flow processes in the late Llandovery, Rhuddnant Grits turbidite system, Welsh Basin. *Geological Journal*, **29**, 167-181.

Cole, P.D., Calder, E.S., Sparks, R.S.J., Clarke, A.B., Druitt, T.H., Young, S.R., Herd, R.A., Harford, C.L. and **Norton, G.E.** (2002) Deposits from dome-collapse pyroclastic flows at Soufrière Hills Volcano, Montserrat. In: *The Eruption of Soufrière Hills Volcano, Montserrat, from 1995 to 1999*, (Eds T.H. Druitt and B.P. Kokelaar), Geological Society of London Memoir 21, 231–262.

Colliat, J.L., Dendani, H., Puech, A. and **Nauroy, J.F.** (2011) Gulf of Guinea deepwater sediments: Geotechnical properties, design issues and installation experiences. In: *Proceedings of the 2nd International Symposium on Frontiers in Offshore Geotechnics* (ISFOG), Perth, Australia, 59-86.

Collinson, J. and **Mountney, N**. (2019) *Sedimentary Structures – 4th edition, Dunedin Academic Press*, Edinburgh, Scotland, 340 pp.

Collinson, J., **Mountney, N.** and **Thompson, D.** (2006) *Sedimentary Structures – 3rd edition*. Terra Publishing, Harpenden, England, 292 pp.

Craig, G.Y. and **Walton, E.K.** (1962) Sedimentary structures and palaeocurrent directions from the Silurian rocks of Kirkcudbrightshire. *Transactions of the Edinburgh Geological Society*, **19**, 100-119.

Crimes, T.P. (1973) From limestones to distal turbidites: a facies and trace fossil analysis in the Zumaya flysch (Paleocene-Eocene), North Spain. *Sedimentology*, **20**, 105-131.

Crimes, T.P. (1976) Sand fans, turbidites, slumps and the origin of the Bay of Biscay: A facies analysis of the Guipuzcoan Flysch. *Palaeogeography, Palaeoclimatology, Palaeoecology*, **19**, 1-15.

Crowell, J.C. (1955) Directional-current structures from the Prealpine Flysch, Switzerland. *Geological Society of America Bulletin*, **66**, 1351-1384.

Crowell, J.C. (1958) Sole markings of graded beds: A discussion. *The Journal of Geology*, **66**, 333-335.

Cummings J.P. and **Hodgson D.M.** (2011a) An agrichnial feeding strategy for deep-marine Paleogene Ophiomorpha group trace fossils. *Palaios*, **26**, 212-224.

Cummings, J.P. and **Hodgson, D.M.** (2011b) Assessing controls on the distribution of ichnotaxa in submarine fan environments, the Basque Basin, Northern Spain. *Sedimentary Geology*, **239**, 162-187.

Cunha, R.S., **Tinterri, R.** and **Muzzi Magalhaes, P.** (2017) Annot Sandstone in the Peïra Cava basin: An example of an asymmetric facies distribution in a confined turbidite system (SE France). *Marine and Petroleum Geology*, **87**, 60-79.

Dade, W.B., Nowell, A.R.M. and **Jumars, P.A.** (1992) Predicting erosion resistance of muds. *Marine Geology*, **105**, 285-297.

Dakin, N., Pickering, K.T., Mohrig, D. and **Bayliss, N.J.** (2013) Channel-like features created by erosive submarine debris flows: Field evidence from the Middle Eocene Ainsa Basin, Spanish Pyrenees. *Marine and Petroleum Geology*, **41**, 62-71.

Dasgupta, P. and **Mann, P.** (2011) Geometrical mechanism of inverse grading in grain-flow deposits: An experimental revelation. *Earth-Science Reviews*, **104**, 186-198.

Davies, A.G. (1982) The reflection of wave energy by undulations on the seabed. *Dynamics of Atmospheres and Oceans*, **6**, 207-232.

Davis, C., Haughton, P., McCaffrey, W., Scott, E., Hogg, N. and **Kitching, D.** (2009) Character and distribution of hybrid sediment gravity flow deposits from the outer Forties fan, Palaeocene Central North Sea, UKCS. *Marine and Petroleum Geology*, **26**, 1919-1939.

De Blasio, F.V., Engvik, L.E. and **Elverhoi, A.** (2006) Sliding of outrunner blocks from submarine landslides. *Geophysical Research Letters*, **33**, L06614.

de Jager, J. (1979) The relation between tectonics and sedimentation along the 'Sillaro line' (northern Appennines, Italy). *Geologica Ultraiectina*, **19**, 1-97.

Denny, M.W. (1989) Invertebrate mucous secretions: functional alternatives to vertebrate paradigms. *Symposia of the Society for Experimental Biology*, **43**, 337-366.

De Rooij, F. and **Dalziel, S.B.** (2001) Time-and space-resolved measurements of deposition under turbidity currents. In: *Particulate Gravity Currents* (Eds W.D. McCaffrey, B.C. Kneller and J. Peakall), *International Association of Sedimentologists Special Publication*, 31, 207–215.

Deville, E., Mascle, A., Callec, Y., Huyghe, P., Lallemant, S., Lerat, O., Mathieu, X., Padron de Carillo, C., Patriat, M., Pichot, T., Loubrieux, B. and **Granjeon, D.** (2015) Tectonics and sedimentation interactions in the east Caribbean subduction zone: an overview from the Orinoco delta and the Barbados accretionary prism. *Marine and Petroleum Geology***, 64**, 76–103.

Dickhudt, P.J., Friedrichs, C.T. and **Sanford, L.P.** (2011) Mud matrix solids fraction and bed erodibility in the York River estuary, USA, and other muddy environments. *Continental Shelf Research*, **31**, S3-S13.

Dirnerová, D. and **Janočko, J.** (2014) Sole structures as a tool for depositional environment interpretation; a case study from the Oligocene Cergowa Sandstone, Dukla Unit (Outer Carpathians, Slovakia). *Geological Quarterly*, **58**, 41-50.

Draganits, E., Schlaf, J., Grasemann, B. and **Argles, T.** (2008) Giant submarine landslide grooves in the Neoproterozoic / Lower Cambrian Phe Formation, Northwest Himalaya: Mechanisms of formation and palaeogeographic implications. *Sedimentary Geology*, **205**, 126-141.

Drake, T.G., Shreve, R.L., Dietrich, W.E., Whiting, P.J. and **Leopold, L.B.** (1988) Bed load transport of fine gravel observed by motion-picture photography. *Journal of Fluid Mechanics*, **192**, 193-217.

Ducassou, E., Migeon, S., Capotondi, L. and **Mascle, J.** (2013) Run-out distance and erosion of debris-flows in the Nile deep-sea fan system: Evidence from lithofacies and micropalaeontological analyses. *Marine and Petroleum Geology*, **39**, 102-123.

Dunbar, C.O. and **Rodgers, J.** (1957) *Principles of Stratigraphy*. Wiley, New York.

Dutkiewicz, A., Müller, R.D., O'Callaghan, S. and **Jónasson, H.** (2015) Census of seafloor sediments in the world's ocean. *Geology*, **43**, 795-798.

Dżułyński, S. (1965) New data on experimental production of sedimentary structures. *Journal of Sedimentary Petrology*, **35**, 196-212.

Dżułyński, S. (1996) Erosional and deformational structures in single sedimentary beds: a genetic commentary. *Annales Societatis Geologorum Poloniae*, **66**, 101-189.

Dżułyński, S. (2001) *Atlas of Sedimentary Structures from the Polish Flysch Carpathians*. 12th meeting of the association of European Geological Societies, 132 pp.

Dżułyński, S. and **Radomski, A.** (1955) Origin of groove casts in the light of turbidity current hypothesis. *Acta Geologica Polonica*, **5**, 47-56.

Dżułyński. S. and **Sanders, J.E.** (1962a) Current marks on firm mud bottoms. *Transactions of the Connecticut Academy of Arts and Sciences*, **42**, 57-96.

Dżułyński. S. and **Sanders, J.E.** (1962b) On some current markings in flysch. *Annales Societatis Geologorum Poloniae*, **32**, 143-146.

Dżułyński. S. and **Simpson, F.** (1966) Experiments on interfacial current markings. *Geologica Romana*, **5**, 197-214.

Dżułyński, S. and **Ślączka, A.** (1958) Directional structures and sedimentation in the Krosno Beds (Carpathian flysch). *Annales Societatis Geologorum Poloniae*, **28**, 205-259.

Dżułyński, S. and **Ślączka, A.** (1960) Sole markings produced by fish bones acting as tools. *Annales Societatis Geologorum Poloniae*, **30**, 249-255.

Dżułyński, S. and **Walton, E.K.** (1963) Experimental production of sole markings. *Transactions of the Edinburgh Geological Society*, **19**, 279-305.

Dżułyński, S. and **Walton, E.K.** (1965) *Sedimentary Features of Flysch and Greywackes*. Developments in Sedimentology 7, Elsevier, Amsterdam, 274 pp.

Dżułyński, S., Ksiazkiewicz, M. and **Kuenen, Ph.H.** (1959) Turbidites in flysch of the Polish Carpathian Mountains. *Geological Society of America Bulletin*, **70**, 1089-1118.

Edwards, D.A., Leeder, M.R., Best, J.L. and **Pantin, H.M. (1994)** On experimental reflected density currents and the interpretation of certain turbidites. *Sedimentology*, **41**, 437-461.

Ehlers, C.J., Chen, J., Roberts, H.H. and **Lee, Y.C.** (2005) The origin of near-seafloor crust zones in deepwater. In: *Proceedings of the International Symposium on Frontiers in Offshore Geotechnics*, ISFOG 2005, Perth, 927-934.

Elder, H.Y. and **Hunter, R.D.** (1980) Burrowing of Priapulus caudatus (Vermes) and the significance of the direct peristaltic wave*. Journal of Zoology*, **191**, 333-351.

Elliott, T. (2000) Megaflute erosion surfaces and the initiation of turbidite channels. *Geology*, **28**, 119–122.

Enos, P. (1969a) Anatomy of a flysch. *Journal of Sedimentary Petrology*, **39**, 680-723.

Enos, P. (1969b) Cloridorme Formation, Middle Ordovician Flysch, Northern Gaspé Peninsula, Quebec. *Geological Society of America Special Paper*, **117**, 66 pp.

Felix, M. and **Peakall, J**. (2006) Transformation of debris flows into turbidity currents: mechanisms inferred from laboratory experiments. *Sedimentology*, **53**, 107-123.

Felix, M., Leszczynzki, S., Slaczka, A., Uchman, A., Amy, L. and **Peakall, J.** (2009) Field expressions of the transformation of debris flows into turbidity currents, with examples from the Polish Carpathians and the French Maritime Alps. *Marine and Petroleum Geology*, **26**, 2011-2020.

Fernandes, S., Sobral, P. and **Costa, M.H.** (2006) Nereis diversicolor effect on the stability of cohesive intertidal sediments. *Aquatic Ecology*, **40**, 567-579.

Fernandez Luque, R. and **Van Beek, R.** (1976) Erosion and transport of bed load sediment. *Journal of Hydraulic Research*, **14**, 127-144.

Fleming, T.P. and **Richards, K.S.** (1982) Uptake and surface adsorption of zinc by the freshwater tubificid oligochaete Tubifex tubifex. *Comparative Biochemistry and Physiology Part C: Comparative Pharmacology*, **71**, 69-75.

Flemings, P.B., Behrmann, J.H., John, C.M. and **Expedition 308 Scientists** (2006) *Gulf of Mexico Hydrogeology. Proc. Int. Ocean Drill. Program*, **38**, Integrated Ocean Drilling Program Management International, Incorporated, College Station, TX.

Fonnesu, M., Haughton, P., Felletti, F. and **McCaffrey, W.** (2015) Short length-scale variability of hybrid event beds and its applied significance. *Marine and Petroleum Geology*, **67**, 583-603.

Fonnesu, M., Patacci, M., Haughton, P.D.W., Felletti, F. and **McCaffrey, W.D.** (2016) Hybrid event beds generated by local substrate delamination on a confined-basin floor. *Journal of Sedimentary Research*, **86**, 929-943.

Fonnesu, M., Felletti, F., Haughton, P.D.W., Patacci, M. and **McCaffrey, W.D.** (2018) Hybrid event bed character and distribution linked to turbidite system sub-environments: The North Appenine Gottero Sandstone (north-west Italy). *Sedimentology*, **65**, 151-190, doi: 10.1111/sed.12376.

Francis, J.R.D. (1973) Experiments on the motion of solitary grains along the bed of a water-stream. *Proceedings of the Royal Society of London A*, **332**, 443-471.

Friend, P.L., Collins, M.B. and **Holligan, P.M.** (2003) Day–night variation of intertidal flat sediment properties in relation to sediment stability. *Estuarine, Coastal and Shelf Science*, **58**, 663-675.

Fuchs, T. (1895) Studien über Fucoiden und Hieroglyphen. *Denkschriften der Kaiserlichen Akademie der Wissenschaften, Mathematisch-Naturwissenschaftliche Klasse, Wien*, **62**, 369-448.

Gee, M.J.R., Gawthorpe, R.L. and **Friedmann, S.J.** (2005) Giant striations at the base of a submarine slide. *Marine Geology*, **214**, 287-294.

Gingras, M.K., Pemberton, S.G., Dashtgard, S. and **Dafoe, L.** (2008) How fast do marine invertebrates burrow? *Palaeogeography, Palaeoclimatology, Palaeoecology*, **270**, 280-286.

Glaessner, M.F. (1958) Sedimentary flow structures on bedding planes. *Journal of Geology*, **66**, 1-7.

Grabowski, R.C., Droppo, I.G. and **Wharton, G.** (2011) Erodibility of cohesive sediment: the importance of sediment properties. *Earth-Science Reviews*, **105**, 101-120.

Gray, J.M.N.T. and **Kokelaar, B.P.** (2010) Large particle segregation, transport and accumulation in granular free-surface flows. *Journal of Fluid Mechanics*, **652**, 105-137.

Grundvåg, S-A., Johannessen, E.P., Helland-Hansen, W. and **Plink-Björklund, P.** (2014) Depositional architecture and evolution of progradationally stacked lobe complexes in the Eocene Central Basin of Spitsbergen. *Sedimentology*, **61**, 535-569.

Grupe, B., Becker, H.J. and **Oebius, H.U.** (2001) Geotechnical and sedimentological investigations of deep-sea sediments from a manganese nodule field of the Peru Basin. *Deep Sea Research Part II: Topical Studies in Oceanography*, **48**, 3593-3608.

Gust, G. (1976) Observations on turbulent-drag reduction in a dilute suspension of clay in sea-water. *Journal of Fluid Mechanics,* **75**, 29–47.

Gust, G. and **Walger, E.** (1976) The influence of suspended cohesive sediments on boundary-layer structure and erosive activity of turbulent sea water flow. *Marine Geology,* **22**, 189–206.

Haines, P.W., Jago, J.B. and **Gum, J.C.** (2001) Turbidite deposition in the Cambrian Kanmantoo Group, South Australia. *Australian Journal of Earth Sciences*, **48**, 465-478.

Hall, J. (1843) *Geology of New York, Part 4*, *Comprising the Survey of the Fourth Geological District*. Charles Van Benthuyson and Sons, Albany, 683 pp.

Hammond, R. A. (1970) The burrowing of Priapulus caudatus. *Journal of Zoology*, **162**, 469-480.

Hampton, M.A. (1970) *Subaqueous Debris Flow and Generation of Turbidity Currents*. Unpublished doctoral dissertation, Stanford University, California, 180 pp.

Hampton, M.A. (1975) Competence of fine grained debris flows. *Journal of Sedimentary Petrology*, **45**, 833–844.

Harms, J.C. (1969) Hydraulic significance of some sand ripples. *Geological Society of America Bulletin*, **80**, 363-396.

Harms, J.C. and **Fahnestock, R.K.** (1965) Stratification, bed forms, and flow phenomena (with and example from the Rio Grande). In: *Primary Sedimentary Structures and their Hydrodynamic Interpretation* (Ed G.V. Middleton), SEPM Special Publication, 12, 84-115.

Haughton, P.D., Barker, S.P. and **McCaffrey, W.D.** (2003) 'Linked' debrites in sand-rich turbidite systems–origin and significance. *Sedimentology*, **50**, 459-482.

Haughton, P., Davis, C., McCaffrey, W. and **Barker, S.** (2009) Hybrid sediment gravity flow deposits classification, origin and significance. *Marine and Petroleum Geology*, **26**, 1900-1918.

Heard, T.G. and **Pickering, K.T.** (2008). Trace fossils as diagnostic indicators of deep-marine environments, Middle Eocene Ainsa-Jaca basin, Spanish Pyrenees. *Sedimentology*, **55**, 809-844.

Heard, T.G., Pickering, K.T. and **Clark, J.D.** (2014) Ichnofabric characterization of a deep-marine clastic system: a subsurface study of the Middle Eocene Ainsa system, Spanish Pyrenees. *Sedimentology*, **61**, 1298-1331.

Henstra, G.A., Grundvåg, S.A., Johannessen, E.P., Kristensen, T.B., Midtkandal, I., Nystuen, J.P., Rotevatn, A., Surlyk, F., Saether, T. and **Windelstad, J.** (2016) Depositional processes and stratigraphic architecture within a coarse-grained rift-margin turbidite system: The Wollaston Forland Group, east Greenland. *Marine and Petroleum Geology*, **76**, 187-209.

Hermidas, N., Eggenhuisen, J.T., Jacinto, R.S., Luthi, S.M., Toth, F. and **Pohl, F.** (2018) A classification of clay-rich subaqueous density flow structures. *Journal of Geophysical Research: Earth Surface*, **123**, 945–966, doi.org/10.1002/2017JF004386.

Hill, A.J., Evans, T.G., Mackenzie, B. and **Thompson, G.** (2011) Deepwater Angola part II: Geotechnical Challenges. In: *Frontiers in Offshore Geotechnics II* (Eds S. Gourvenec and D. White), 215-220.

Hiscott, R.N. (1994) Traction-carpet stratification in turbidites – fact or fiction. *Journal of Sedimentary Research*, **64**, 204–208.

Hiscott, R.N., Pickering, K.T., Bouma, A.H., Hand, B.M., Kneller, B.C., Postma, G. and **Soh, W.** (1997) Basin-floor fans in the North Sea: Sequence stratigraphic models vs. sedimentary facies: Discussion. *AAPG Bulletin*, **81**, 662-665.

Hodgson, D.M. (2009) Origin and distribution of bipartite beds in sand-rich submarine fans: Constraints from the Tanqua depocentre, Karoo Basin, South Africa. *Marine and Petroleum Geology*, **26**, 1940–1956.

Hofstra, M., Hodgson, D.M., Peakall, J. and **Flint, S.S.** (2015) Giant scour-fills in ancient channel-lobe transition zones: Formative processes and depositional architecture. *Sedimentary Geology,* **329**, 98-114.

Houwing, E.J. (1999) Determination of the critical erosion threshold of cohesive sediments on intertidal mudflats along the Dutch Wadden Sea coast. *Estuarine, Coastal and Shelf Science*, **49**, 545-555.

Howe, M.P.A. (1999) The Silurian fauna (graptolite and nautiloid) of the Niarbyl Formation, Isle of Man. In: *In Sight of the Suture: the Palaeozoic Geology of the Isle of Man in its Iapetus Ocean Context* (Eds N.H. Woodcock, D.G. Quirk, W.R. Fitches and R.P. Barnes). *Geological Society London Special Publications*, **160**, 177-187.

Hsu, K.J. (1959) Flute- and groove-casts in the Prealpine Flysch, Switzerland. *American Journal of Science*, **257**, 529–536.

Hubbard, S.M., Covault, J.A., Fildani, A. and **Romans, B.W.** (2014). Sediment transfer and deposition in slope channels: Deciphering the record of enigmatic deep-sea processes from outcrop. *Geological Society of America Bulletin*, **126**, 857-871.

Hughes Clarke, J.E. (2016) First wide-angle view of channelized turbidity currents links migrating cyclic steps to flow characteristics. *Nature Communications*, **7**:11896.

Ilstad, T., Marr, J.G., Elverhøi, A. and **Harbitz, C.B.** (2004a) Laboratory studies of subaqueous debris flows by measurements of pore-fluid pressure and total stress. *Marine Geology*, **213**, 404-414.

Ilstad, T., Elverhøi, A., Issler, D. and **Marr, J.G.** (2004b) Subaqueous debris flow behaviour and its dependence on the sand/clay ratio: a laboratory study using particle tracking. *Marine Geology*, **213**, 415–438.

Iverson, R.M. (1997) The physics of debris flows. *Reviews of Geophysics*, **35**, 245-296.

Iverson, R.M. (2005) Regulation of landslide motion by dilatancy and pore-pressure feedback. *Journal of Geophysical Research: Earth Surface*, **110**, F02015.

Iverson, R.M., Reid, M.E. and **LaHusen, R.G.** (1997) Debris-flow mobilization from landslides. *Annual Review of Earth & Planetary Science*, **25**, 85-138.

Iverson, R.M., Reid, M.E., Iverson, N.R., LaHusen, R.G., Logan, M., Mann, J.E. and **Brien, D.L.** (2000) Acute sensitivity of landslide rates to initial soil porosity. *Science*, **290**, 513‑516.

Iverson, R.M., Logan, M., LaHusen, R.G. and **Berti, M.** (2010) The perfect debris flow? Aggregated results from 28 largescale experiments. *Journal of Geophysical Research*, **115**, F03005.

Jackson, C.A-L., Zakaria, A.A., Johnson, H.D., Tongkul, F. and **Crevello, P.D.** (2009) Sedimentology, stratigraphic occurrence and origin of linked debrites in the West Crocker Formation (Oligo-Miocene), Sabah, NW Borneo. *Marine and Petroleum Geology*, **26**, 1957-1973.

Jobe, Z.R., Bernhardt, A. and **Lowe, D.R.** (2010) Facies and architectural asymmetry in a conglomerate-rich submarine channel fill, Cerro Toro Formation, Sierra del Toro, Magallanes Basin, Chile. *Journal of Sedimentary Research*, **80**, 1085‑1108.

Johansson, M. and **Stow, D.A.V.** (1995) A classification scheme for shale clasts in deep water sandstones. In: *Characterization of Deep Marine Clastic Systems*, (Eds A.J. Hartley, and D.J. Prosser), *Geological Society Special Publication,* 94, 221-241.

Johns, D.D., Mutti, E., Rosell, J. and **Seguret, M.** (1981) Origin of a thick, redeposited carbonate bed in Eocene turbidites of the Hecho Group, South-central Pyrenees, Spain. *Geology*, **9**, 161–164.

Johnson, C.G., Kokelaar, B.P., Iverson, R.M., Logan, M., LaHusen, R.G. and **Gray, J.M.N.T.** (2012) Grain-size segregation and levee formation in geophysical mass flows. *Journal of Geophysical Research – Earth Surface*, **117**, F01032.

Jørgensen, K.D. and **Posner, A.S.** (1959) Study of the setting of plaster. *Journal of Dental Research*, **38**, 491-499.

Kamphuis, J.W. and **Hall, K.R.** (1983) Cohesive material erosion by unidirectional current. *Journal of Hydraulic Engineering*, **109**, 49-61.

Kane, I.A., McCaffrey, W.D., Peakall, J. and **Kneller, B.C.** (2010) Submarine channel levee shape and sediment waves from physical experiments. *Sedimentary Geology*, **223**, 75-85.

Kane, I.A., Pontén, A.S.M., Vangdal, B., Eggenhuisen, J.T., Hodgson, D.M. and **Spychala, Y.T.** (2017). The stratigraphic record and processes of turbidity current transformation across deep-marine lobes. *Sedimentology*, **64**, 1236-1273.

Kastens, K.A. (1984) Earthquakes as a triggering mechanism for debris flows and turbidites on the Calabrian Ridge. *Marine Geology*, **55**, 13-33.

Kelling, G. and **Walton, E.K.** (1957) Load-cast structures: Their relationship to upper-surface structures and their mode of formation. *Geological Magazine*, **94**, 481-491.

Kelling, G., Walton, E.K. and **Simpson, F.** (2007) The contribution of Stanislaw Dżułyński to flysch sedimentology: A 'western' perspective. *Annales Societatis Geologorum Poloniae*, **77**, 93-103.

Kenrick, P., Wellman, C.H., Schneider, H. and **Edgecombe, G.D.** (2012) A timeline for terrestrialization: consequences for the carbon cycle in the Palaeozoic. *Philosophical Transactions of the Royal Society of London, Series B*, **367**, 519–536.

Klaucke, I., Hesse, R. and **Ryan, W.B.F.** (1997) Flow parameters of turbidity currents in a low sinuosity giant deep-sea channel. *Sedimentology*, **44**, 1093–1102.

Knaust, D., Warchol, M. and **Kane, I.A.** (2014) Ichnodiversity and ichnoabundance: Revealing depositional trends in a confined turbidite system. *Sedimentology*, **61**, 2218-2267.

Kneller, B.C. and **Branney, M.J.** (1995) Sustained high-density turbidity currents and the deposition of thick massive sands. *Sedimentology*, **42**, 607–616.

Kneller, B. and **McCaffrey, W.** (1999) Depositional effects of flow nonuniformity and stratification within turbidity currents approaching a bounding slope: Deflection, reflection, and facies variation. *Journal of Sedimentary Research*, **69**, 980-991.

Kneller, B. and **McCaffrey, W.D.** (2003) The interpretation of vertical sequences in turbidite beds: the influence of longitudinal flow structure. *Journal of Sedimentary Research*, **73**, 706–713.

Krecic, M.R. and **Hanes, D.M.** (1997) An analysis of particle saltation dynamics. *Coastal Engineering, 1996*, Volume 4, Proceedings 25th International Conference, Sept. 2-6, 1996, Orlando, Fl., 3846-3859.

Kuenen, Ph.H. (1953) Significant features of graded bedding. *AAPG Bulletin*, **37**, 1044-1066.

Kuenen, Ph.H. (1957) Sole markings of graded greywacke beds. *The Journal of Geology*, **65**, 231-258.

Kuenen, Ph.H. (1966) Matrix of turbidites: experimental approach. *Sedimentology*, **7**, 267–297.

Kuenen, Ph.H. and **Sanders, J.E.** (1956) Sedimentation phenomena in Kulm and Flozleeres graywackes, Saverland and Oberharz, Germany. *American Journal of Science*, **254**, 649-671.

Kuenen, Ph.H. and **Ten Haaf, E.** (1958) Sole markings of graded greywacke beds: A reply. *The Journal of Geology*, **66**, 335-337.

Kuijpers, A., Nielsen, T., Akhmetzhanov, A., de Haas, H., Kenyon, N.H. and **van Veering, T.C.E.** (2001) Late Quaternary slope instability on the Faeroe margin: mass flow features and timing of events. *Geo-Marine Letters*, **20**, 149-159.

Kuo, M. and **Bolton, M.** (2013) The nature and origin of deep ocean clay crust from the Gulf of Guinea. *Géotechnique*, **63**, 500-509.

Labaume, P., Mutti, E. and **Seguret, M.** (1987) Megaturbidites – a depositional model from the Eocene of the SW-Pyrenean Foreland Basin. *Geo-Marine Letters*, **7**, 91–101.

Lanteaume, M., Beaudoin, B. and **Campredon, R.** (1967) *Figures Sédimentaires du Flysch Grés D'Annot du Synclinal de Peira-Cava*. Centre National de la Reserche Scientifique, 104 pp.

Lee, H-Y. and **Hsu, I-S.** (1994) Investigation of saltating particle motions. *Journal of Hydraulic Engineering*, **120**, 831-845.

Leeder, M. (2011) *Sedimentology and Sedimentary Basins: From Turbulence to Tectonics*. Wiley-Blackwell, Oxford, 768 pp.

Leszczyński, S. (1989) Characteristics and origin of fluxo-turbidites from the Carpathian flysch (Cretaceous-Palaeogene), south Poland. *Annales Societatis Geologorum Poloniae*, **59**, 351-390.

Li, M.Z. and **Gust, G.** (2000) Boundary layer dynamics and drag reduction in flows of high cohesive sediment suspensions. *Sedimentology*, **47**, 71–86.

Lovell, J.P.B. (1969) Tyee Formation: A study of proximality in turbidites. *Journal of Sedimentary Petrology*, **39**, 935-953.

Lowe, D.R. (1976a) Grain flow and grain flow deposits. *Journal of Sedimentary Petrology*, **46**, 188-199.

Lowe, D.R. (1976b) Subaqueous liquefied and fluidised sediment flows and their deposits. *Sedimentology*, **23**, 285–308.

Lowe, D.R. (1979) Sediment gravity flows: Their classification and some problems of application to natural flows and deposits. In: *Geology of Continental Slopes*, (Eds L.J. Doyle and O.H. Pilkey, Jr.), *SEPM Special Publication*, 27, 75-82.

Lowe, D.R. (1982) Sediment gravity flows. 2. Depositional models with special reference to high density turbidity currents. *Journal of Sedimentary Petrology*, **52**, 279–298.

Lundkvist, M., Grue, M., Friend, P.L. and **Flindt, M.R.** (2007) The relative contributions of physical and microbiological factors to cohesive sediment stability. *Continental Shelf Research*, **27**, 1143-1152.

Luthi, S.M., Hodgson, D.M., Geel, C.R., Flint, S.S., Goedbloed, J.W., Drinkwater, N.J. and **Johannessen, E.P.** (2006) Contribution of research borehole data to modelling of fine-grained turbidite reservoir analogues, Permian Tanqua-Karoo basin-floor fans (South Africa). *Petroleum Geoscience*, **12**, 175-190.

Macdonald, H.A., Wynn, R.B., Huvenne, V.A., Peakall, J., Masson, D.G., Weaver, P.P. and **McPhail, S.D.** (2011a) New insights into the morphology, fill, and remarkable longevity (>0.2 m.y.) of modern deep-water erosional scours along the northeast Atlantic margin. *Geosphere*, **7**, 845-867.

Macdonald, H.A., Peakall, J., Wignall, P.B. and **Best, J.** (2011b) Sedimentation in deep-sea lobe-elements: implications for the origin of thickening-upward sequences. *Journal of the Geological Society of London*, **168**, 319–331.

Major, J.J. and **Iverson, R.M.** (1999) Debris-flow deposition: effects of pore-fluid pressure and friction concentrated at flow margins. *Geological Society of America Bulletin*, **111**, 1424–1434.

Malarkey, J., Baas, J.H., Hope, J.A., Aspden, R.J., Parsons, D.R., Peakall, J., Paterson, D.M., Schindler, R.J., Ye, L., Lichtman, I.D., Bass, S.J., Davies, A.G., Manning, A.J. and **Thorne, P.D.** (2015) The pervasive role of biological cohesion in bedform development. *Nature Communications*, **6**, 6257.

Malkowski, M.A., Sharman, G.R., Graham, S.A. and **Fildani, A.** (2017) Characterisation and diachronous initiation of coarse clastic deposition in the Magallanes-Austral foreland basin, Patagonian Andes. *Basin Research*, **29**, 298-326.

Malkowski, M.A., Jobe, Z.R., Sharman, G.R. and **Graham, S.A.** (2018) Downslope facies variability within deep-water channel systems: Insights from the Upper Cretaceous Cerro Toro Formation, southern Patagonia. *Sedimentology*, **65**, 1918-1946, doi: 10.1111/sed.12452

Màngano, M.E., Buatois, L.A., Wilson, M. and **Droser, M.** (2016) The Great Ordovician biodiversification event. In: *The Trace-Fossil Record of Major Evolutionary Events*, (Eds M.G. Màngano and L.A. Buatois), Topics in Geobiology, 39, 127-156.

Marr, J.G., Harff, P.A., Shanmugam, G. and **Parker, G.** (2001) Experiments on subaqueous sandy gravity flows: The role of clay and water content in flow dynamics and depositional structures. *Geological Society of America Bulletin*, **113**, 1377-1386.

McBride, E.F. (1962) Flysch and associated beds of the Martinsburg-Formation (Ordovician), central Appalachians. *Journal of Sedimentary Petrology*, **32**, 39-91.

McCave, I.N. (1984) Erosion, transport and deposition of fine-grained marine sediments. In: *Fine-grained Sediments: Deep Sea Processes and Facies* (Eds D.A.V. Stow and D.J.W. Piper), *Geological Society London Special Publications*, **15**, 35-69.

McCave, I.N., Manighetti, B. and **Robinson, S.G.** (1995) Sortable silt and fine sediment size/composition slicing: Parameters for palaeocurrent speed and palaeoceanography. *Paleoceanography*, **10**, 593-610.

Meadows, P.S. and **Meadows, A.** (Eds) (1991) *The Environmental Impact of Burrowing Animals and Animal Burrows*, Clarendon Press, Oxford, UK, 368 pp.

Meadows, A. and **Meadows, P.S.** (1994) Bioturbation in deep sea Pacific sediments. *Journal of the Geological Society*, **151**, 361-375.

Meadows, P.S. and **Tait, J.** (1989) Modification of sediment permeability and shear strength by two burrowing invertebrates. *Marine Biology*, **101**, 75-82.

Meadows, P.S., Tait, J. and **Hussain, S.A.** (1990) Effects of estuarine infauna on sediment stability and particle sedimentation. *Hydrobiologia*, **190**, 263-266.

Meadows, P.S., Reichelt, A.C., Meadows, A. and **Waterworth, J.S.** (1994) Microbial and meiofaunal abundance, redox potential, pH and shear strength profiles in deep sea Pacific sediments. *Journal of the Geological Society*, **151**, 377-390.

Mehta, A.J., Hayter, E.J., Parker, W.R., Krone, R.B. and **Teeter, A.M.** (1989) Cohesive sediment transport I: Process description. *Journal of Hydraulic Engineering*, **115**, 1076-1093.

Middleton, G.V. (1967) experiments on density and turbidity currents. III Deposition of sediment. *Canadian Journal of Earth Sciences*, **4**, 475-505.

Middleton, G.V. (1970) Experimental studies related to problems of flysch sedimentation. In: *Flysch Sedimentology in North America*, (Ed J. Lajoie), *The Geological Association of Canada Special Paper*, 7, 253-272.

Middleton, G.V. and **Hampton, M.A.** (1973) Sediment gravity flows: mechanics of flow and deposition. In: *Turbidites and Deep-water Sedimentation* (Eds G.V. Middleton and A.H. Bouma), SEPM Pacific Section short course, 1-38.

Middleton, G.V. and **Hampton, M.A.** (1976) Subaqueous sediment transport and deposition by sediment gravity flows. In: *Marine Sediment Transport and Environmental Management* (Eds D.H. Stanley and D.J.P. Swift), John Wiley & Sons, New York, 197-218.

Miller, M.C. and **Komar, P.D.** (1977) The development of sediment threshold curves for unusual environments (Mars) and for inadequately studied materials (foram sands). *Sedimentology*, **24**, 709-721.

Mohrig, D., Ellis, C., Parker, G., Whipple, K.X. and **Hondzo, M.** (1998) Hydroplaning of subaqueous debris flows. *Geological Society of America Bulletin*, **110**, 387-394.

Moore, H.B. (1931) The specific identification of faecal pellets. *Journal of the Marine Biological Association of the United Kingdom*, **17**, 359-365.

Mulder, T. and **Alexander, J.** (2001) Abrupt change in slope causes variation in the deposit thickness of concentrated particle-driven density currents. *Marine Geology*, **175**, 221-235.

Mulder, T., **Migeon, S., Savoye, B.** and **Faugères, J-C.** (2002) Reply to discussion by Shanmugam on Mulder et al. (2001, Geo-Marine Letters 21: 86-93) Inversely graded turbidite sequences in the deep Mediterranean. A record of deposits from flood-generated turbidity currents? *Geo-Marine Letters*, **22**, 112-120.

Murakami, K. and **Hanada, M.** (1956) Studies on the viscosity of Plaster of Paris. *Gypsum and Lime*, **22**, 1179-1183.

Murray, J.M., Meadows, A. and **Meadows, P.S.** (2002) Biogeomorphological implications of microscale interactions between sediment geotechnics and marine benthos: a review. *Geomorphology*, **47**, 15-30.

Mutti, E. (1992) *Turbidite Sandstones*. Istituto di Geologia Universitá di Parma & AGIP, San Donato Milanese, 275 pp.

Mutti, E. and **Nilsen, T.H.** (1981) Significance of intraformational rip-up clasts in deep-sea fan deposits. In: *International Association of Sedimentologists, 2^{nd} European Regional Meeting*, Bologna, 117-119.

Mutti, E. and **Normark W.R.** (1987) Comparing examples of modern and ancient turbidite systems: Problems and concepts. In: *Marine Clastic Sedimentology: Concepts and Case Studies* (Eds J.K. Legget and G.G. Zuffa), Graham & Trotman, 1-38.

Mutti, E., Ricci Lucchi, F. and **Roveri, M.** (2002) *Revisiting Turbidites of the Marnoso-arenacea Formation and their Basin-Margin Equivalents: Problems with Classic Models*. Excursion Guidebook. Workshop organized by Dipartimento di Scienze della Terra (Universita` di Parma) and Eni-Divisione Agip, 64th EAGE Conference and Exhibition, Florence, Italy, May 27–30, 120 pp.

Mutti, E., Tinterri, R., Benevelli, G., di Biase, D. and **Cavanna G.** (2003) Deltaic, mixed and turbidite sedimentation of ancient foreland basins. *Marine and Petroleum Geology*, **20**, 733-755.

Mutti, E., Benoulli, D., Ricci Lucchi, F. and **Tinterri, R.** (2009) Turbidite and turbidity currents from Alpine 'flysch' to the exploration of continental margins. *Sedimentology*, **56**, 267–318.

Muzzi Magalhaes, P. and **Tinterri, R.** (2010) Stratigraphy and depositional setting of slurry and contained (reflected) beds in the Marnoso-arenacea Formation (Langhian-Serravallian) Northern Apennines, Italy. *Sedimentology*, **57**, 1685-1720.

Nissen, S.E., Haskell, N.L., Steiner, C.T. and **Cotterill, K.L.** (1999) Debris flow outrunner blocks, glide tracks, and pressure ridges identified on the Nigerian continental slope using 3-D seismic coherency. *The Leading Edge*, **18**, 595-599.

Oehmig, R. (1993) Entrainment of planktonic foraminifera: Effect of bulk density. *Sedimentology*, **40**, 869-877.

Orr, J.R. (2001) Colonization of the deep-marine environment during the early Phanerozoic: the ichnofaunal record. *Geological Journal*, **36**, 265-278.

Ortiz-Karpf, A., Hodgson, D.M., Jackson, C.A.-L. and **McCaffrey, W.D.** (2017) Influence of seabed morphology and substrate composition on mass-transport flow processes and pathways: Insights from the Magdalena Fan, offshore Colombia. *Journal of Sedimentary Research*, **87**, 189-209.

Panagiotopoulos, I., Voulgaris, G. and **Collins, M.B.** (1997) The influence of clay on the threshold of movement of fine sandy beds. *Coastal Engineering*, **32**, 19-43.

Pantin, H.M. (1979) Interaction between velocity and effective density in turbidity flow: phase-plane analysis, with criteria for autosuspension. *Marine Geology*, **31**, 59-99.

Parchure, T.M. and **Mehta, A.J.** (1985) Erosion of soft cohesive sediment deposits. *Journal of Hydraulic Engineering*, **111**, 1308-1326.

Parkash, B. and **Middleton, G.V.** (1970) Downcurrent textural changes in Ordovician turbidite greywackes. *Sedimentology*, **14**, 259-293.

Parker, G., Fukushima, Y. and **Pantin, H.M.** (1986) Self-accelerating turbidity currents. *Journal of Fluid Mechanics*, **171**, 145-181.

Parkes, R.J., Cragg, B.A. and **Wellsbury, P.** (2000) Recent studies on bacterial populations and processes in subseafloor sediments: a review. *Hydrogeology Journal*, **8**, 11-28.

Parnell, K.E. and **Kofoed-Hansen, H.** (2001) Wakes from large high-speed ferries in confined coastal waters; management approaches with examples from New Zealand and Denmark. *Coastal Management*, **29**, 217-237.

Parsons, D.R., Schindler, R.J., Hope, J.A., Malarkey, J., Baas, J.H., Peakall, J., Manning, A.J., Ye, L., Simmons, S., Paterson, D.M., Aspden, R.J., Bass, S.J., Davies, A.G., Lichtman, I.D. and **Thorne, P.D.** (2016) The role of biophysical cohesion on subaqueous bed form size. *Geophysical Research Letters*, **43**, 1566-1573.

Patacci, M., Haughton, P.D.W. and **McCaffrey, W.D.** (2014) Rheological complexity in sediment gravity flows forced to decelerate against a confining slope, Braux, SE France. *Journal of Sedimentary Research*, **84**, 270-277.

Paull, C.K., Talling, P.J., Maier, K.L., Parsons, D., Xu, J., Caress, D.W., Gwiazda, R., Lundsten, E.M., Anderson, K., Barry, J.P., Chaffey, M., O'Reilly, T., Rosenberger, K.J., Gales, J.A., Kieft, B., McGann, M., Simmons, S.M., McCann, M., Sumner, E.J., Clare, M.A. and **Cartigny, M.J.** (2018) Powerful turbidity currents driven by dense basal layers. *Nature Communications*, **9**:4114.

Payros, A., Pujalte, V. and **Orue-Etxebarria, X.** (1999) The South Pyrenean Eocene carbonate megabreccias revisited: new interpretation based on evidence from the Pamplona Basin. *Sedimentary Geology*, **125**, 165–194.

Peakall, J. and **Sumner, E.J.** (2015) Submarine channel flow processes and deposits: A process-product perspective. *Geomorphology*, **244**, 95-120.

Peakall, J., Ashworth, P. and **Best, J.,** (1996) Physical modelling in fluvial geomorphology: Principles, applications and unresolved issues. In: *The Scientific Nature of Geomorphology* (Eds B.L. Rhoads and C.E. Thorn), John Wiley and Sons, Chichester, 221-253.

Peakall, J., McCaffrey, W.D. and **Kneller, B.C.** (2000) A process model for the evolution, morphology, and architecture of sinuous submarine channels. *Journal of Sedimentary Research*, **70**, 434–448.

Pett, J.W. and **Walker, R.G.** (1971) Relationship of flute cast morphology to internal sedimentary structures in turbidites. *Journal of Sedimentary Petrology*, **41**, 114-128.

Pettijohn, F.J. and **Potter, P.W.** (1964) *Atlas and Glossary of Primary Sedimentary Structures*. Springer-Verlag, Berlin, 370 pp.

Piasecka, E.D., Stokes, C.R., Winsborrow, M.C.M. and **Andreassen, K.** (2018) Relationship between mega-scale glacial lineations and iceberg ploughmarks on the Bjørnøyrenna Palaeo-Ice Stream bed, Barents Sea. *Marine Geology*, **402**, 153-164.

Pickering, K.T. and **Hiscott, R.N**. (1985) Contained (reflected) turbidity currents from the Middle Ordovician Cloridorme Formation, Quebec, Canada: An alternative to the antidune hypothesis. *Sedimentology*, **32**, 373-394.

Pickering, K.T. and **Hiscott, R.N.** (2016) *Deep Marine Systems: Processes, Deposits, Environments, Tectonics and Sedimentation*. AGU / Wiley, 657 pp.

Pilotti, M. and **Menduni, G.** (1997) Application of lattice gas techniques to the study of sediment erosion and transport caused by laminar sheetflow. *Earth Surface Processes and Landforms*, **22**, 885-893.

Piper, D.J.W., Cochonat, P. and **Morrison, M.L.** (1999) The sequence of events around the epicentre of the 1929 Grand Banks earthquake: initiation of debris flows and turbidity current inferred from sidescan sonar. *Sedimentology*, **46**, 79–97.

Pirmez, C. and **Imran, J.** (2003) Reconstruction of turbidity currents in Amazon Channel. *Marine and Petroleum Geology*, **20**, 823–849.

Pittari, A. and **Cas, R.A.F.** (2004) Sole marks at the base of the late Pleistocene Abrigo Ignimbrite, Tenerife: implications for transport and depositional processes at the base of pyroclastic flows. *Bulletin of Volcanology*, **66**, 356-363.

Posamentier, H.W. and **Kolla, V.** (2003) Seismic geomorphology and stratigraphy of depositional elements in deep-water settings. *Journal of Sedimentary Research*, **73**, 367–388.

Postma, G., Nemec, W. and **Kleinspehn, K.L.** (1988) Large floating clasts in turbidites – a mechanism for their emplacement. *Sedimentary Geology*, **58**, 47–61.

Potter, P.E. and **Pettijohn, F.J.** (1963) *Paleocurrents and Basin Analysis*. Academia Press, New York, 296 pp.

Poulos, S. (2001) The contribution of near-bed currents to modern sedimentation processes in the deep waters of the Hellenic Arc-Trench system, eastern Mediterranean. *Geo-Marine Letters*, **20**, 201-208.

Prior, D.B., Bornhold, D.B. and **Johns, M.W.** (1984) Depositional characteristics of a submarine debris flow. *Journal of Geology*, **92**, 707-727.

Ptasinski, P.K., Nieuwstadt, F.T.M., van den Brule, B.H.A.A. and **Hulsen, M.A.** (2001) Experiments in turbulent pipe flow with polymer additives at maximum drag reduction. *Flow, Turbulence and Combustion*, **66**, 159–182.

Ptasinski, P.K., Boersma, B.J., Nieuwstadt, F.T.M., Hulsen, M.A., van den Brule, B.H.A.A. and **Hunt, J.C.R.** (2003) Turbulent channel flow near maximum drag reduction: Simulations, experiments and mechanisms. *Journal of Fluid Mechanics*, **490**, 251–291.

Pyles, D.R. and **Jennette, D.C.** (2009) Geometry and architectural associations of co-genetic debrite-turbidite beds in basin margin strata, Carboniferous Ross Sandstone (Ireland): Applications to reservoirs located on the margins of structurally confined submarine fans. *Marine and Petroleum Geology*, **26**, 1974-1996.

Raudkivi, A.J. (1997) Ripples on stream bed. *Journal of Hydraulic Engineering*, **123**, 58-64.

Rees, A.I. (1983) Experiments on the production of transverse grain alignment in a sheared dispersion. *Sedimentology*, **30**, 437-448.

Reimnitz, E., **Barnes, P.W., Toimil, L.J.** and **Melchoir, J.** (1977) Ice gouge recurrence and rates of sediment reworking, Beaufort Sea, Alaska. *Geology*, **5**, 405-408.

Remacha, E. and **Fernández, L.P.** (2003) High-resolution correlation patterns in the turbidite systems of the Hecho Group (south-central Pyrenees, Spain). *Marine and Petroleum Geology*, **20**, 711-726.

Remacha, E., Fernández, L.P. and **Maestro, E.** (2005) The transition between sheet-like lobe and basin-plain turbidites in the Hecho Basin (South-Central Pyrenees, Spain). *Journal of Sedimentary Research*, **75**, 798-819.

Reynolds, S. and **Gorsline, D.S.** (1992) Clay microfabric of deep-sea, detrital mud(stone)s, California continental borderland. *Journal of Sedimentary Research*, **62**, 41-53.

Ricci Lucchi, F. (1969a) Considerazioni sulla formazione di alcune impronte da corrente. *Giornale di Geologia*, **36**, 363–438.

Ricci Lucchi, F. (1969b) Channelised deposits in the Middle Miocene Flysch of Romagna (Italy). *Giornale di Geologia*, **36**, 203-282.

Ricci Lucchi, F. (1978) Turbidite dispersal in a Miocene deep-sea plain: the Marnoso-arenacea of the northen Apennines. *Geologie en Mijnbouw*, **57**, 559-576.

Ricci Lucchi, F. (1986) The Oligocene to recent foreland basins of the Northern Apennines. In: *Foreland Basins*, (Eds P.A. Allen and P. Homewood), IAS Special Publication 8, 105-139.

Ricci Lucchi, F. (1995) *Sedimentographica: A Photographic Atlas of Sedimentary Structures*, 2nd ed. Columbia University Press, New York, 255 pp.

Rice, M.A. (1991) Grain shape effects on aeolian sediment transport. In: *Aeolian Grain Transport 1: Mechanics* (Eds. O.E Barndorff-Nielsen & Willetts, B.B.), Acta Mechanica Supplementum 1, Springer-Verlag, 159-166.

Richardson, K. and **Carling, P.** (2005) A Typology of Sculpted Forms in Open Bedrock Channels. *Geological Society of America Special Publication,* **392**, 108 pp.

Righetti, M. and **Lucarelli, C.** (2007) May the Shields theory be extended to cohesive and adhesive benthic sediments? *Journal of Geophysical Research: Oceans*, **112**, C05039.

Roberts, J., Jepsen, R., Gotthard, D. and **Lick, W.** (1998) Effects of particle size and bulk density on erosion of quartz particles. *Journal of Hydraulic Engineering*, **124**, 1261-1267.

Rodríguez-Tovar, F.J. and **Hernández-Molina, F.J.** (2018) Ichnological analysis of contourites: Past, present and future. *Earth-Science Reviews*, **182**, 28-41.

Rubinow, S. and **Keller, J.** (1961) The transverse force on a spinning sphere moving in a viscous fluid. *Journal of Fluid Mechanics*, **11**, 447-459.

Rücklin, H. (1938) Stromungsmarken im Unteren Muschelkalk des Saarlands [Flute casts in the Lower Muschelkalk of the Saarland]. *Senckenbergiana Lethaea*, **20**, 94-114.

Sanders, J.E. (1965) Primary sedimentary structures formed by turbidity currents and related resedimentation mechanisms. In: *Primary Sedimentary Structures and their Hydrodynamic Interpretation* (Ed G.V. Middleton), *SEPM Special Publication*, 12, 192-219.

Sato, H. (1956) Experimental investigation of a laminar separated layer. *Journal of the Physical Society of Japan*, **11**, 702-709.

Sato, H. (1959) Further investigations on the transition of two-dimensional separated layers at subsonic speeds. *Journal of the Physical Society of Japan*, **14**, 1797-1810.

Schwab, W.C., Lee, H.J., Twichell, D.C., Locat, J., Nelson, C.H., McArthur, W.G. and **Kenyon, N.H.** (1996) Sediment mass-flow processes on a depositional lobe, outer Mississippi Fan. *Journal of Sedimentary Research*, **66**, 916-927.

Seizilles, G., Lajeunesses, E., Devauchelle, O. and **Bak, M.** (2014) Cross-stream diffusion in bedload transport. *Physics of Fluids*, **26**, 013302.

Sestini, G. and **Curcio, M.** (1965) Aspetti quantitative delle impronte di fondo da corrente nelle torbiditie dell Apennino toscoemiliano. *Bollettino della Società Geologica Italiana*, **84**, 1-26.

Sgro, L., Mistri, M. and **Widdows, J.** (2005) Impact of the infaunal Manila clam, Ruditapes philippinarum, on sediment stability. *Hydrobiologia*, **550**, 175-182.

Shchepetkina, A., Gingras, M.K. and **Pemberton, S.G.** (2018) Modern observations of floccule ripples: Petitcodiac River estuary, New Brunswick, Canada. *Sedimentology*, **65**, 582-596, doi:10.1111/sed.12393.

Shrock, R.R. (1948) *Sequence in Layered Rocks: A Study of Features and Structures Useful for Determining Top and Bottom or Order of Succession in Bedded and Tabular Rock Bodies*. McGraw-Hill, 507 pp.

Singer, J.K. and **Anderson, J.B.** (1984) Use of total grain-size distributions to define bed erosion and transport for poorly sorted sediment undergoing simulated bioturbation. *Marine Geology*, **57**, 335-359.

Skempton, A. (1954) Discussion of the structure of inorganic soil. *Journal of the Soil Mechanics and Foundations Division, Proceedings of the American Society of Civil Engineers*, **80**, 19-22.

Slackza, A. and **Unrug, R.** (1976) Trends of textural variation in turbidite sandstones: The Cergowa Sandstone (Oligocene, Outer Carpathians). A*nnales Societatis Geologorum Poloniae*, **46**, 55-75.

Smerdon, E.T. and **Beasley, R.P.** (1959) Relation of compaction and other soil properties to erosion resistance of soils. *Transactions, American Society of Agriculture Engineers*, **8**.

Smith, N.D. (1972) Flume experiments on the durability of mud clasts. *Journal of Sedimentary Petrology*, **42**, 378-383.

Sohn, Y.K. (1997) On traction-carpet sedimentation. *Journal of Sedimentary Research*, **67**, 502–509.

Sohn, Y.K. (2000) Depositional processes of submarine debris flows in the Miocene fan deltas, Pohang Basin, SE Korea with special reference to flow transformation. *Journal of Sedimentary Research*, **70**, 491-503.

Soomere, T. (2007) Nonlinear components of ship wake waves. *Transactions of the ASME*, **60**, 120-138.

Soulsby, R.L. and **Whitehouse, R.J.S.** (1997) Threshold of sediment motion in coastal environments. In: *Pacific Coasts and Ports '97: Proceedings of the 13th Australasian Coastal and Ocean Engineering Conference and the 6th Australasian Port and Harbour Conference; Volume 1*, Christchurch, N.Z., Centre for Advanced Engineering, University of Canterbury, 145-150.

Southern, S.J., Patacci, M., Felletti, F. and **McCaffrey, W.D.** (2015) Influence of flow containment and substrate entrainment upon sandy hybrid event beds containing a co-genetic mud-clast-rich division. *Sedimentary Geology*, **321**, 105-121.

Soutter, E.L., Kane, I.A. and **Huuse, M.** (2018) Giant submarine landslide triggered by Paleocene mantle plume activity in the North Atlantic. *Geology*, **46**, 511-514.

Sparks, R.S.J., Gardeweg, M.C., Calder, E.S. and **Matthews, S.J.** (1997) Erosion by pyroclastic flows on Lascar Volcano, Chile. *Bulletin of Volcanology*, **58**, 557–565.

Sparks, R.S.J., Barclay, J., Calder, E.S., Herd, R.A., Komorowski, J-C., Luckett, R., Norton, G.E., Ritchie, L.J., Voight, B. and **Woods, A.W.** (2002) Generation of a debris avalanche and violent pyroclastic density current on 26 December (Boxing Day) 1997 at Soufrière Hills Volcano, Montserrat. In: *The Eruption of Soufrière Hills Volcano, Montserrat, from 1995 to 1999* (Eds T.H. Druitt and B.P. Kokelaar), *Geological Society of London Memoir*, 21, 409–434.

Spychala, Y.T., Hodgson, D.M., Flint, S.S. and **Mountney, N.P.** (2015) Constraining the sedimentology and stratigraphy of submarine intraslope lobe deposits using exhumed examples from the Karoo Basin, South Africa. *Sedimentary Geology*, **322**, 67-81.

Spychala, Y.T., Hodgson, D.M. and **Lee, D.R.** (2017a) Autogenic controls on hybrid bed distribution in submarine lobe complexes. *Marine and Petroleum Geology*, **88**, 1078-1093, doi:10.1016/j.marpetgeo.2017.09.005

Spychala, Y.T., Hodgson, D.M., Prélat, A., Kane, I.A., Flint, S.S. and **Mountney, N.P.** (2017b) Frontal and lateral submarine lobe fringes: Comparing sedimentary facies, architecture and flow processes. *Journal of Sedimentary Research*, **87**, 75-96.

Stanley, D.J. (1982) Welded slump-graded sand couplets: evidence for slide generated turbidity currents. *Geo-marine Letters*, **2**, 149-155.

Stevenson, C.J., Talling, P.J., Sumner, E.J., Masson, D.G., Frenz, M. and **Wynn, R.B.** (2014). On how thin submarine flows transported large volumes of sand for hundreds of kilometres across a flat basin plain without eroding the sea floor. *Sedimentology*, **61**, 1982–2019.

Stevenson, C.J., Jackson, C.A-L., Hodgson, D.M., Hubbard, S.M. and **Eggenhuisen, J.** (2015) Sediment bypass in deep-water systems. *Journal of Sedimentary Research*, **85**, 1058-1081.

Sumner, E.J., Amy, L. and **Talling, P.J.** (2008) Deposit structure and processes of sand deposition from a decelerating sediment suspension. *Journal of Sedimentary Research*, **78**, 529–547.

Sumner, E.J., Talling, P.J. and **Amy, L.A.** (2009) The deposits of flows transitional between turbidity currents and debris flow. *Geology*, **37**, 991–994.

Sutherland, T.F., Grant, J. and **Amos, C.L.** (1998) The effect of carbohydrate production by the diatom Nitzschia curvilineata on the erodibility of sediment. *Limnology and Oceanography*, 43, 65-72.

Talling, P.J. (2013) Hybrid submarine flows comprising turbidity current and cohesive debris flow: Deposits, theoretical and experimental analyses, and generalized models. *Geosphere*, **9**, 460-488.

Talling P.J., Peakall, J., Sparks, R.S.J., ÓCofaigh, C.S., Dowdeswell, J.A., Felix, M., Wynn, R.B., Baas, J.H., Hogg, A.J., Masson, D.G., Taylor, J. and **Weaver, P.P.E.** (2002) Experimental constraints on shear mixing rates and processes: implications for the dilution of submarine debris flows. In:

Glacier-influenced Sedimentation on High-Latitude Continental Margins (Eds J.A. Dowdeswell and C.S. ÓCofaigh), *Geological Society of London Special Publication*, 203, 89-103.

Talling, P.J., Amy, L.A., Wynn, R.B., Peakall, J. and **Robinson, M.** (2004) Beds comprising debrite sandwiched within co-genetic turbidite: origin and widespread occurrence in distal depositional environments. *Sedimentology*, **51**, 163-194.

Talling, P.J., Amy, L.A. and **Wynn, R.B.** (2007a) New insights into the evolution of large volume turbidity currents; comparison of turbidite shape and previous modelling results. *Sedimentology*, **54**, 737–769.

Talling, P.J., Amy, L.A., Wynn, R.B., Blackbourn, G. and **Gibson, O.** (2007b) Turbidity current evolution deduced from extensive thin turbidites: Marnoso-arenacea Formation (Miocene), Italian Apennines. *Journal of Sedimentary Research*, **77**, 172–196.

Talling, P.J., Wynn, R.B., Masson, D.G., Frenz, M., Cronin, B.T., Schiebel, R., Akhmetzhanov, A.M., Dallmeier-Tiessen, S., Benetti, S., Weaver, P.P.E., Georgiopoulou, A., Zühlsdorff, C. and **Amy, L.A.** (2007c) Onset of submarine debris flow deposition far from original giant landslide. *Nature*, **450**, 541–544.

Talling, P.J., Wynn, R.B., Rixon, R., Schmidt, D., Sumner, E. and **Amy, L.A.** (2010) How did submarine flows transport boulder sized mud clasts to the fringes of the Mississippi Fan? *Journal of Sedimentary Research*, **80**, 829–851.

Talling, P.J., Masson, D.G., Sumner, E.J. and **Malgesini, G.** (2012a) Subaqueous sediment density flows: Depositional processes and deposit types. *Sedimentology*, **59**, 1937-2003.

Talling, P.J., Malgesini, G., Sumner, E.J., Amy, L.A., Felletti, F., Blackbourn, G., Nutt, C., Wilcox, C., Harding, I.C. and **Akbari, S.** (2012b) Planform geometry, stacking pattern, and extra-basinal origin of low strength and intermediate strength cohesive debris flow deposits in the Marnoso-arenacea Formation, Italy. *Geosphere*, **8**, 1207-1230.

Talling, P.J., Malgesini, G. and **Felletti, F.** (2013a) Can liquefied debris flows deposit clean sand over large areas of seafloor? Field evidence from the Marnoso-arenacea Formation, Italian Apennines. *Sedimentology*, **60**, 720-762.

Talling, P.J., Paull, C.K. and **Piper, D.J.W.** (2013b) How are subaqueous sediment density flows triggered, what is their internal structure and how does it evolve? Direct observations from monitoring of active flows. *Earth-Science Reviews*, **125**, 244-287.

Tanaka, K. (1970) Sedimentation of the Cretaceous flysch sequence in the Ikusgumbetsu area, Hokkaido, Japan. *Geological Survey of Japan Report*, **236**, 102 pp.

Tarhan, L.G. (2018a) The early Paleozoic development of bioturbation – Evolutionary and geobiological consequences. *Earth-Science Reviews*, **178**, 177-207.

Tarhan, L.G. (2018b) Phanerozoic shallow marine sole marks and substrate evolution. *Geology*, **46**, 755-758.

Tarhan, L.G., Droser, M.L., Planavsky, N.J. and **Johnston, D.T.** (2015) Protracted development of bioturbation through the early Palaeozoic Era. *Nature Geoscience*, **8**, 865-871.

Ten Haaf, E. (1959) Graded beds of the northern Apennines. PhD thesis, Rijksuniv, Groningen, 102 p.

Thomsen, L. and **Gust, G.** (2000) Sediment erosion thresholds and characteristics of resuspended aggregates on the western European continental margin. *Deep Sea Research Part I: Oceanographic Research Papers*, **47**, 1881-1897.

Tinterri, R. and **Muzzi Magalhaes, P.** (2011) Synsedimentary structural control on foredeep turbidites related to basin segmentation: facies response to the increase in tectonic confinement (Marnoso-arenacea Formation, Miocene, Northern Apennines, Italy). *Marine and Petroleum Geology*, **67**, 81-110.

Tinterri, R. and **Tagliaferri, A.** (2015) The syntectonic evolution of foredeep turbidites related to basin segmentation: Facies response to the increase in tectonic confinement (Marnoso-arenacea Formation, Northern Apennines, Italy). *Marine and Petroleum Geology*, **67**, 81-110.

Tinterri, R, Drago, M., Consomi, A., Davoli, G. and **Mutti, E.** (2003) Modelling subaqeous bipartite sediment gravity flows on the basis of outcrop constraints: first results. *Marine and Petroleum Geology*, **20**, 911–933.

Tinterri, R., **Muzzi Magalhaes, P., Tagliaferri, A.** and **Cunha, R.S.** (2016) Convolute laminations and load structures in turbidites as indicators of flow reflections and decelerations against bounding slopes. Examples from the Marnoso-arenacea Formation (northern Italy) and Annot Sandstones (south eastern France). *Sedimentary Geology*, **344**, 382-407.

Trevor, J.H. (1978) The dynamics and mechanical energy expenditure of the polychaetes Nephtys cirrosa, Nereis diversicolor and Arenicola marina during burrowing. *Estuarine and Coastal Marine Science*, **6**, 605-619.

Uchman, A. and **Wetzel, A.** (2011) Deep-sea ichnology: The relationships between depositional environment and endobenthic organisms. In: *Deep-sea Sediments* (Eds H. Hüneke and T. Mulder), Developments in Sedimentology, 63, 517-556.

Vangriesheim, **A., Khripounoff, A.** and **Crassous, P.** (2009) Turbidity events observed in situ along the Congo submarine channel. *Deep Sea Research Part II: Topical Studies in Oceanography*, **56**, 2208-2222.

Van Vliet, A. (2007) Submarine fans and associated sediments of the Tertiary Coastal Range of Guipúzcoa, Spain. In: *Atlas of Deep-water Outcrops* (Eds T.H. Nilsen, R.D. Shrew, G.S. Steffens and J.R.J. Studlick), AAPG Studies in Geology 56 (and Shell International Exploration and Production), 341-347.

Vogt, P.R., Crane, K. and **Sundvor, E.** (1994) Deep Pleistocene iceberg plowmarks on the Yermak Plateau: sidescan and 3.5 kHz evidence for thick calving ice fronts and a possible marine ice sheet in the Arctic Ocean. *Geology*, **22**, 403-406.

Vrolijk, P.J. and **Southard, J.B.** (1997) Experiments on rapid deposition of sand from high-velocity flows. *Geoscience Canada*, **24**, 45–54.

Walker, R.C. (1965) The origin and significance of the internal sedimentary structures of turbidites. *Proceedings of the Yorkshire Geological Society*, **35**, 1-32.

Walker, R.C. (1967) Turbidite sedimentary structures and their relationship to proximal and distal depositional environments. *Journal of Sedimentary Petrology*, **37**, 25-43.

Walker, R.C. (1970) Review of the geometry and facies organization of turbidites and turbidite bearing basins. In: *Flysch Sedimentology in North America* (Ed J. Lajoie), T*he Geological Association of Canada Special Paper*, 7, 219-251.

Wang, Z. and **Plate, E.C.H.J.** (1996) A preliminary study on the turbulence structure of flows of non-Newtonian fluid. *Journal of Hydraulic Research,* **34**, 345–361.

Wetzel, A., (2006) Theodor Fuchs' experiments on the formation of solemarks in Flysch. *Ichnology Newsletter*, **27**, 16-19.

Wiberg, P.L. and **Smith, J.D.** (1985) A theoretical model for saltating grains in water. *Journal of Geophysical Research*, **90**, 7341-7354.

Widdows, J., Brinsley, M.D. and **Pope, N.D.** (2009) Effect of Nereis diversicolor density on the erodability of estuarine sediment. *Marine Ecology Progress Series*, **378**, 135-143.

Williams, G. (1964) Some aspects of the eolian saltation load. *Sedimentology*, **3**, 257-287.

Winn, R.D., Jr. and **Dott, R.H., Jr.** (1977) Large-scale traction produced structures in deep-water fan-channel conglomerates in southern Chile. *Geology*, **5**, 41-44.

Winn, R.D., Jr. and **Dott, R.H., Jr.** (1979) Deep-water fan-channel conglomerates of Late Cretaceous age, southern Chile. *Sedimentology*, **26**, 203-228.

Winston, J.E. and **Anderson, F.E.** (1971) Bioturbation of sediments in a northern temperate estuary. *Marine Geology*, **10**, 39-49.

Winterwerp, J.C. and **W.G.M. van Kesteren** (2004) *Introduction to the Physics of Cohesive Sediments in the Marine Environment*, Developments in Sedimentology, 56, Elsevier, New York, 466 pp.

Winterwerp, J.C., van Kesteren, W.G.M., van Prooijen, B. and **Jacobs, W.** (2012) A conceptual framework for shear flow–induced erosion of soft cohesive sediment beds. *Journal of Geophysical Research: Oceans*, **117**, C10020.

Wood, A. and **Smith, A.J.** (1958) The sedimentation and sedimentary history of the Aberystwyth Grits (Upper Llandoverian). *Quarterly Journal of the Geological Society*, **114**, 163-195.

Yanniotis, S., Skaltsi, S. and **Karaburnioti, S.** (2006) Effect of moisture content on the viscosity of honey at different temperatures. *Journal of Food Engineering*, **72**, 372-377.

Yin, D., Peakall, J., Parsons, D., Chen, Z., Macdonald Averill, H., Wignall, P. and **Best, J.** (2016) Bedform genesis in bedrock substrates: Insights into formative processes from a new experimental approach and the importance of suspension-dominated abrasion. *Geomorphology*, **255**, 26-38.

Zavala, C. and **Arcuri, M.** (2016) Intrabasinal and extrabasinal turbidites: Origin and distinctive characteristics. *Sedimentary Geology*, **337**, 36-54.

Zavala, C., Arcuri, M. and **Blanco Valiente, L.** (2012) The importance of plant remains as a diagnostic criteria for the recognition of ancient hyperpycnites. *Revue de Paléobiologie*, **11**, 457–469.

Figure captions

Figure 1. Schematic models for transitional flows: (A-E) transitional flows over a plane bed as a function of increasing clay concentration (top to bottom), depicted in sections parallel to flow (modified from Baas *et al*., 2009). The viscous sublayer (vsl) increases in thickness from ~1 mm in turbulent flows as clay content increases, and shows a marked jump in thickness in the UTPF regime; (F-J) transitional flows over a transverse bedform as a function of increasing clay concentration (top to bottom) showing the changing fluid dynamic features in the leeside of the bedform. Views are depicted parallel to flow (modified from Baas & Best, 2008). Flow is from left to right. See text for further details.

Figure 2. Morphological relationships for current ripples formed under different transitional flows. (A) Equilibrium ripple height, and (B) equilibrium ripple wavelength, as a function of sediment concentration (kaolinite clay) and transitional flow regime. TF = turbulent flow, TETF = turbulence-enhanced transitional flow, LTPF = lower transitional plug flow, UTPF = upper transitional plug flow, QLPF = quasi-laminar plug flow. Modified from Baas *et al*. (2011).

Figure 3. Estimation of the maximum clast size that can be supported by the yield strength (matrix strength) of a mud-rich fluid, and by buoyancy, for increasing kaolin concentrations. Modified from Talling *et al*. (2012) and Talling (2013).

Figure 4. Plots of undrained shear strength against depth for cohesive sediments from a range of modern deep-water locations worldwide (WD = water depth). Grey filled polygon indicates expected shear strength for each site assuming normal consolidation during burial (defined as virgin consolidation by Skempton, 1954). All sites feature apparently over-consolidated sediments in the top one metre, despite the lack of significant post-depositional loading.

Figure 5. (A) Sample of near-seafloor sediment from offshore Angola (*c*. 1500 m water depth), illustrating the reworking by polychaete worms of background matrix into faecal pellets that line a burrow (modified from Kuo & Bolton, 2013). (B) Box core from western Mediterranean (*c*. 800 m water depth), showing contrast between high water content upper benthic boundary layer, and underlying consolidating clay sediment.

Figure 6. (A) Relationship between remoulded shear strength and bed shear stress. Points *a* to *d* indicate the effects of a flow which exerts the same shear stress, on beds with different remoulded shear strengths. Where lower initial strengths occur, floc erosion (erosion of individual flocs) or surface erosion (erosion of surface layers as a result of the top of the bed liquefying) regimes are

bypassed, leading to mass erosion (where 'lumps' of material are removed following local failure within the bed). Remoulded here refers to the shear strength following failure (where failure is the peak shear strength, as in Fig. 4) and prior to reaching the minimum shear strength that results from complete deformation. (B) Biostabilising effect of EPS (Extra-cellular polymeric substances) observed in the East Frisian Wadden Sea, Germany. As EPS surface concentration increases, so too does the erosion threshold. Points are shaded relative to the density of macrozoobenthos stabilisers. Both figures modified from Winterwerp & van Kesteren, 2004).

Figure 7. Flute morphology for the 'ideal flute', a parabolic flute (A), and flutes types as seen in planform (B). For simplicity, only the main flute types are shown, and asymmetric forms are not included. Based on Allen (1971a, 1984).

Figure 8. Examples of flutes. (A) Large parabolic-transitional (bulbous) flutes on the base of a submarine channel, Lower Silurian Aberystwyth Grits, Wales; (B) Parabolic flutes, Aberystwyth Grits, Wales. Note the mixture of flutes, with some exhibiting prominent median ridges, whilst others exhibit simple smooth shapes; (C) Spindle flutes with some flutes exhibiting a pronounced spiralling pattern, referred to as twisted flutes by Allen (1971a), middle Ordovician Cloridorme Formation, Gaspé Peninsula, Quebec, Canada. Finger for scale.

Figure 9. Schematic evolution of flutes from an initial bed defect, showing stable and unstable developmental paths. V is the time-averaged areal mean erosion rate, a parameter that changes over time, t, and was measured in the experiments from repeated profiles; X is the initial length of the defect. In addition to the bed streamlines shown in planform for the final stable and unstable forms, the flow fields are shown longitudinally and in cross-section. These patterns were derived from experiments using clear water flows over plaster-of-Paris beds. Based on Allen (1971a).

Figure 10. Examples of grooves. (A) A series of smooth parallel grooves. Total width of parallel grooves ~0.4 m. Lower Silurian, Aberystwyth Grits, Wales; (B) Rounded grooves exhibiting occasional cross-cutting, Aberystwyth Grits, Wales, maximum width across groove field ~1 m; (C) Parallel grooves, middle Ordovician Cloridorme Formation, Quebec, Canada. Lens cap for scale, diameter 58 mm; (D) Grooves from the Miocene Marnoso-arenacea Formation, Italian Apennines, exhibiting a relatively smooth form. Hammer for scale, 33 cm long; (E) Close up of groove, showing internal striations, Cloridorme Formation, Quebec, Canada. Lens cap for scale, diameter 77 mm.

Figure 11. Examples of grooves, illustrating the relationships between sole structures and the overlying beds. (A) Grooves beneath massive Bouma A bed, updip of a clast-rich hybrid event bed, Miocene Marnoso-arenacea Formation, Italy (location shown in Bed 5 planform map, Figure 14). (B) Grooves beneath a hybrid event bed, Lower Silurian Aberystwyth Grits, Wales, featuring a sandy debrite division (H3 division of Haughton *et al*., 2009) shown by the lighter layer in the middle of the bed. (C) Grooves on lower surface cut by younger prod marks at a high angle to the grooves (palaeoflow of prods towards base of photo). The grooved surface is overlain by rippled sands, representing the Bouma C division, with a strong palaeoflow component orientated in the direction of the grooves, and approximately transverse to the flow direction indicated by the prod marks. Yellow scale bar is 10 cm. (D) Grooves, cut by later flute marks; flow direction from top left to bottom right. The grooves and flutes are overlain by a Bouma B division, however there is insufficient definition of the laminae for photographic reproduction. Examples C and D are from samples in the collection of the Natural Sciences Education Centre at the Jagiellonian University, Kraków, Poland.

Figure 12. Photograph showing the formation of linear, parallel, flat-bottomed grooves bounded by lateral ridges, by a debris flow in the Angelico Basin, Calabrian Ridge, eastern Mediterranean Sea. Note how the groove width appears to match the size of the clasts. Modified from Kastens (1984).

Figure 13. Cutaway sketches showing a moving-frame view of tool behaviour and groove formation in a subaerial debris flow head. (A) Initial descent of tool (clast) towards the base, (B) initial cutting of groove, (C) completion of groove cutting and uplift of the tool into the flow, and (D) lateral movement of the clast. Note that the groove is being cut in a downstream direction, but that the base of the flow behind the head is moving more slowly than the front speed, therefore in a moving-frame of reference as shown here the groove appears to be cut upstream. Flow dynamics modified from Johnson *et al*. (2012).

Figure 14. (A) Planform distribution of grooves, and clast-rich and clast-poor cohesive debrite intervals for Beds 1, 3, 5 and 6 of the Miocene Marnoso-arenacea Formation, Italian Apennines (Bed numbers after Amy & Talling, 2006). The debrite intervals are parts of hybrid beds. In the case of Bed 5, grooves are present for >40 km, and extend over areas up to ~300 km^2. Talling *et al*. (2007a, 2012b) provide information on the broader context of these beds. (B, C, D) Representative cross-sections showing the nature of sedimentation above the grooved intervals; note spacing between logs is schematic. (B) The Ridracoli section for Bed 3 shows a downstream transition from a turbidite to a hybrid bed with the main grooved section underlying a clast-poor hybrid bed, with some grooves also present beneath the turbidite (location shown as line i to i’). (C) The Pianetto transect illustrates grooves beneath a hybrid bed showing lateral variability between a clast-rich and clast-poor debritic unit (Modified from Talling *et al*., 2012b); location shown as line ii to ii’. (D) Bed 5 deposits are summarised for the three eastern downstream areas (locations shown as line iii to iii’ in A), illustrating a hybrid bed with a clast-rich debrite overlying the grooves (Modified from Talling *et al*., 2013a).

Figure 15. Plan view of a subaqueous debris flow experiment showing parallel grooves behind a detached head (right), with the main part of the flow shown on the left hand side, inside a 15 cm wide semi-circular channel (reproduced from Middleton & Hampton (1973) after Hampton (1970)).

Figure 16. Examples of chevrons. (A) Uninterrupted chevrons (*c*. 3 cm in width) changing downstream (to the left) into a groove mark (*c*. 1 cm in width). This suggests that a particle moved down through the flow until it started sliding along the bed, at which point it ceased to produce chevrons. (B) Close up of A showing detail of the uninterrupted chevrons. A and B from the Lower Silurian Aberystwyth Grits, Wales. (C) Interrupted chevrons, showing flow from right to left. From the middle Ordovician Cloridorme Formation, Gaspé Peninsula, Quebec, Canada.

Figure 17. Schematic showing the different types of chevron marks, reflecting the relative height of the clast with respect to the bed.

Figure 18. Summary of the different mechanisms that may potentially form grooves and chevrons. (A) Low-density turbidity current; (B) high density turbidity current (HDTC) with traction carpet; (C) high density turbidity current (HDTC) with a high concentration basal layer; (D) granular flow; (E) liquefied / fluidised flow. White arrows show flow direction.

Figure 18 (continued) Summary of the different mechanisms that may potentially form grooves and chevrons. (F) nearly liquefied debris flow (equivalent to the 'liquefied debris flow' of Talling *et al*., (2012a)); (G) laminar plug flow with slip (debris flow); (H) quasi-laminar plug flow (debris flow) – grooves, showing cutting by clasts attached to the base of the plug; (I) quasi-laminar plug flow (debris flow) – chevrons, substrate shows chevrons in cross-section (see Fig. 17) being formed by bow waves from clasts carried at the base of the plug. White arrows show flow direction; black arrows in G, H and I show relative velocities and slip with respect to the base.

Figure 19. Models of hybrid-bed generation. (A) Forerunning turbidity current that cuts grooves, followed by a multi-layered flow, with high-density flow (HDF) overlain by a plug flow, and in turn a low-density flow (LDF). Modified from Fonnesu *et al*. (2016). (B) Standard model of hybrid-bed formation with deposition of sand from a forerunning turbidity current, followed by deposition of a clast-rich debrite, 'L' and 'T' represent laminar and turbulent flow respectively. The resulting deposit consists of sand at the base, an overlying clast-rich debrite, and finer-grained deposits (silts or sands) at the top, to give a hybrid-bed. Modified from Haughton *et al*. (2009). (C) Debris flow with either a forerunning turbidity current depositing sand, or sand separating and settling at a late stage from the laminar plug. Modified from Talling (2013).

Figure 20. Models for groove formation by flows forming hybrid beds. (A) Model for grooves found up-dip of a hybrid-bed deposit. A bypassing debris flow, with or without a forerunning turbidity current, cuts a grooved surface, and a later turbidite is deposited on top of the grooved surface. (B-E) Models for hybrid beds with grooves at the base. (B) A flow with a debris flow component and a forerunning turbidity current. The head of the turbidity current erodes unconsolidated mud, and mud clasts, undergoing transformation into a debris flow, producing longitudinal segregation from frontal debris flow, through turbidity current, and back into a second debris flow component. (C) Longitudinal flow segregation, with multiple debrite components from initial conditions (*e.g.*, periodic retrogressive failure) or from separation and break-up of an initially single debris flow (*e.g.*, Felix *et al*., 2009). The first debris flow cuts the grooves and is then followed successively by turbiditic and debritic components. (D) A single debris flow, with the frontal part cutting the grooves, followed by later separation and settling of sand from a laminar clast-rich plug flow (see Fig. 19C). (E) An initial debris flow cuts a grooved surface and bypasses down-dip. Given that debris flows deposit *en masse*, then the grooves may be left in pristine form on the sediment surface, or may be covered by a thin layer of unconsolidated mud from minor flow transformation of the top of the debris flow,

and any subsequent hemipelagic deposition. If a turbidity current is generated prior to a thicker consolidated mud developing it may ‘ingest’ any unconsolidated mud, and then at some point deposit directly onto the grooved surface. In this case, one flow cuts the erosive surface and an entirely separate flow accounts for the deposit.

Figure 21. Examples of discontinuous tool marks. (A) Prod (Pr) and skim marks (Sk), with large groove (Gr) displaying internal striations, in the centre. Prod mark at top right, shows internal striae suggesting a lack of rotation in the impinging particle (see text for details). Two sets of tool marks are observed, with the second set (~ENE-WSW in terms of photo orientation) cutting the lowermost set. This suggests that the earlier tool marks represent a bypass surface. Example from middle Carboniferous Quebrada de las Lajas, Argentina. Lens cap for scale, diameter 58 mm; (B) Prod and skim (bounce) marks superimposed on earlier flutes, Oligocene Krosno beds, Outer Carpathians, Poland; (C) Prod and skim (bounce) marks eroded by later flutes, Outer Carpathians, Poland. Examples B and C are from samples in the collection of the Natural Sciences Education Centre at the Jagiellonian University, Kraków, Poland.

Figure 22. Styles of discontinuous tool marks as seen in cross-section (x-y) and planform (x-z). Modified from Allen (1984).

Figure 23. Proposed formative flow conditions for discontinuous tool marks. TF = turbulent flow, TETF = turbulence-enhanced transitional flow, LTPF = lower transitional plug flow, UTPF = upper transitional plug flow, and QLPF = quasi-laminar plug flow.

Figure 24. A process-orientated conceptual model for the longitudinal distribution of flutes and tool marks. (A) The distribution of flutes and tool marks is shown for a flow that is increasing in cohesion with longitudinal distance, as hypothesised for instance for many hybrid event beds. (B) The

distribution of flutes and tool marks for flows that decrease in cohesion with distance; note that the order of the sole structures with distance is reversed relative to A. Note that transformations can start and finish anywhere along the transport path, that flows may also vary temporally at-a-point, and that flutes and tool marks will vary with substrate conditions (see main text for details). TF = turbulent flow, TETF = turbulence-enhanced transitional flow, LTPF = lower transitional plug flow, UTPF = upper transitional plug flow, QLPF = quasi-laminar plug flow, LPF = laminar plug flow (see Fig. 1 and accompanying text for more detail on transitional flow types).

Figure 25. Evolution of the classic Bouma sequence in pictorial form. Bouma (1962) initially defined 5 divisions. Blatt *et al*. (1972) added an erosive base to the A-division a decade later, and Middleton & Hampton (1973, 1976) then explicitly linked the erosive base on the A-division to flutes and tool marks. The combination of the Blatt *et al*. (1972) and Middleton & Hampton (1973, 1976) figures gives us the present form of the Bouma sequence, and in many cases this explicitly links grooves, as well as flutes and other tool marks, to the base of the A-division (*e.g.*, Collinson *et al*., 2006 as pictured here).

Figure 26. Revised Bouma sequence in pictorial form, highlighting the time gap between the basal surface and the basal sand–rich division, which can either be the Bouma A, B, or C division. The nature of the erosive surface provides information on the flow that cut the bed and bypassed down-dip. Grooves indicate erosion by a debritic flow component, and therefore a debrite will be located down-dip unless flow transformation has occurred. Flutes indicate that a turbulent flow, or a weaker transitional flow (TETF, LTPF, lower UTPF), formed the surface and a turbidite will be located down-dip, unless flow transformation has subsequently occurred. For simplicity, discontinuous tool marks are not shown. However, prod marks are likely linked to weaker transitional flows, and skim marks, and prod marks with upstream striae, to stronger transitional flows (see text for discussion). There is

evidence from some examples that the basal surface may even represent a separate flow event to the overlying turbidite and thus there is no genetic linkage (see text for details).

Table 1. Flute and groove occurrence as a function of Bouma division.

Table 2. Overview of some biological modifications to geomechanical behaviour of cohesive substrates that can affect the nature of erosion.

Table 3. Context of the major field areas considered, and the distribution of grooves and hybrid beds within them.

	Commencing Bouma Division			% Per Division		
	A	B	C	A	B	C
Bouma (1962) - Peïra Cava, France‡						
Total beds	106	92	684			
Flutes	20	12	9	18.9	13.0	1.3
Grooves	31	14	2	29.3	15.2	0.3
Crimes (1973) – Zumaia, Spain*						
Total	147	471	439			
Flutes alone	7	17	17	4.8	3.6	3.9
Grooves alone	14	19	15	9.5	4.0	3.2
Flutes and grooves together	13	29	47	8.3	6.2	10.0
Pett & Walker (1971) – Cloridorme & St. Roch Fm, Canada; & New York †						
Total	40	155	69			
Flutes	34	45	30	85.0	29.0	43.5
Small grooves and skim marks	1	29	23	2.5	18.7	33.3
Large grooves	2	3	0	5.0	1.9	0

‡From the proximal part of the basin, interpreted as channel-lobe transition in the lower part of the section, and proximal basin-plain in the upper part (see Table 3 for context). He also reports data for the Marnoso arenacea, Italy, and the Zollhaus Flysch, Switzerland, however total numbers of beds studied and thus flutes and grooves observed are very small (22 and 13 respectively).

*From basin-plain deposits (see Table 3 for context).

†Note that there are also several other categories of discontinuous tool marks plus organic structures, that are only found in T_B and T_C beds, and not in T_A beds. Cloridorme outcrops represent basin-plain deposits at the base, moving up towards lobes at the top (see Table 3 for context).

Modification Type	**Biological Process(es) Responsible**	**Reference Source**
Increased shear strength	Crustacean and polychaete burrows improve permeability, increase dewatering and hence increase shear strength	Meadows & Tait (1989)
Enhanced compaction	Internal burrow pressures result in localised/differential compaction	Hammond (1970); Elder & Hunter (1980); Trevor (1978); Murray *et al.* (2002)
Enhanced adhesion or interparticle-bonding	Formation of biologically-induced flocs, biofilms, or inter-particle bonding by EPS	Fleming & Richards (1982); Denny (1989); Bromley (1996); Meadows *et al.* (1990); Reynolds & Gorsline (1992)
Armouring of sediment surface	Winnowing brings finer sediment to surface, which is removed by currents, leaving an armouring of coarser sediments	Singer & Anderson (1984)
Loss of anisotropy/heterogeneity	Bioturbation mixes sediment vertically and laterally	Winston & Anderson (1971); Gingras *et al.* (2008)
Lateral variations in substrate strength	Spatially variable density of benthic colonisation results in localised differences in magnitude of modification	Murray *et al.* (2002)
Enhanced bed roughness	Seafloor expression of burrows provides (biogenic) roughness at the sediment-flow interface	Meadows & Meadows (1991); Bromley (1996); Davies (1982); Poulos (2001)
Reworking of cohesive sediments into faecal pellets	Cohesive sediment excreted as bonded pellets by invertebrates such as polychaetes that line burrows (e.g. *Ophiomorpha*)	Moore (1931); Colliat *et al.* (2011); Kuo & Bolton (2013)

Field Area	Age	Basin Type	Environments	Confined/ Unconfined	Spatial distribution of grooves	Grooves and facies	Hybrid prone	Other
Cloridorme Formation, Gaspé Peninsula, Quebec, Canada	Ordovician	Foreland[3]	Basin plain at base[3]; lobes towards top[4].	Confined – at base; flow reflection from margins and thick mud caps on thick-bedded calcareous wackes suggests ponding.[3]	Not stated; appear to be throughout ~145 km section. Correlate over ~11 km section at W[1-2]. No clear changes in sole marks longitudinally; but moving up/down stratigraphy. No change in detailed ~5 km section at top. See also[5].	Associated with: calcisiltites (turbidites) – *1% grooved*; calcareous wackes (75% turbidites; 25% hybrids) – *8%*; greywacke hybrid beds – *11-26%*[1-2].	Yes – abundant hybrid beds	Reflected bedforms in thick calcareous wackes (TCW)[3,6]. Examples shown are turbidites[3]. 55% of TCW beds[1-2] have flutes, 8% grooved, but mixture of turbidites & hybrid beds[1].
Marnoso-arenacea Formation, Italy	Miocene	Foreland[7], later transitioning to a piggyback basin[8].	Basin plain in younger (inner stage[9]) deposits, MTCs and lobes in older (outer stage[9])[10]deposits. Note: inner and outer stages record the evolution of the basin as the MAF closed[10].	Confined – younger parts due to large flows[11]; older parts, due to tectonically controlled sub-basins[12].	In inner stage - present across outcrop although missing in most distal locations[11]. Very rarely described in outer stage[13,14].	Associated with[10,11,15], and upstream from[11], hybrid beds (both clast-rich & clast-poor)[15]; also with thin, fine-grained sandstones (F9 facies *sensu*[12] = to T_B & T_C)[16].	Abundant hybrid beds[8,15]. Vary from >30-40% (Units I,II), to >5-10% (III, IV)[10] to ~10-20% (VI)[8] in inner stage, decreasing to almost zero in transition to outer stage[8].	Hybrid beds present across the basin apart from most distal regions, here they transform to thinly bedded sands and silts[11]. New data on groove distribution and relationships to hybrid beds are shown in Figure 14.
Peïra Cava Annot Sandstone, France	Upper Eocene to Oligocene	Foreland Basin, consisting of a series of complex ponded sub-basins[17, 18].	Proximal (Data of[20]), channel-lobe transition[19]; changes vertically to proximal basin-plain[18]. Central – proximal basin-plain[18]. Distal, basin-plain[18,19].	Confined in the main, although some lobes are recognised[18]. Strongly ponded at the distal end[18,19].	Grooves are present across the basin, from proximal to distal, with the possible exception of the most distal ponded basin in the NE[18,20].	Grooves linked primarily to T_A and T_B beds, with rare T_C beds[20] (Table 1). No subsequent detailed linkage to facies.	Hybrid beds (& mass transport deposits) very rare, and decrease as a proportion of beds down-stream[19, 21].	See Fig, 7 of [19] for a detailed plot of hybrid beds (and mass transport deposits) with longitudinal distance.
Zumaia, Guipúzcoa region, Basque Basin, N. Spain	Late Cretaceous to Eocene. Section of[22] Palaeocene to L. Eocene	Probably formed as an oblique-slip (pull apart basin[23].	Proximal is channel-lobe transition zone, changing downdip to lobes and basin-plain at Zumaia itself[24].	Unconfined for lobe deposits[24], basin-plain sheets may be confined.	Areal palaeocurrents are shown, however flutes and grooves are not separated[25].	Grooves associated with T_A, T_B and T_C in Zumaia section[22], and at base of localised slump[25].	Absent from Palaeocene to Lower Eocene. Some hybrid beds from Mid-Eocene[26].	Recurrence intervals suggest that basin-plain deposits are likely the product of disintegrating slides[27,28].

[1-2]Enos, 1969a,b; [3]Pickering & Hiscott, 1985; [4]Awadallah & Hiscott, 2004; [5]Measurement positions of data from Pett & Walker, 1971 (see Table 1) is not sub-divided into the Cloridorme, nor are the Cloridorme sections stated; [6]Edwards et al., 1994; [7]Ricci Lucchi, 1978; [8]Tinterri & Tagliaferri, 2015; [9]Ricci Lucchi, 1986; [10]Muzzi Magalhaes & Tinterri, 2010; [11]Amy & Talling, 2006; [12]Mutti *et al.,* 2003; [13]Mutti *et al*., 2002; [14]de Jager, 1979; [15]Talling *et al*., 2004; [16]Tinterri & Muzzi Magalhaes, 2011; [17]Apps *et al*., 2004; [18]Amy *et al*., 2007 (for groove areal distribution see their Fig. 11); [19]Cunha *et al*., 2017; [20]Bouma, 1962 (see his figure 19); [21]Stanley, 1982; [22]Crimes, 1973; [23]van Vliet, 2007; [24]Cummings & Hodgson, 2011b; [25]Crimes, 1976; [26]Unpublished data of the authors; [27]Clare *et al*., 2014; [28]Clare *et al*., 2015.

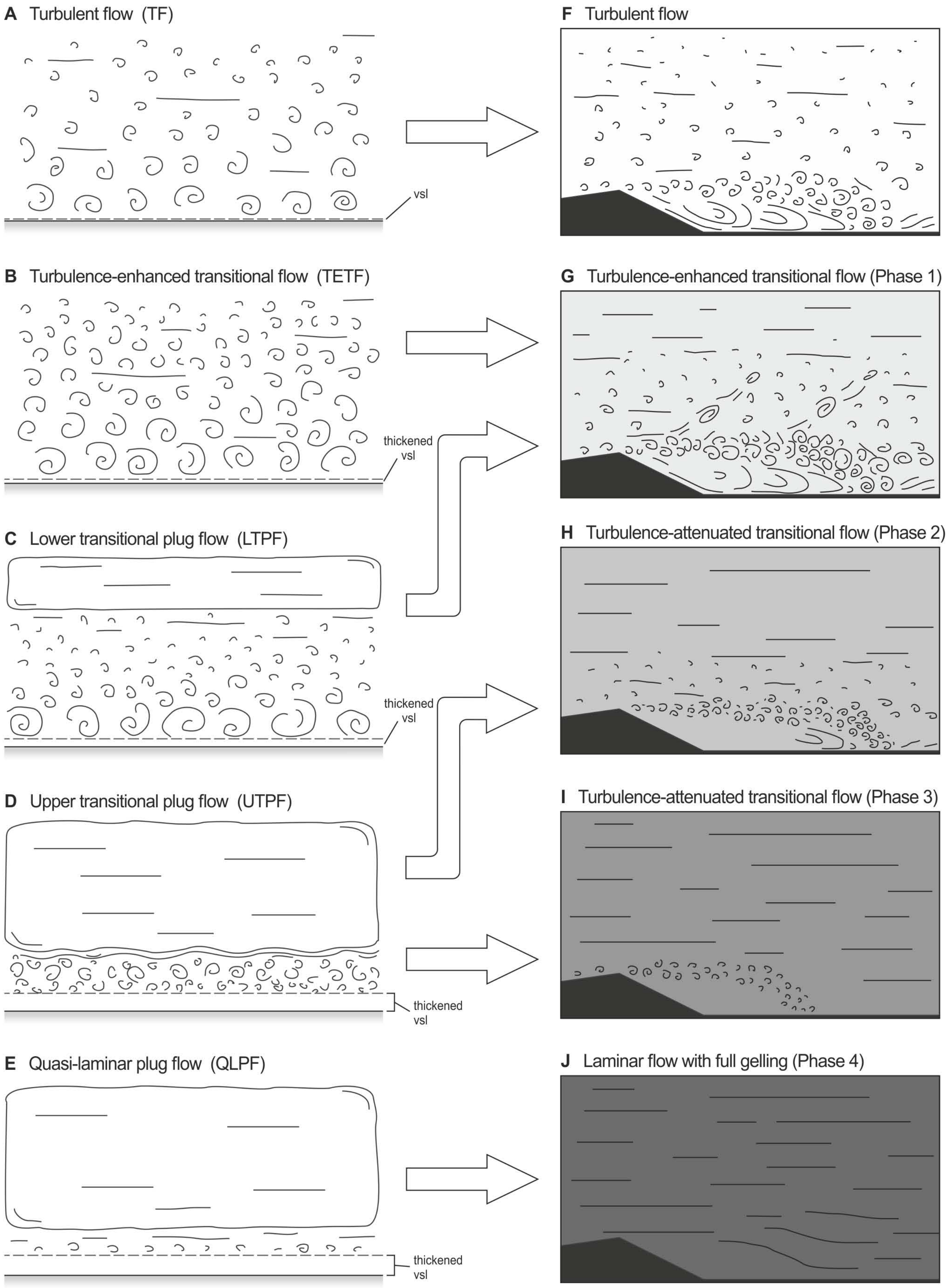
A Turbulent flow (TF)
vsl
B Turbulence-enhanced transitional flow (TETF)
thickened vsl
C Lower transitional plug flow (LTPF)
thickened vsl
D Upper transitional plug flow (UTPF)
thickened vsl
E Quasi-laminar plug flow (QLPF)
thickened vsl
F Turbulent flow
G Turbulence-enhanced transitional flow (Phase 1)
H Turbulence-attenuated transitional flow (Phase 2)
I Turbulence-attenuated transitional flow (Phase 3)
J Laminar flow with full gelling (Phase 4)

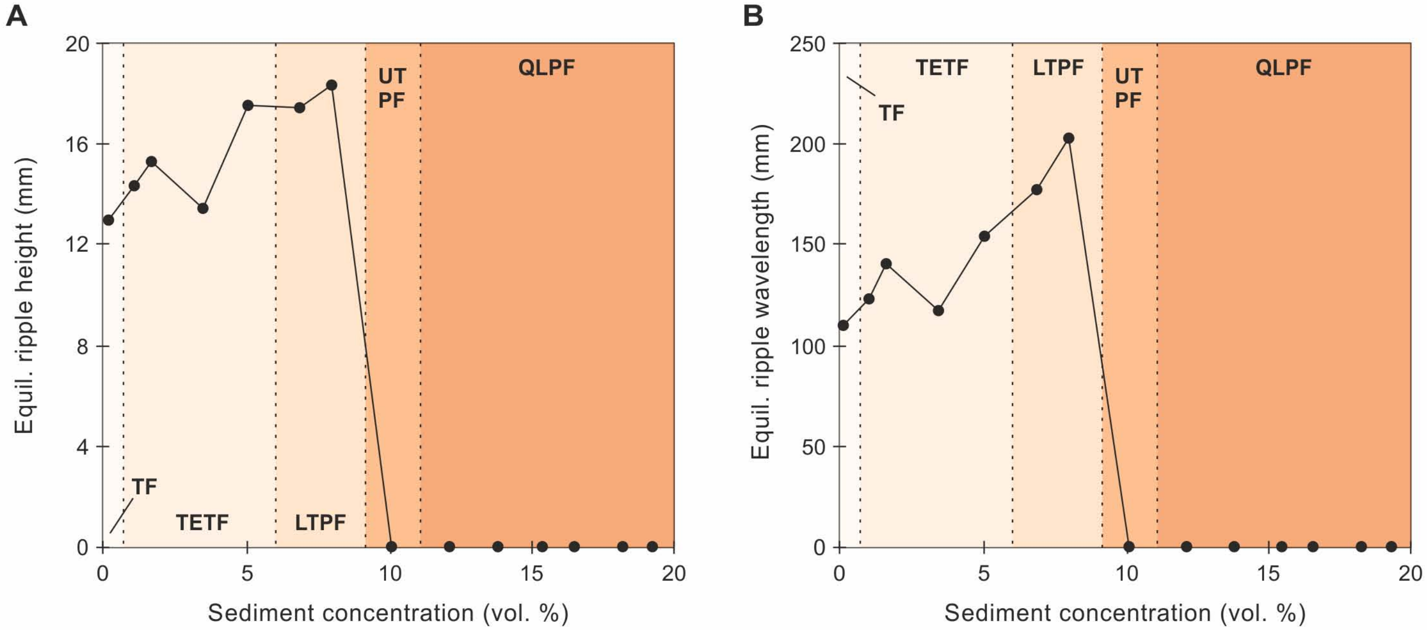
A
Equil. ripple height (mm)
Sediment concentration (vol. %)
TF
TETF
LTPF
UT PF
QLPF
B
Equil. ripple wavelength (mm)
Sediment concentration (vol. %)
TF
TETF
LTPF
UT PF
QLPF

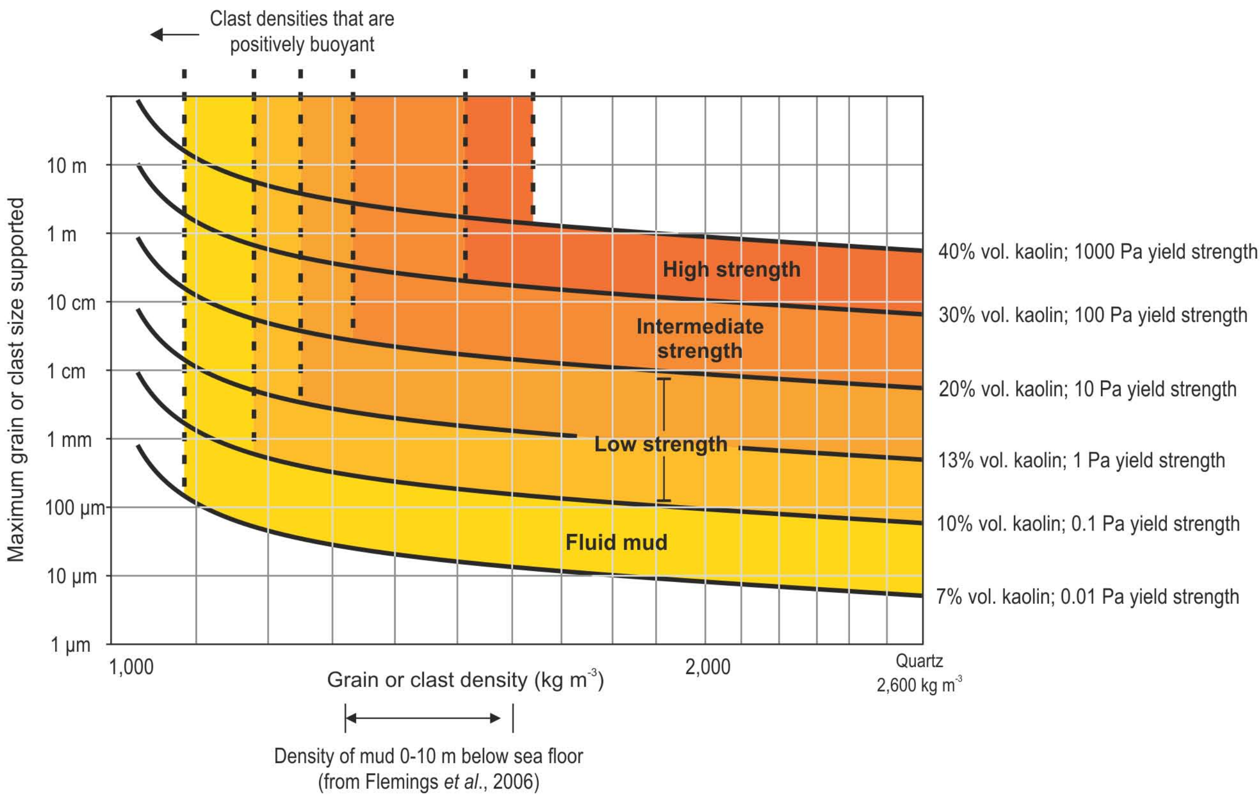

Clast densities that are positively buoyant
Maximum grain or clast size supported
10 m
1 m
10 cm
1 cm
1 mm
100 µm
10 µm
1 µm
1,000
2,000
Quartz 2,600 kg m^{-3}
Grain or clast density (kg m^{-3})
High strength
Intermediate strength
Low strength
Fluid mud
40% vol. kaolin; 1000 Pa yield strength
30% vol. kaolin; 100 Pa yield strength
20% vol. kaolin; 10 Pa yield strength
13% vol. kaolin; 1 Pa yield strength
10% vol. kaolin; 0.1 Pa yield strength
7% vol. kaolin; 0.01 Pa yield strength
Density of mud 0-10 m below sea floor (from Flemings *et al.*, 2006)

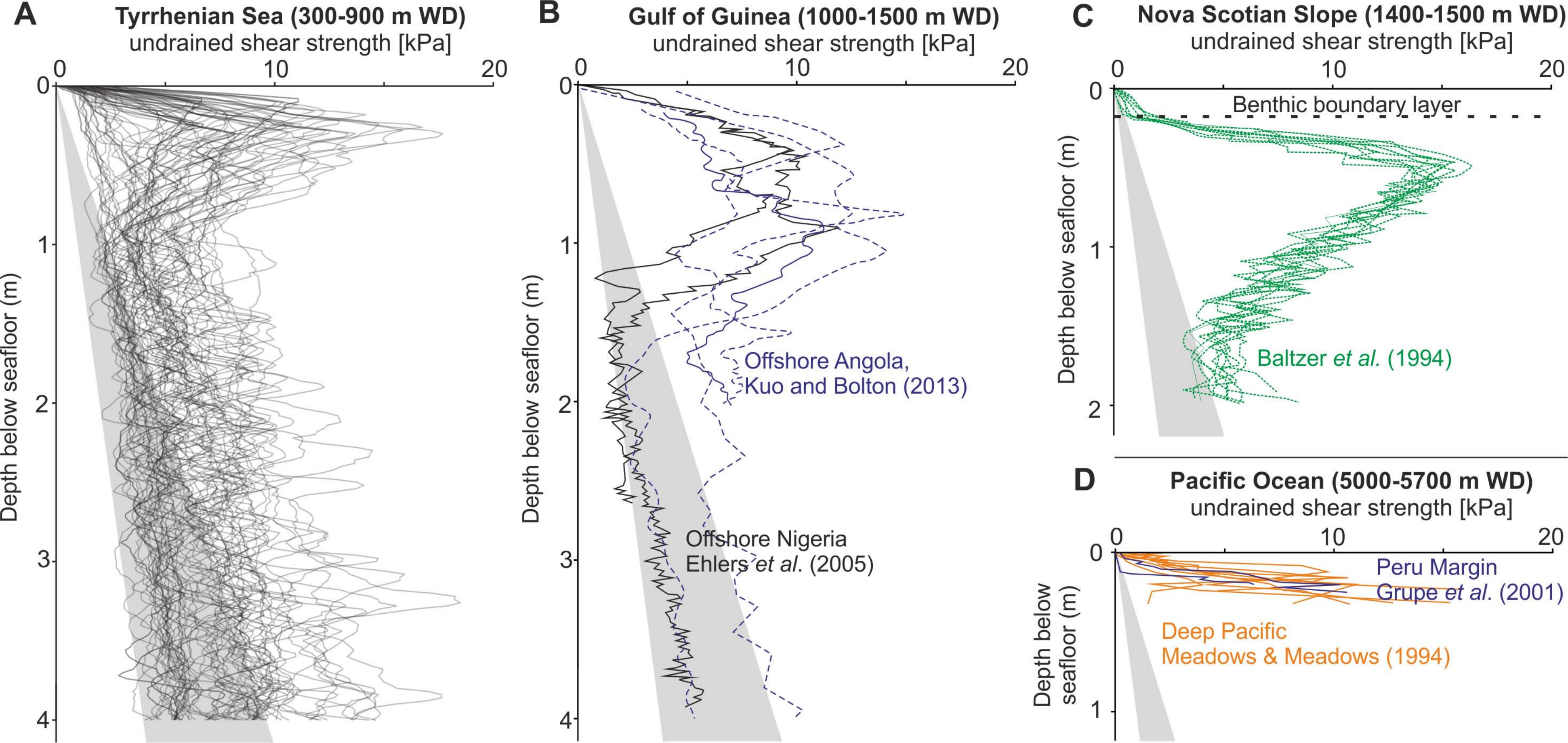
A
Tyrrhenian Sea (300-900 m WD)
undrained shear strength [kPa]
0
10
20
Depth below seafloor (m)
0
1
2
3
4
B
Gulf of Guinea (1000-1500 m WD)
undrained shear strength [kPa]
0
10
20
Depth below seafloor (m)
0
1
2
3
4
Offshore Angola,
Kuo and Bolton (2013)
Offshore Nigeria
Ehlers et al. (2005)
C
Nova Scotian Slope (1400-1500 m WD)
undrained shear strength [kPa]
0
10
20
Depth below seafloor (m)
0
1
2
Benthic boundary layer
Baltzer et al. (1994)
D
Pacific Ocean (5000-5700 m WD)
undrained shear strength [kPa]
0
10
20
Depth below seafloor (m)
0
1
Peru Margin
Grupe et al. (2001)
Deep Pacific
Meadows & Meadows (1994)

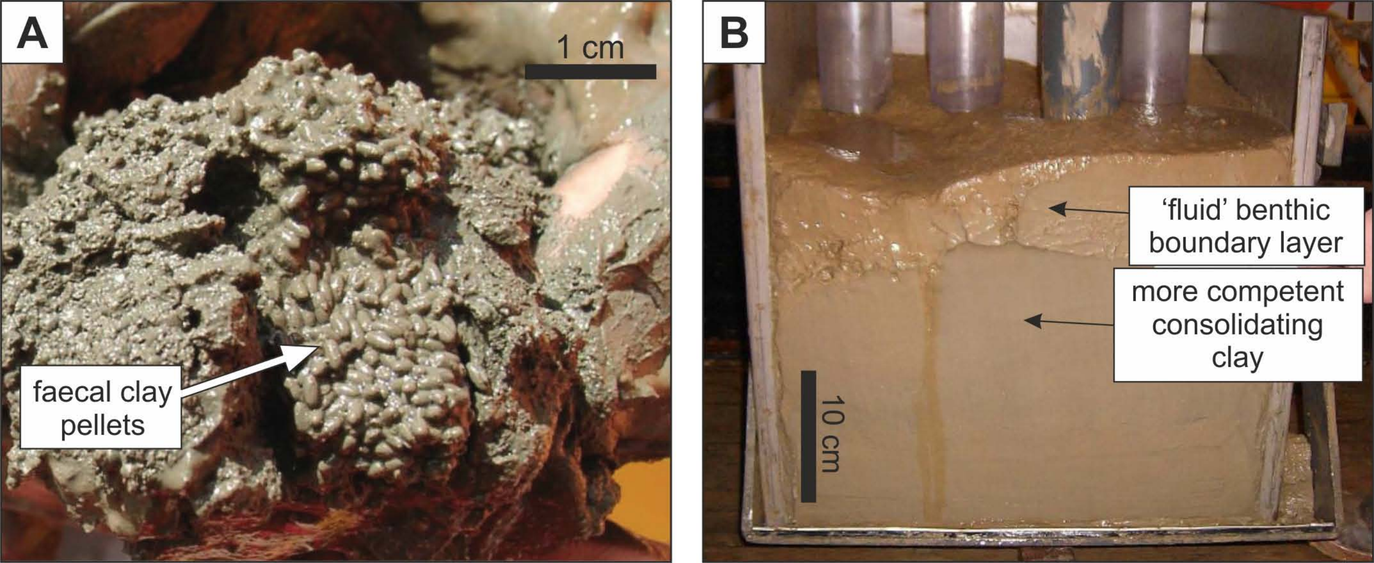
A
1 cm
faecal clay
pellets
B
'fluid' benthic
boundary layer
more competent
consolidating
clay
10 cm

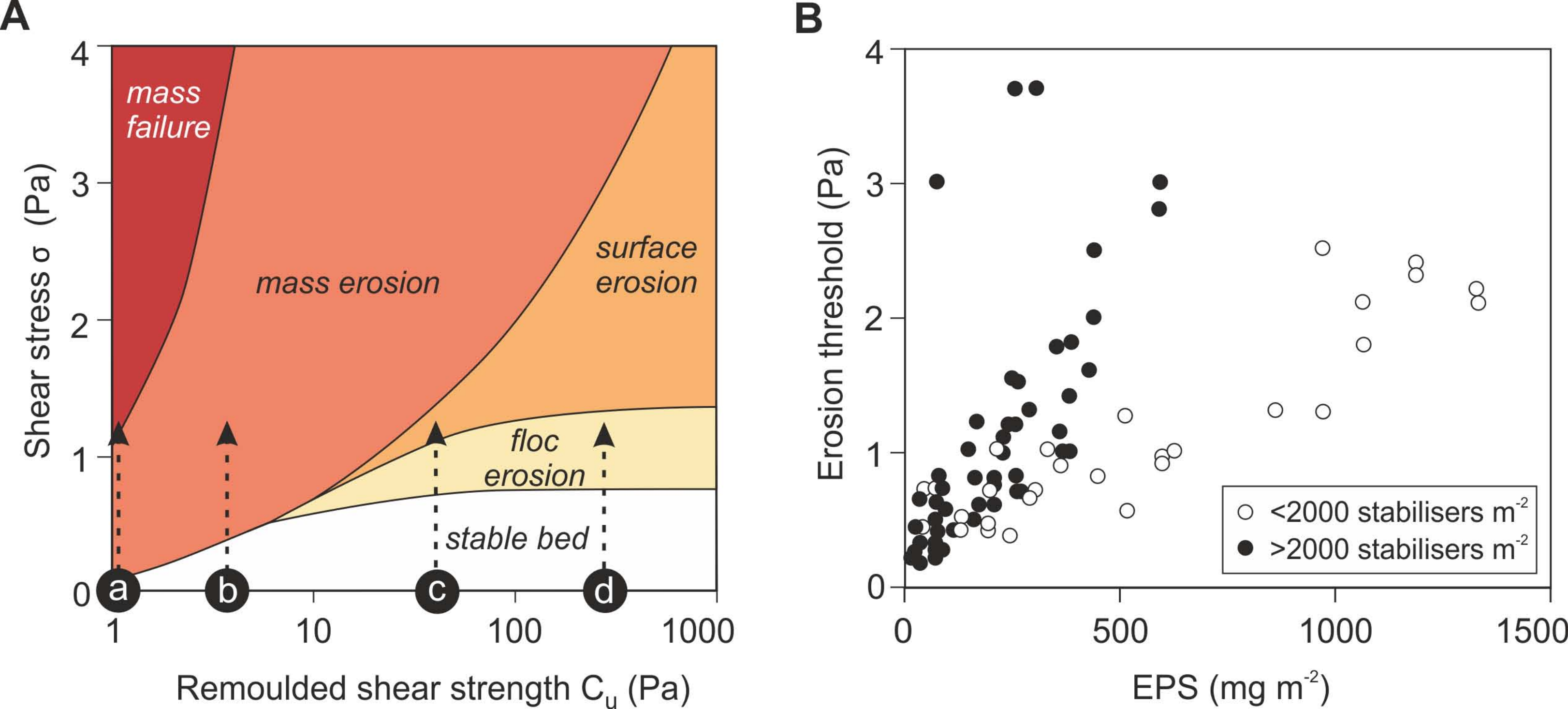
A
B
mass failure
mass erosion
surface erosion
floc erosion
stable bed
a
b
c
d
Shear stress σ (Pa)
Remoulded shear strength C_u (Pa)
0
1
2
3
4
1
10
100
1000
Erosion threshold (Pa)
EPS (mg m^{-2})
0
500
1000
1500
<2000 stabilisers m^{-2}
>2000 stabilisers m^{-2}

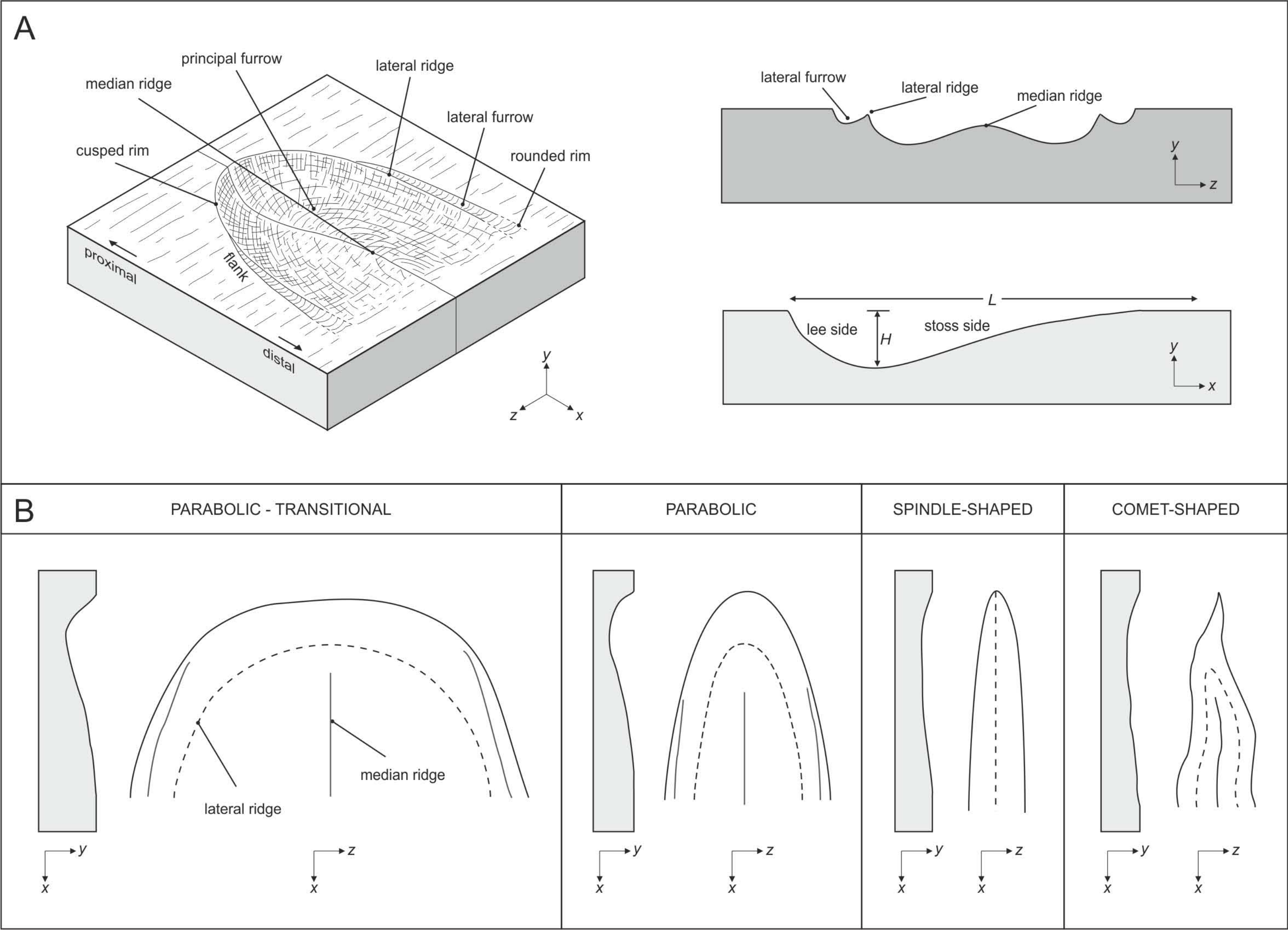
A
principal furrow
lateral ridge
median ridge
lateral furrow
cusped rim
rounded rim
flank
proximal
distal
y
z
x
lateral furrow
lateral ridge
median ridge
y
z
L
lee side
H
stoss side
y
x
B
PARABOLIC - TRANSITIONAL
PARABOLIC
SPINDLE-SHAPED
COMET-SHAPED
lateral ridge
median ridge
y
x
z
x

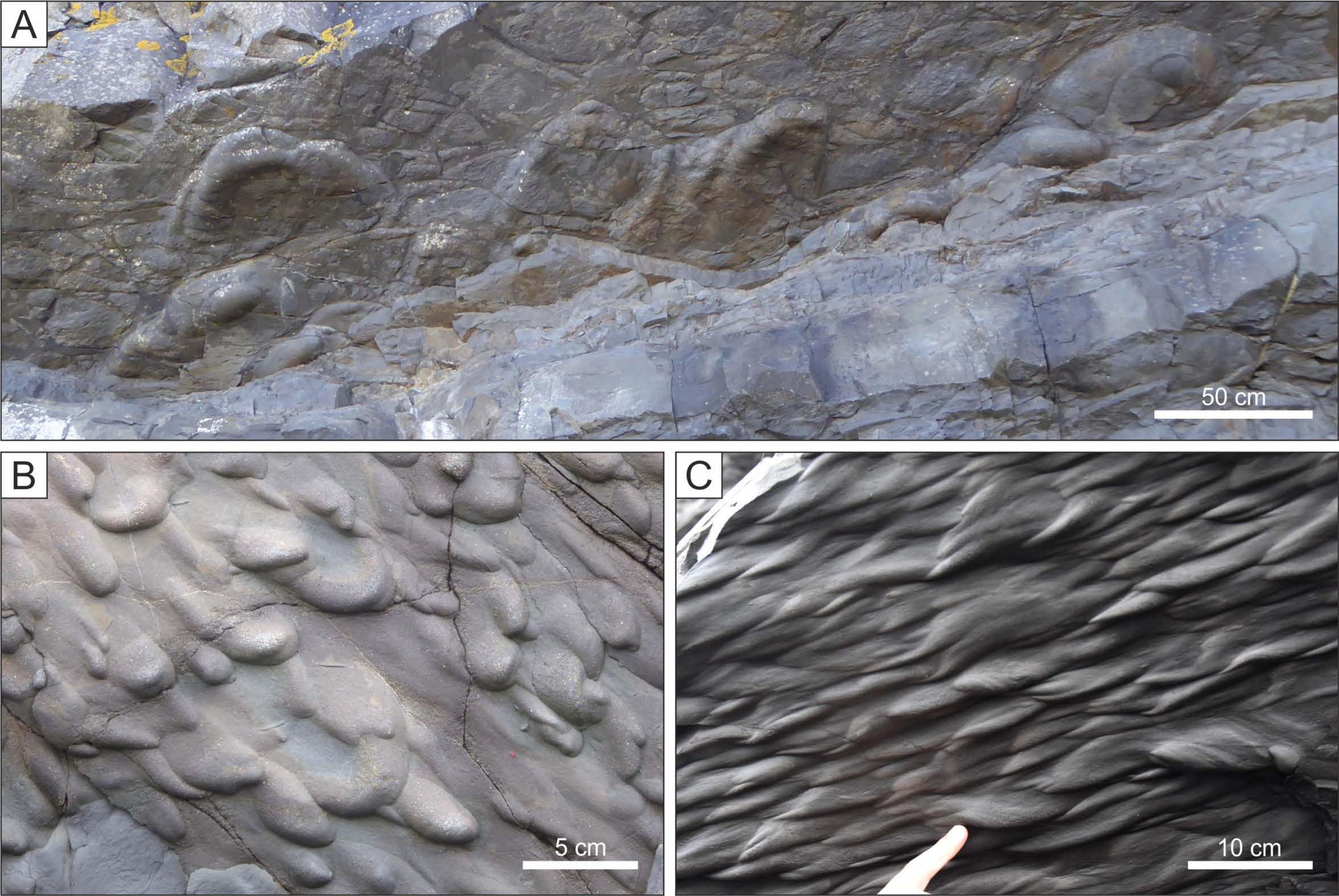
A
50 cm
B
5 cm
C
10 cm

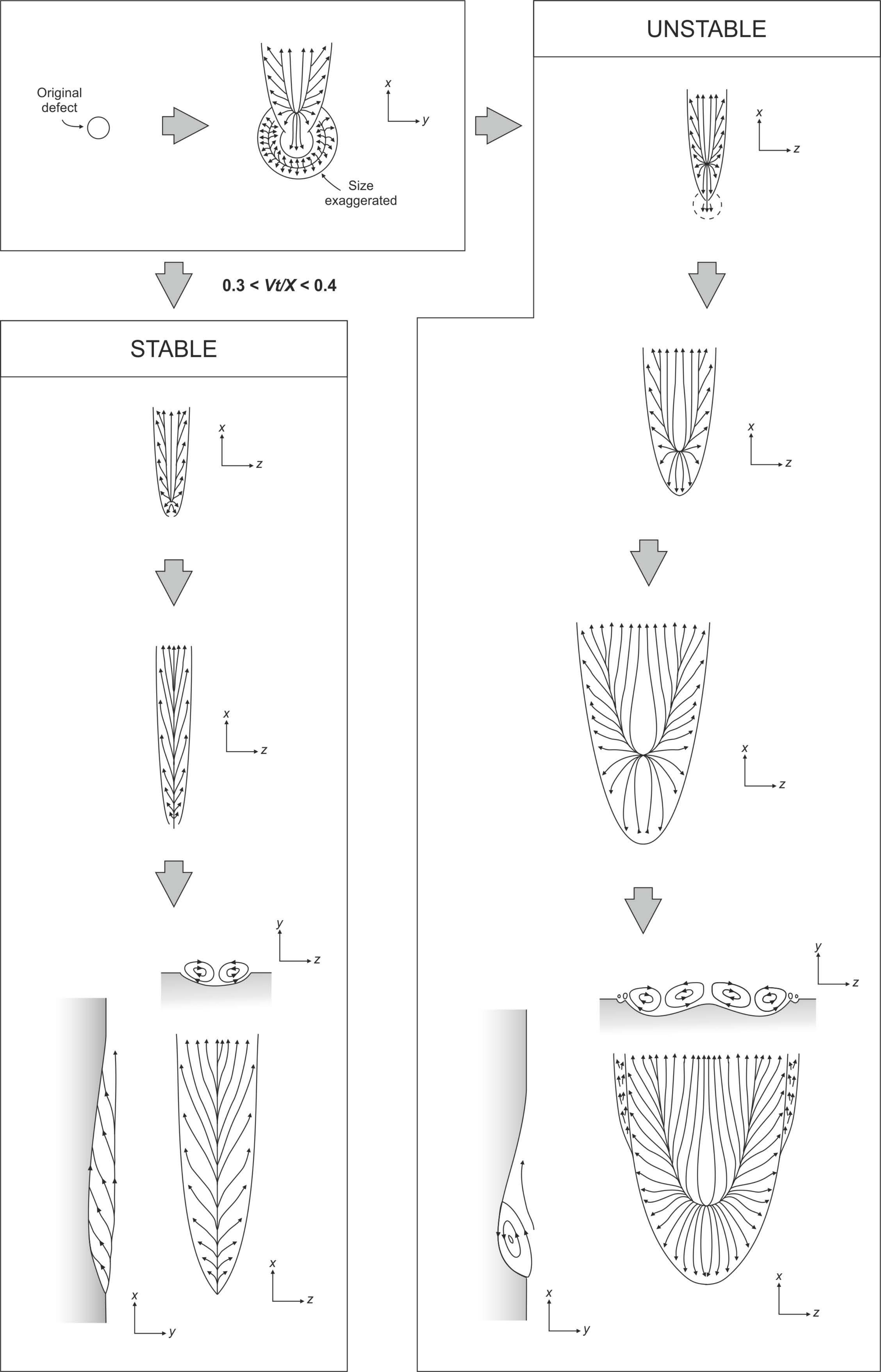

Original defect
Size exaggerated
x
y
0.3 < Vt/X < 0.4
STABLE
z
UNSTABLE

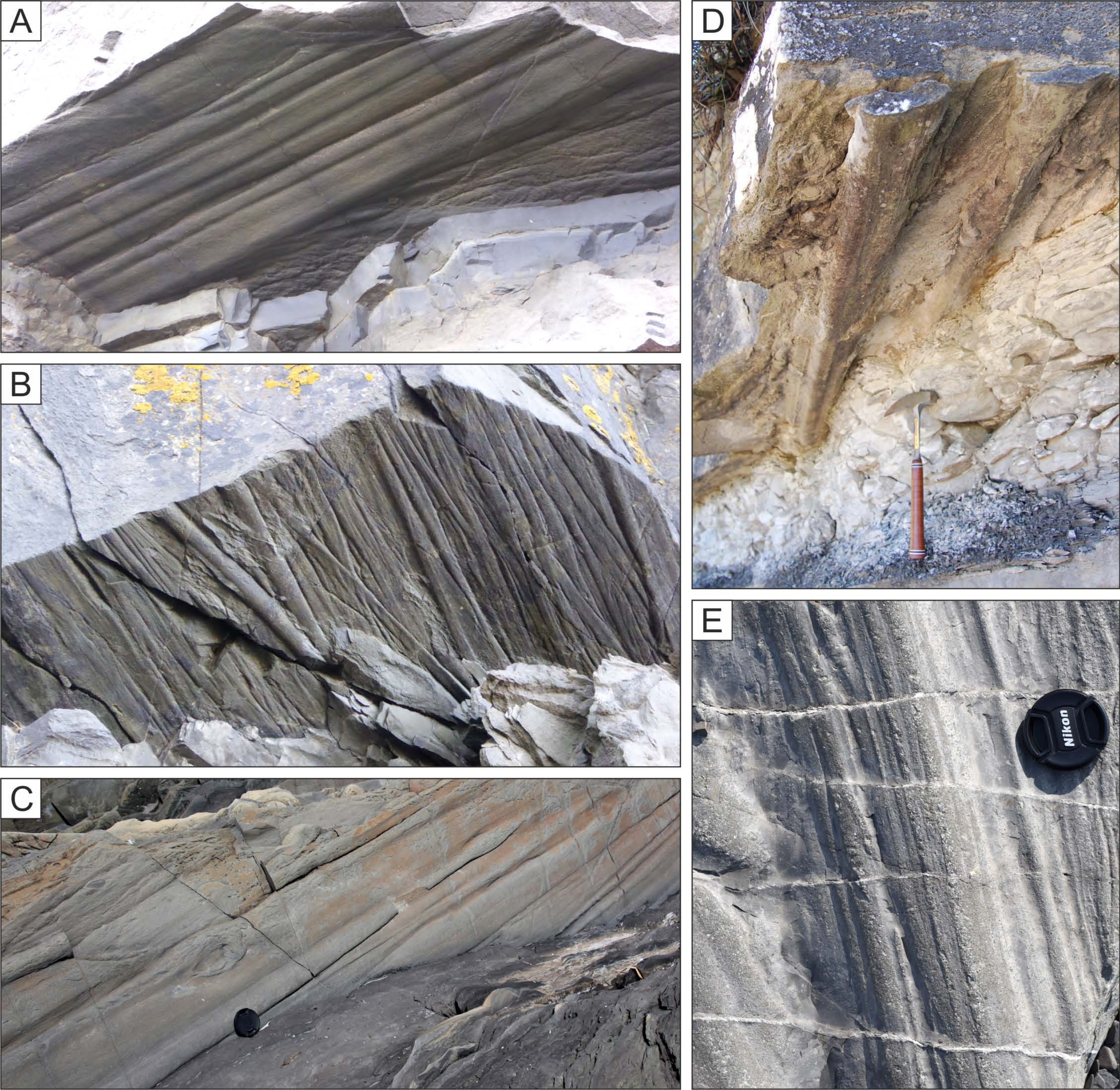
A
B
C
D
E
Nikon

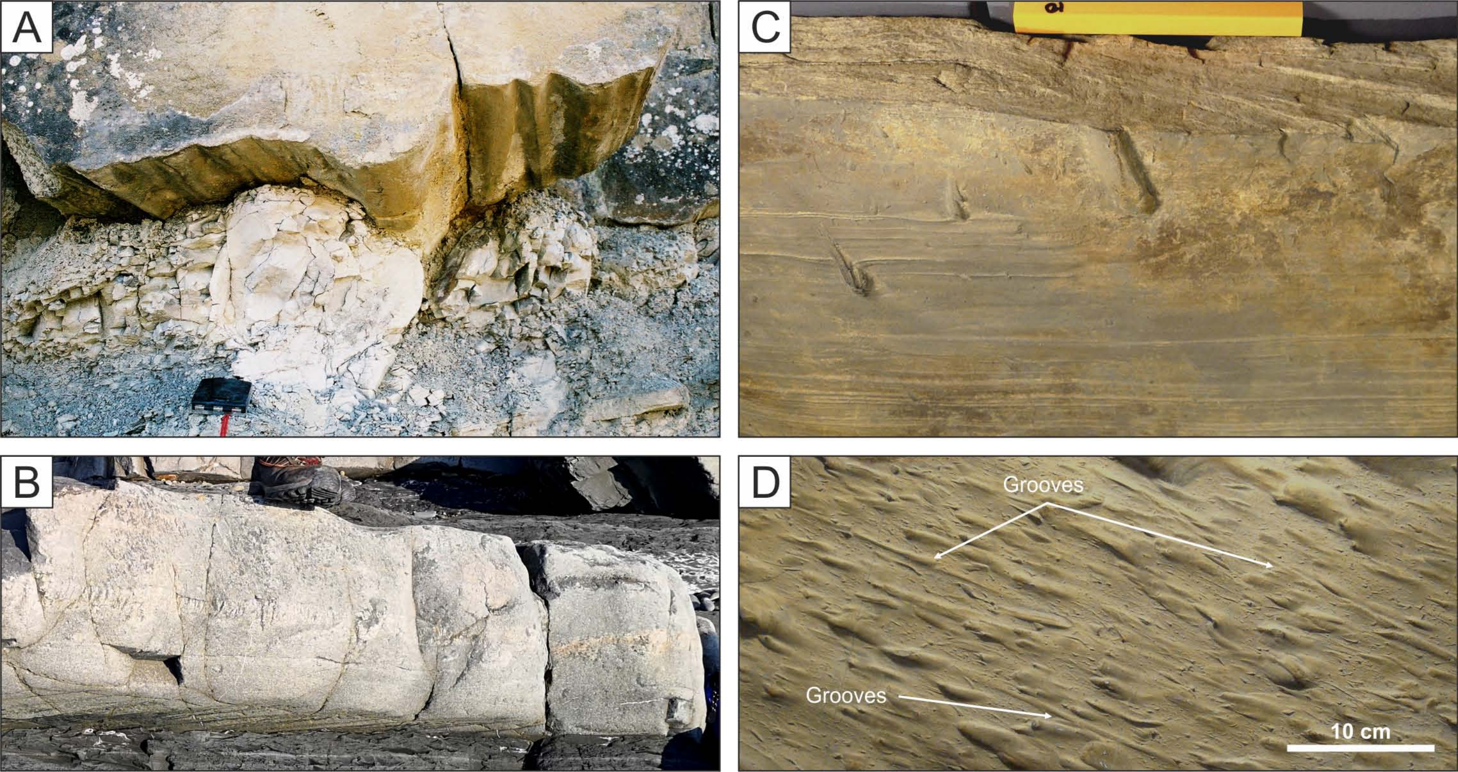
A
B
C
D
Grooves
Grooves
10 cm

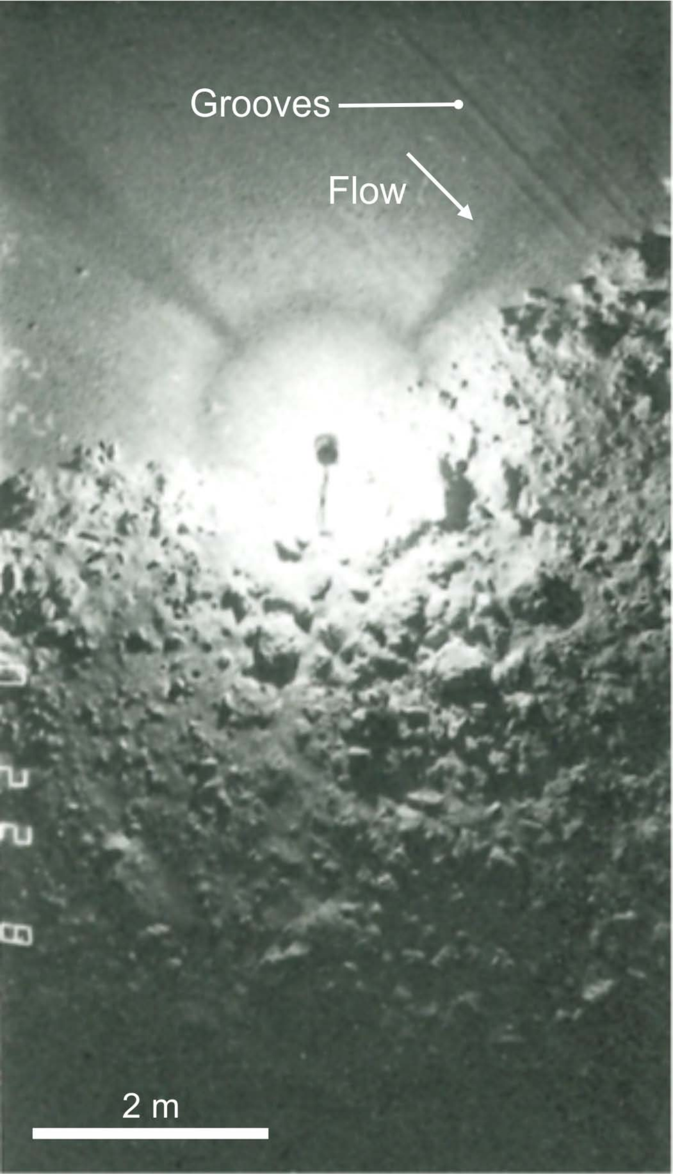
Grooves
Flow
2 m

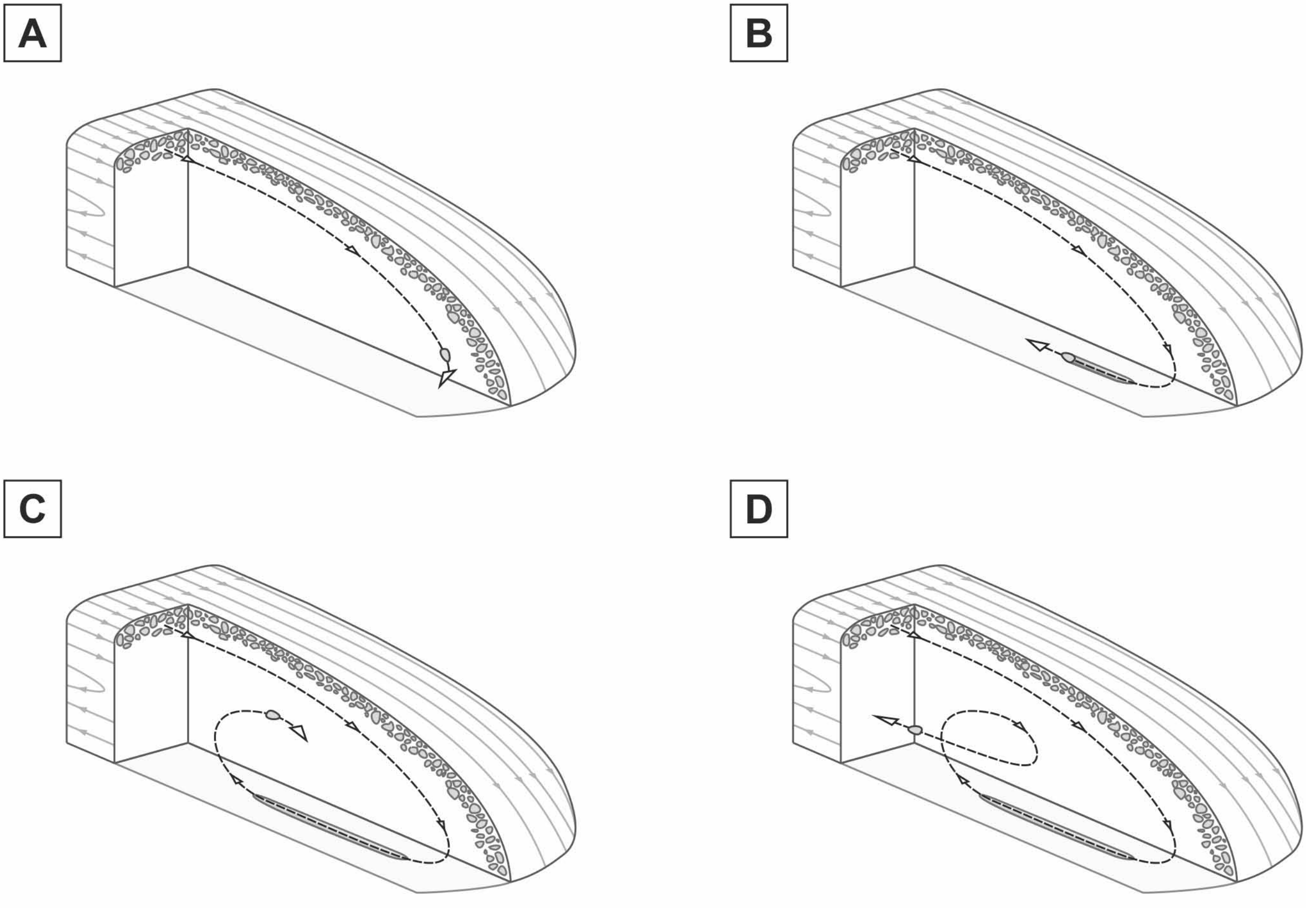
A
B
C
D

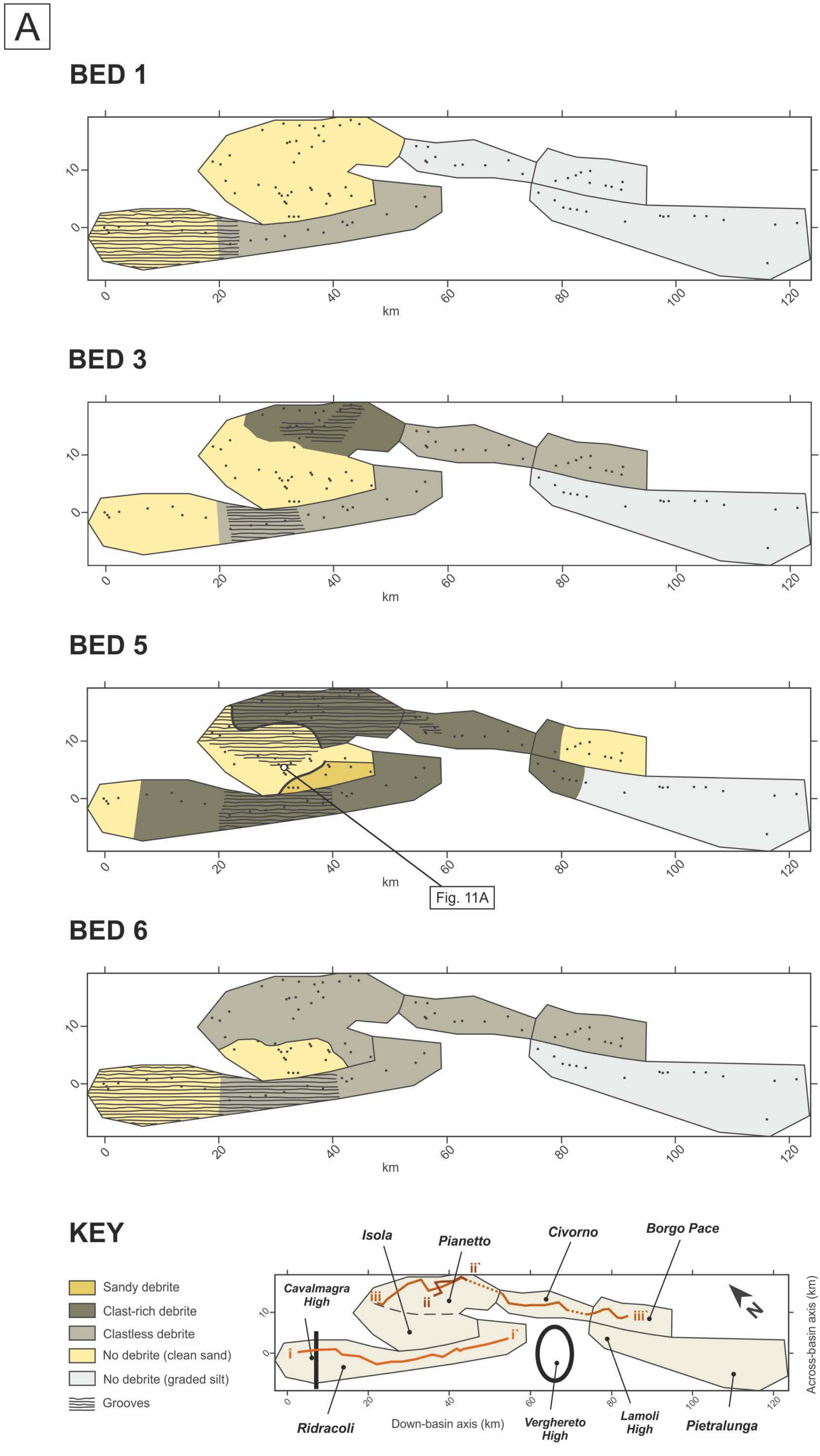

A
BED 1
BED 3
BED 5
Fig. 11A
BED 6
km
KEY
Sandy debrite
Clast-rich debrite
Clastless debrite
No debrite (clean sand)
No debrite (graded silt)
Grooves
Isola
Pianetto
Civorno
Borgo Pace
Cavalmagra High
Ridracoli
Verghereto High
Lamoli High
Pietralunga
Down-basin axis (km)
Across-basin axis (km)
N

B
BED 3 Ridracoli transect
i
Flow direction
i`
metres
2
1
0
C
BED 3 Pianetto transect
ii
ii`
Across-flow direction
Down-flow direction
D
BED 5
iii
iii`
Flow direction
Pianetto
Civorno
Borgo Pace
DATA GAP
DATA GAP
KEY
Mud-poor (clean) sandstone
Mud-rich sandstone
Turbidite mudstone
Planar parallel lamination
Undular parallel lamination
Ripple cross lamination
Swirly fabric
Mudstone clasts (>2 cm)
Mudstone chips (<2 cm)
Sandstone clasts
Basal grooves (>2 cm) infilled with mm-scale granules
Grain size break overlain by coarser sandstone

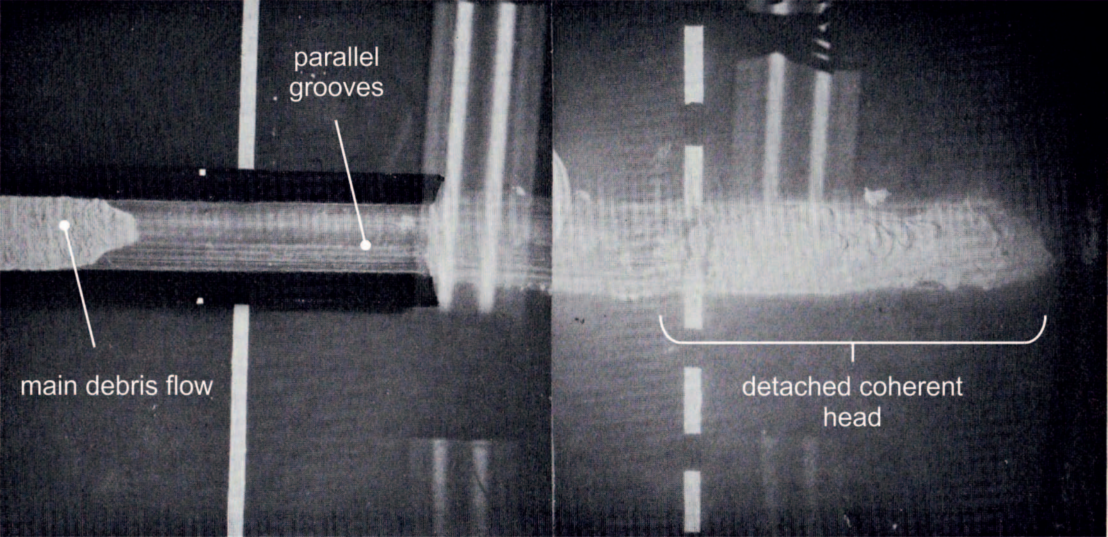
parallel grooves
main debris flow
detached coherent head

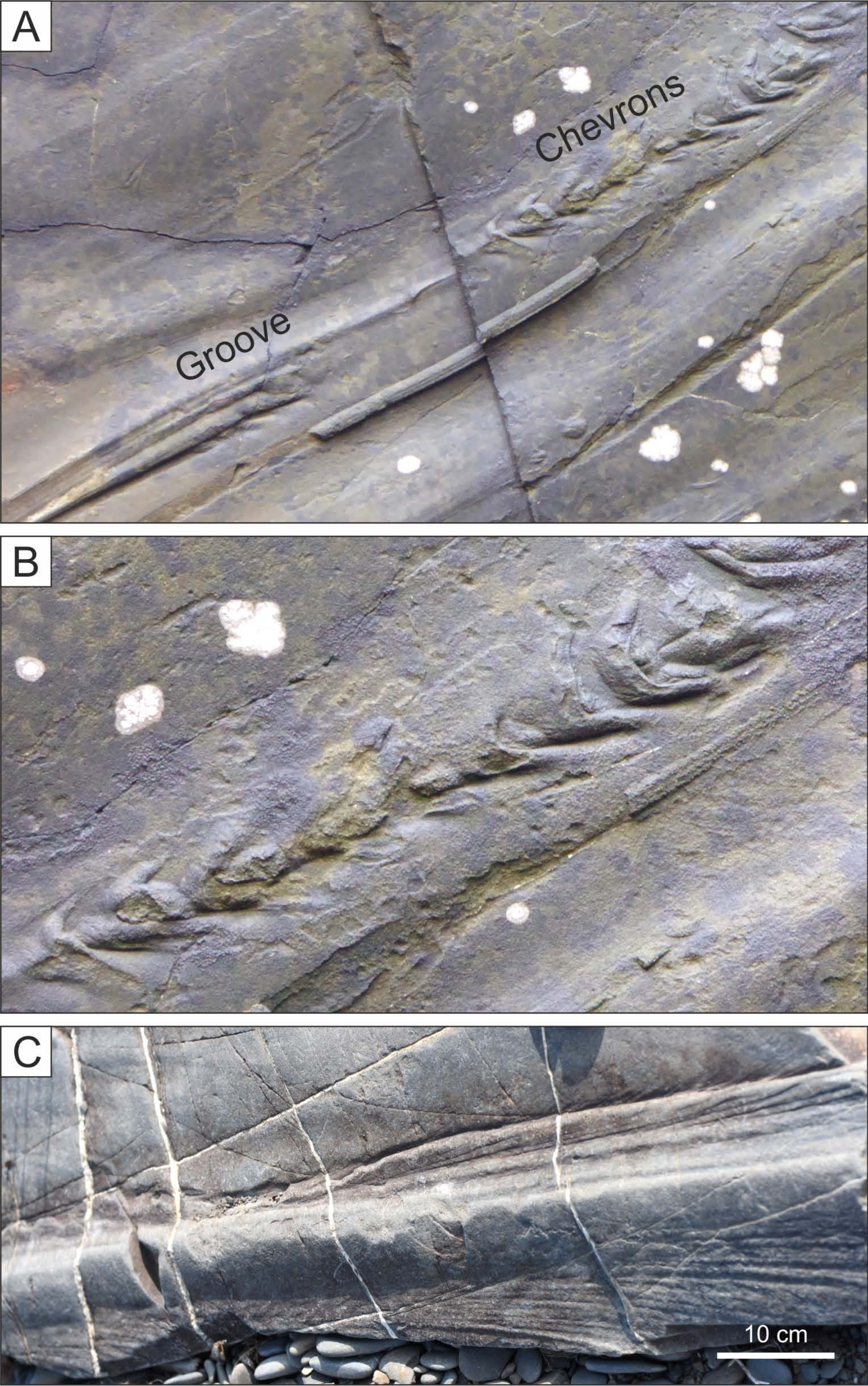
A
Chevrons
Groove
B
C
10 cm

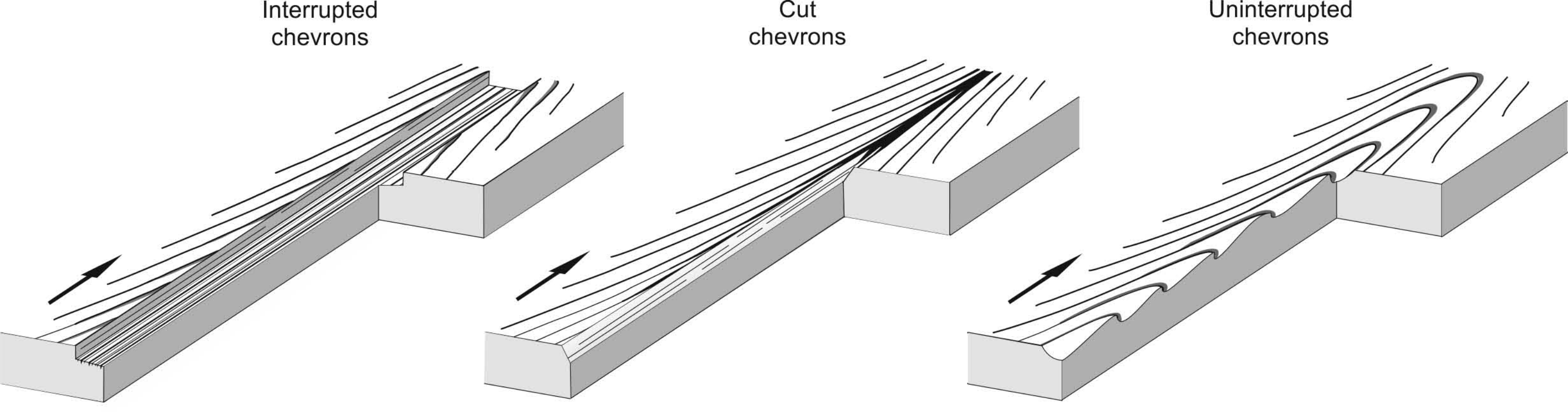
Interrupted chevrons
Cut chevrons
Uninterrupted chevrons

A Low-density turbidity current

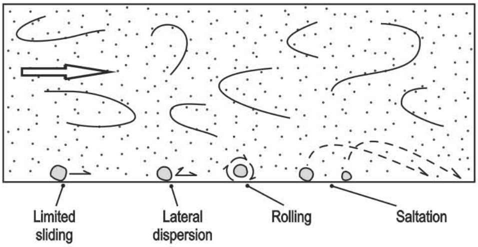

Weaknesses

- Clasts slide for very short distances (<1 grain diameter).
- When overpassing, particles tend to roll.
- Particles rapidly disperse laterally.

B HDTC - traction carpet

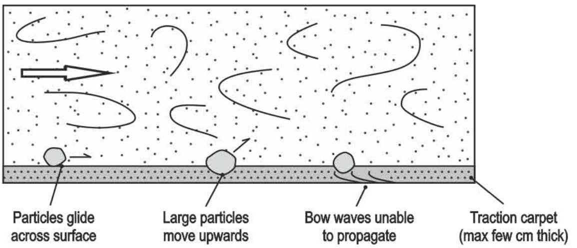

Weaknesses

- Traction carpets thinner than diameter of particles forming many grooves.
- Large particles move away from the bed or glide along the top interface of traction carpet.
- Cannot explain presence of groove marks under T_C beds.
- Bow waves cannot propagate to form chevrons.

C HDTC - high-concentration basal layer

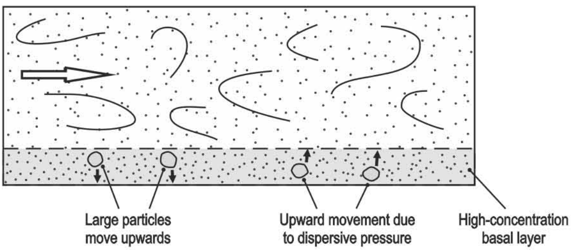

Weaknesses

- Large particles will not remain at a fixed height.
- Large particles may preferentially settle.
- If dispersive pressure is important then large particles may rise.
- If turbulence is extinguished then a very limited tractional signature is produced.

D Granular flow

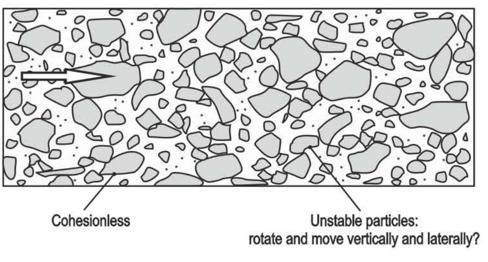

Weaknesses

- Grooves not reported in subaqueous settings.
- Cohesionless flow - clasts likely not fixed in position.
- Restricted to slopes of a few degrees.

E Liquefied/fluidised flow

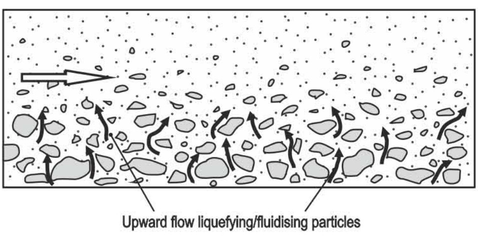

Weaknesses

- Flows have no strength and cannot hold a tool in place.
- Unlikely to liquefy/fluidise large particles.

F Nearly liquefied debris flow

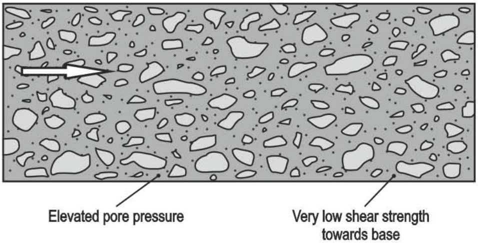

Weaknesses

- Shear strength at base very low.
- Unlikely to be sufficient to hold clasts firmly in place.
- Shear strength higher at front - possible grooves there.

G Laminar plug flow with slip (debris flow)

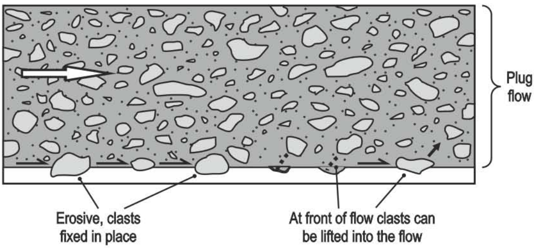

Strengths

- Cohesive strength to hold particles in fixed positions.
- Full of clasts (tools).
- Clasts uplifted at flow front.

H Quasi-laminar plug flow (debris flow) - grooves

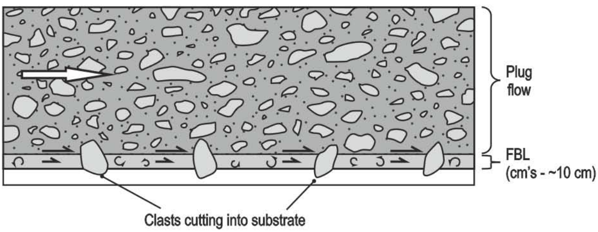

Strengths

- Cohesive strength to hold particles in fixed positions.
- Full of clasts (tools).
- Clasts uplifted at flow front.
- Clasts attached to base of plug penetrate through more fluidal basal layer (FBL).

I Quasi-laminar plug flow (debris flow) - chevrons

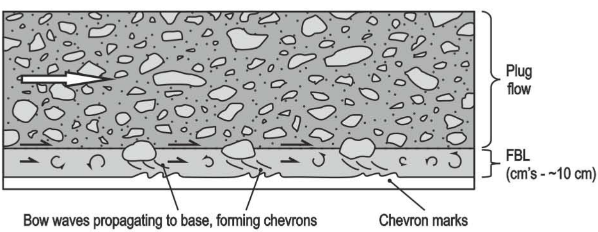

Strengths

- Cohesive strength to hold particles in fixed positions.
- Full of clasts (tools).
- Clasts uplifted at flow front.
- More fluidal basal layer (FBL) allows propagation of bow waves.

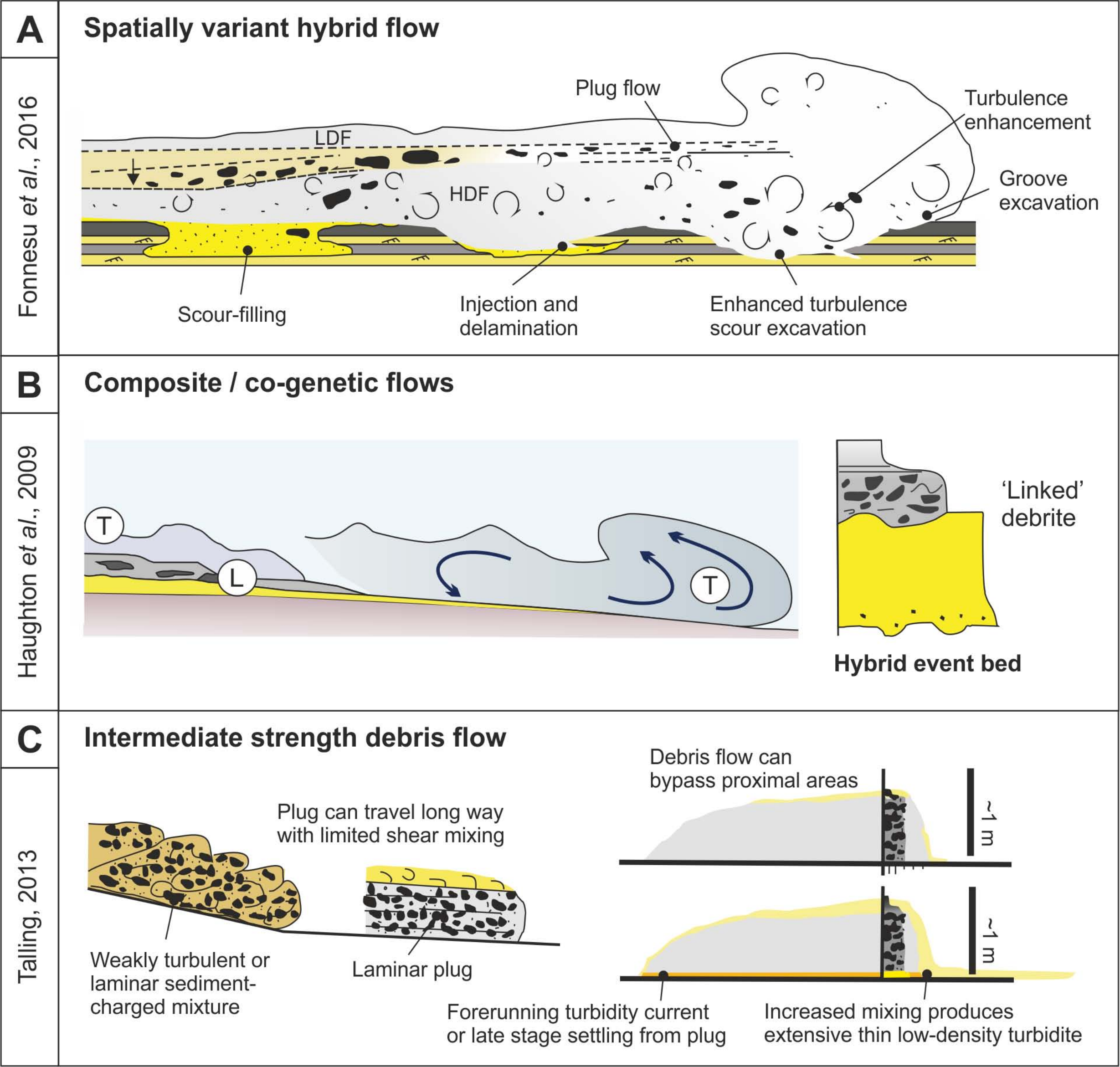
A
Spatially variant hybrid flow
Fonnesu et al., 2016
Plug flow
LDF
HDF
Turbulence enhancement
Groove excavation
Scour-filling
Injection and delamination
Enhanced turbulence scour excavation
B
Composite / co-genetic flows
Haughton et al., 2009
T
L
T
'Linked' debrite
Hybrid event bed
C
Intermediate strength debris flow
Talling, 2013
Debris flow can bypass proximal areas
Plug can travel long way with limited shear mixing
~1 m
~1 m
Weakly turbulent or laminar sediment-charged mixture
Laminar plug
Forerunning turbidity current or late stage settling from plug
Increased mixing produces extensive thin low-density turbidite

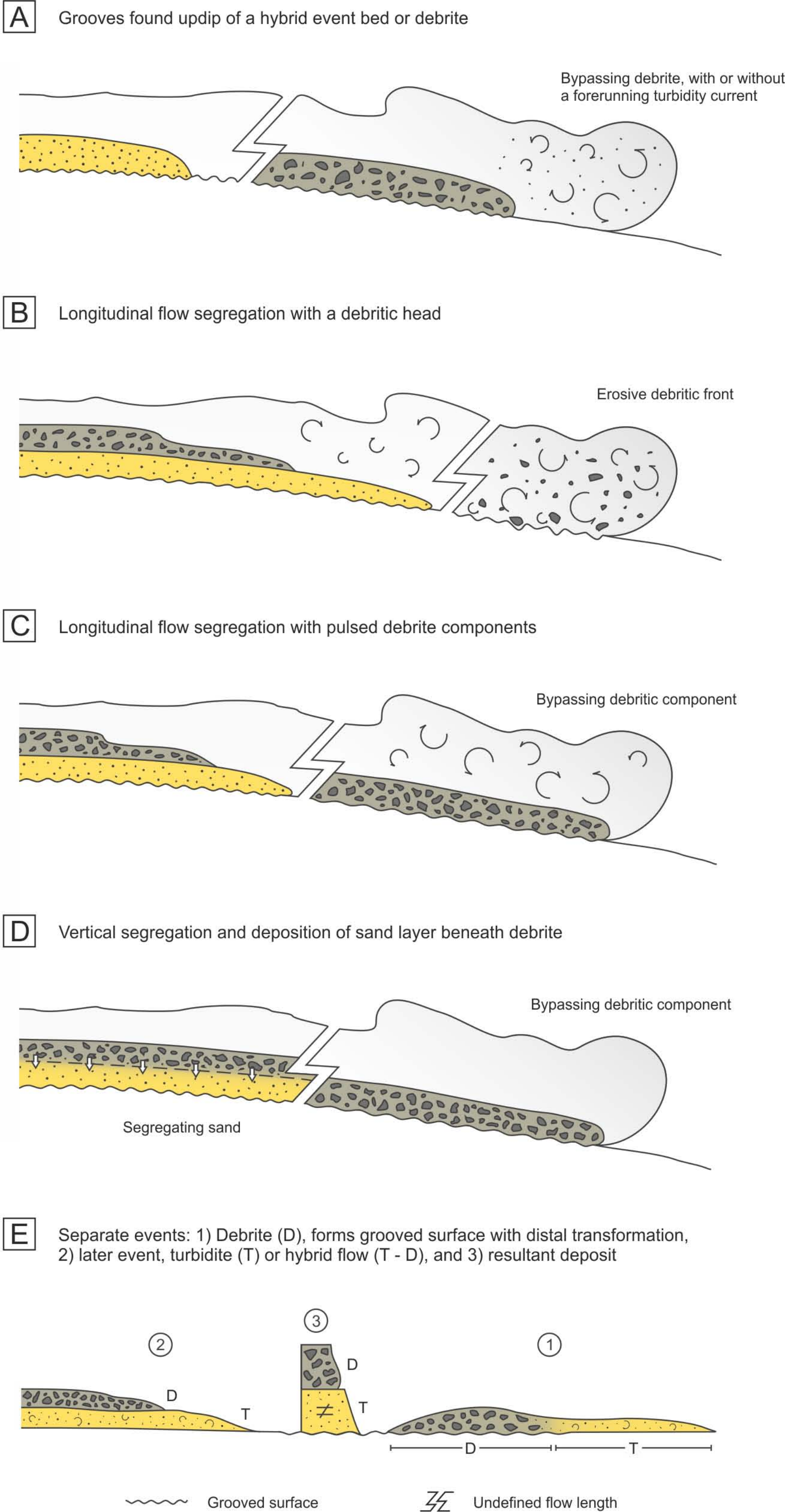
A
Grooves found updip of a hybrid event bed or debrite
Bypassing debrite, with or without
a forerunning turbidity current
B
Longitudinal flow segregation with a debritic head
Erosive debritic front
C
Longitudinal flow segregation with pulsed debrite components
Bypassing debritic component
D
Vertical segregation and deposition of sand layer beneath debrite
Bypassing debritic component
Segregating sand
E
Separate events: 1) Debrite (D), forms grooved surface with distal transformation,
2) later event, turbidite (T) or hybrid flow (T - D), and 3) resultant deposit
2
D
T
3
D
T
1
D
T
Grooved surface
Undefined flow length


A
Gr
Pr
Sk
Sk
Sk
Sk
Sk
Canon
B
Polish Geological Society
C
Polish Geological Society

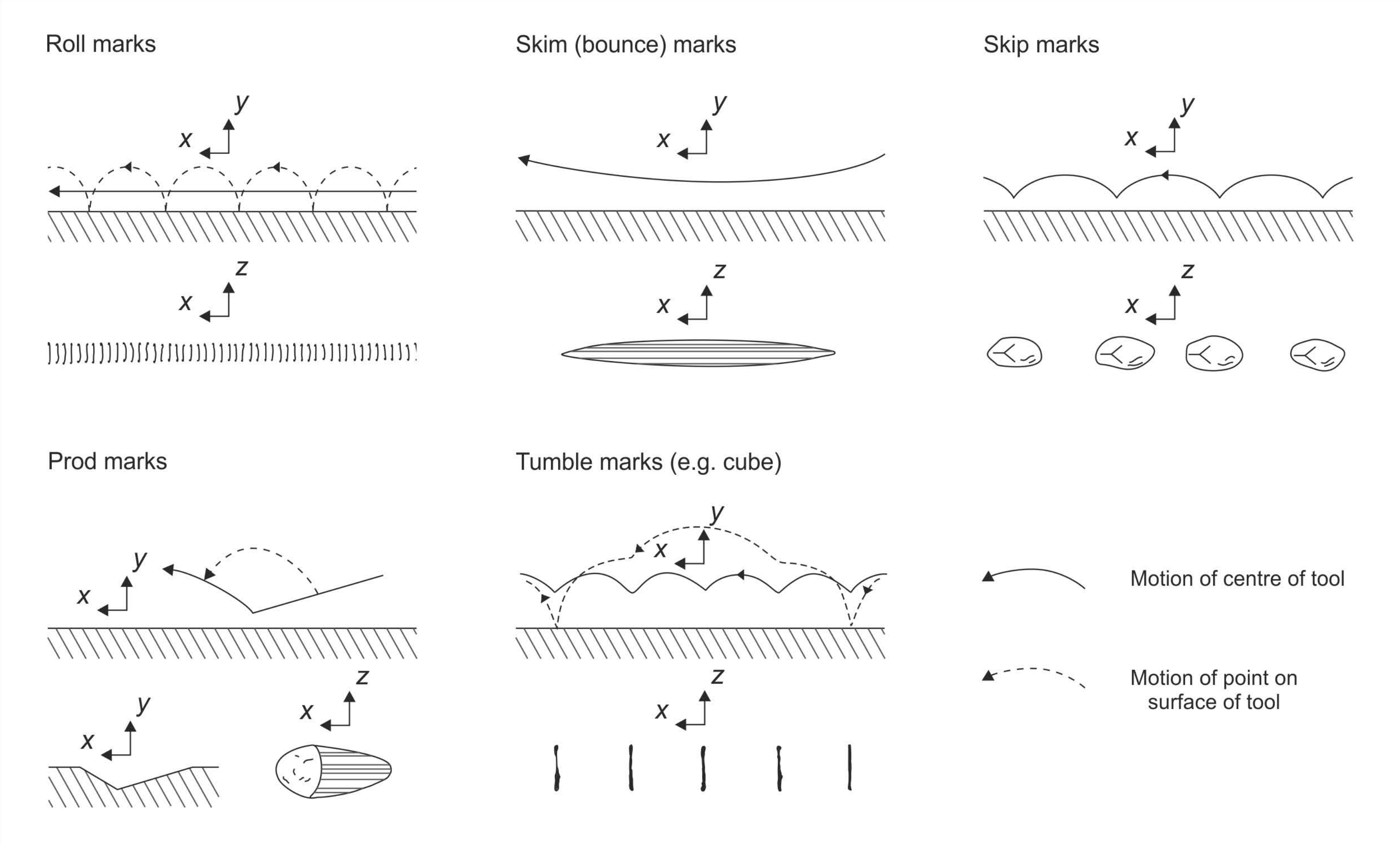
Roll marks
Skim (bounce) marks
Skip marks
y
x
z
Prod marks
Tumble marks (e.g. cube)
Motion of centre of tool
Motion of point on surface of tool

Roll marks

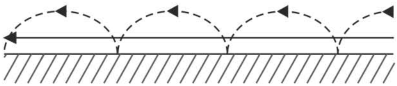

- Low turbulence, low buoyancy.
- However, need relatively planar beds.
- TF, TETF or LTPF.

Prod marks

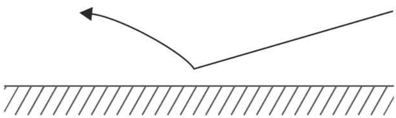

- Ballistic profiles.
- No fine striae at upstream end - likely upper UTPF.
- With fine striae - no grain rotation, stronger transitional flows, uppermost part of UTPF.

Skim marks

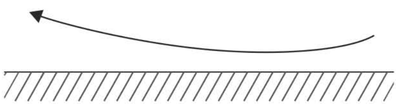

- Buoyant force important.
- Uppermost UTPF.
- Longer skim marks likely lower part of QLPF.
- Grains not 'bouncing' so 'bounce marks' is inappropriate.

Skip marks

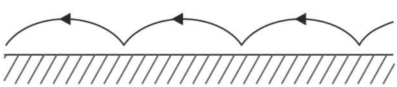

- Shorter relative hop length, stronger transitional flows.
- Likely upper UTPF.

Skip marks - gentle arcs

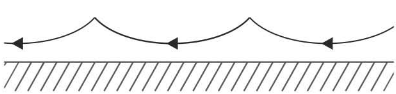

- Buoyant force important.
- Close to forming grooves.
- Likely lower QLPF.
- Cohesive strength insufficient to hold clasts at a constant flow height.

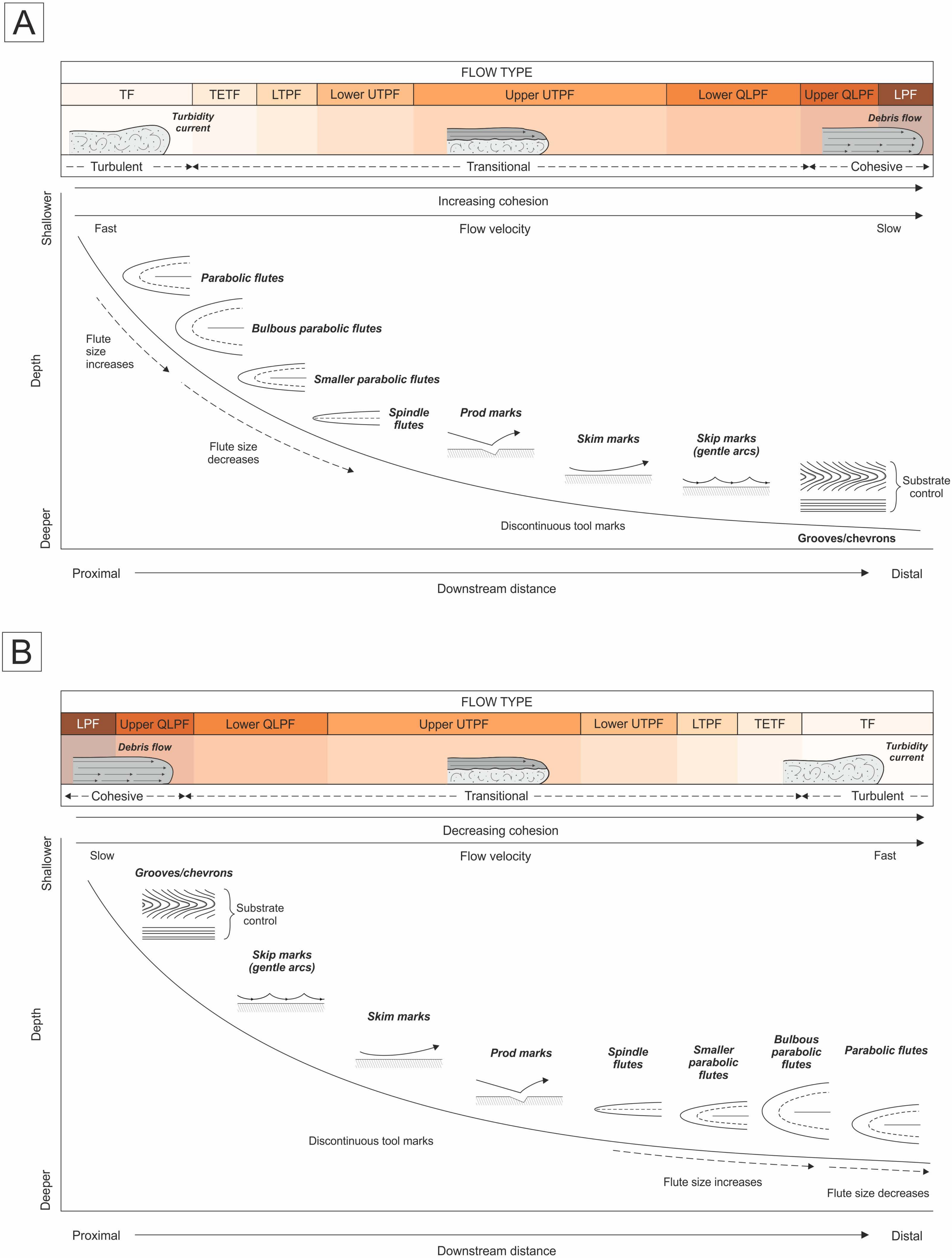

A
FLOW TYPE
TF
TETF
LTPF
Lower UTPF
Upper UTPF
Lower QLPF
Upper QLPF
LPF
Turbidity current
Debris flow
Turbulent
Transitional
Cohesive
Increasing cohesion
Fast
Flow velocity
Slow
Shallower
Depth
Deeper
Parabolic flutes
Bulbous parabolic flutes
Flute size increases
Smaller parabolic flutes
Spindle flutes
Prod marks
Skim marks
Skip marks (gentle arcs)
Flute size decreases
Substrate control
Discontinuous tool marks
Grooves/chevrons
Proximal
Distal
Downstream distance
B
FLOW TYPE
LPF
Upper QLPF
Lower QLPF
Upper UTPF
Lower UTPF
LTPF
TETF
TF
Debris flow
Turbidity current
Cohesive
Transitional
Turbulent
Decreasing cohesion
Slow
Flow velocity
Fast
Shallower
Depth
Deeper
Grooves/chevrons
Substrate control
Skip marks (gentle arcs)
Skim marks
Prod marks
Spindle flutes
Smaller parabolic flutes
Bulbous parabolic flutes
Parabolic flutes
Discontinuous tool marks
Flute size increases
Flute size decreases
Proximal
Distal
Downstream distance

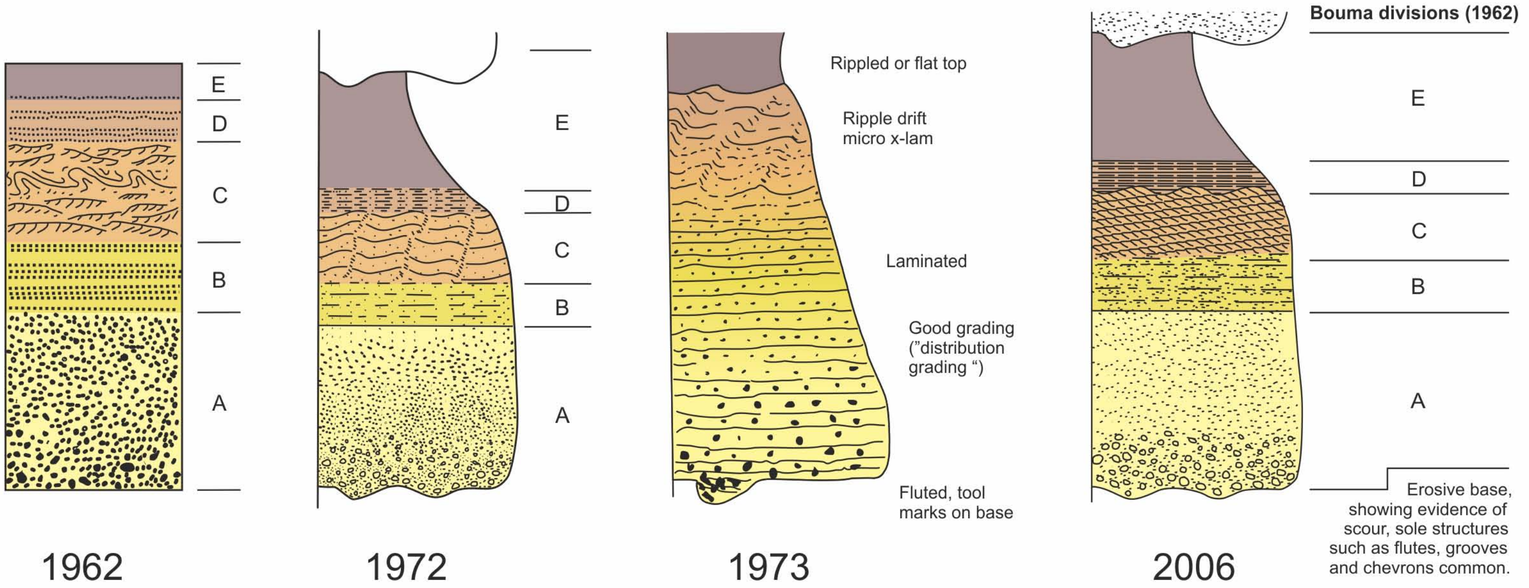
Bouma divisions (1962)
E
D
C
B
A
E
D
C
B
A
Rippled or flat top
Ripple drift
micro x-lam
Laminated
Good grading
("distribution
grading ")
Fluted, tool
marks on base
E
D
C
B
A
Erosive base,
showing evidence of
scour, sole structures
such as flutes, grooves
and chevrons common.
1962
1972
1973
2006

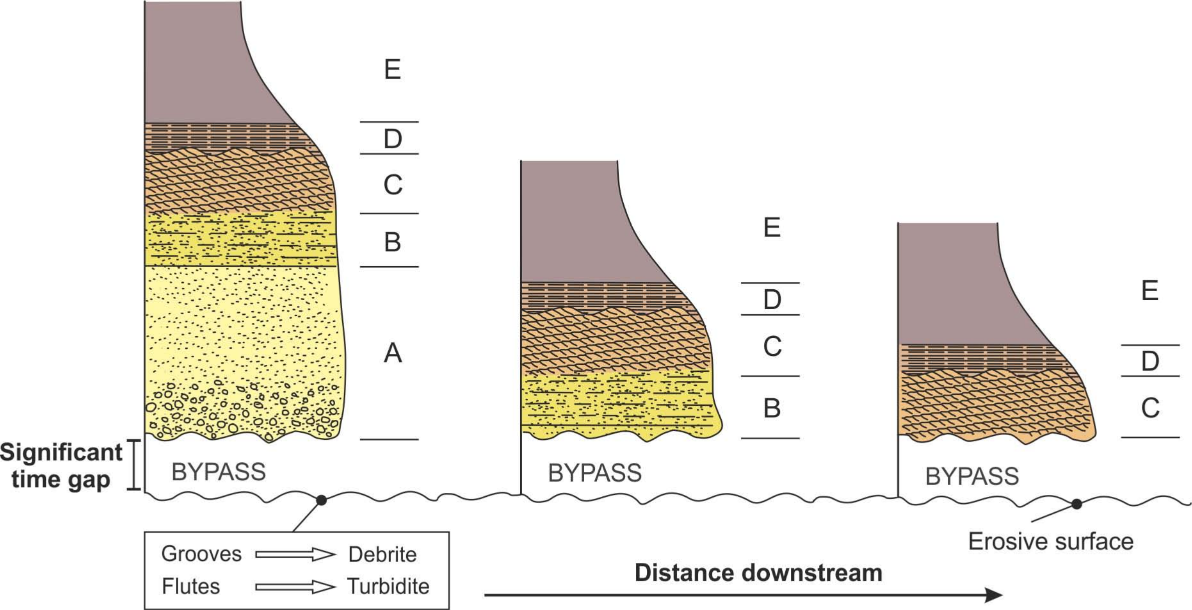
E
D
C
B
A
Significant time gap
BYPASS
E
D
C
B
BYPASS
E
D
C
BYPASS
Grooves
Debrite
Flutes
Turbidite
Distance downstream
Erosive surface